HOW DO ANIMALS GLIDE IN THEIR NATURAL HABITAT? A HOLISTIC APPROACH USING THE FLYING LIZARD *DRACO DUSSUMIERI*

Pranav Chandrakant Khandelwal

A dissertation submitted to the faculty at the University of North Carolina at Chapel Hill in partial fulfillment of the requirements for the degree of Doctor of Philosophy in the Department of Biology.

Chapel Hill
2021

Approved by:

Tyson L. Hedrick

Laura A. Miller

Karin Pfennig

Kenneth J. Lohmann

John J. Socha

ABSTRACT

Pranav Chandrakant Khandelwal: How do animals glide in their natural habitat?
A holistic approach using the flying lizard *Draco dussumieri*
(Under the direction of Tyson L. Hedrick)

Gliding is a common form of aerial locomotion used by a diverse set of animals to perform behaviors essential for their survival. Behaviors like foraging, avoiding predators, seeking mates, and/or territorial aggression are influenced by selective pressures that can lead to differences in glide performance. Furthermore, the glide performance is dictated by the physics of the animal's morphology and the environment in which it is performed. To understand the complex interplay between the animal's morphology, behavior, and the environment and how it shapes glide performance, I ask an overarching question, how do animals glide in their natural habitat? I answer this question using a non-invasive motion capture technique in the natural habitat of the flying lizard *Draco dussumieri.*

In Chapter 2, I describe in detail the gliding aerodynamics and the performance envelope used by *Draco*. In doing so, I discover a potential aerodynamic strategy that maximizes glide performance in terms of distance traveled and height lost. Chapter 3 extends the kinematic and aerodynamic analysis to an individual level looking at the influence of sex and body size on gliding performance. It shows the expected detrimental effects of isometric scaling of body size on aerodynamics but reveals compensatory changes in glide behavior to account for larger body size. Furthermore, I also show subtle glide performance differences within and among sexes, suggesting influences of selective pressure and ontogeny. Finally, I describe how gliding is

actually implemented in the natural habitat. In Chapter 4, I focus on the sensory and environmental context looking at how *Draco* account for spatial complexity and tune their glide execution to reach their desired target. In doing so, I show that *Draco* primarily rely on vision to gather environmental information and use a path planning strategy to navigate their spatially cluttered environment.

Overall, my findings provide the first holistic analysis of gliding showing how various intrinsic (sex, size, behavior) and extrinsic (environment) factors influence glide execution and performance. It presents a more biologically relevant picture of gliding than most studies conducted thus far and emphasizes the importance of observing behavior in the animal's natural habitat.

To my family and friends and all the curious minds

ACKNOWLEDGEMENTS

My PhD journey has been quite a roller coaster ride with its fair share of highs and lows. What has made the ride even more memorable are the people who accompanied and supported me, giving me the comfort and belief to power on during the lows and cherishing all the highs to make them all the more precious.

My PhD would not have been possible without the love and support of my sisters and parents. They gave me the courage to pursue ideas and opportunities which at times I was not sure I was capable of. Though we are many thousands of miles apart, they have always looked out for me. I would especially like to thank my wife for hopping onto this crazy ride and moving countries to stay with me and support me.

I would like to thank my lab mate, Jonathan, for being my sounding board and always coming to my rescue, from settling in a new country to transitioning to my next journey. My roommates Aatish and Sandeep, for providing a home away from home. I thank them for all the stress buster cooking and movie nights and sharing the ups and downs of my PhD together.

My friends Prasanth, Gaurav, Vinay, Tanvi, Thejasvi, Animakshi, Ritwika, and Preeti for providing me a healthy support system and critical feedback when I needed the most. My close family in the US for welcoming me with open arms and keeping me rooted throughout my journey.

My current and former lab mates – Laura, Aaron, Dennis, and Jeremy for providing a wonderful working environment and all the constructive discussions on science and life. I am grateful to many academics including Sanjay, Namrata, Hema, Shanki, and Archana, they have played a crucial role in shaping my academic journey thus far.

I am grateful to my advisor Tyson Hedrick for giving me the opportunity to pursue my ideas and beliefs, and showing how cool technology can be applied to research. I thank him for taking the leap of faith and allowing me to undertake the first field trip on flying lizards without knowing what might come out of it, that has ultimately shaped my PhD! His work ethic, commitment, and approach to research has had a strong positive influence on me. I thank him for his patience during my journey, I am sure I have put that to test multiple times! Finally, I am grateful to him for always supporting me through the various setbacks that I have faced and giving me a gentle nudge when I needed it.

My committee – Karin Pfennig, Laura Miller, Kenneth Lohman, and Jake Socha for guiding and supporting me through my research. I would also like to thank Kenlyn and Barbara in the Biology department for supporting me and lending a thoughtful ear whenever I needed it.

I would also like to thank Steve, Shankar, Priyanka, Reuben, Marisha, Roshni, Dhiraj, Raghu, Sunil, Geetesh, Saroja and all the 257 backers who placed their trust in me and shared my curiosity and awe of flying lizards. I will cherish each and every moment that I have spent at the Agumbe Rainforest Research Station.

Finally, I would like to thank my undergraduate and school friends and everyone that I have known during this memorable journey.

TABLE OF CONTENTS

LIST OF TABLES

LIST OF FIGURES

CHAPTER 1: INTRODUCTION

My dissertation focuses on gliding behavior in the flying lizard *Draco dussumieri* in its natural habitat. It aims to present a holistic perspective on how flying lizards generate and manipulate aerodynamic forces to execute glides, how glide execution varies with body size and the sex of the individual, and finally how gliding is implemented in the lizard's spatially cluttered environment. In doing so, I present a case for using *Draco* as a convenient system to study gliding animals and highlight the importance of studying locomotory behavior in the animal's natural habitat. Finally, I also present a novel methodology to collect high quality real-world data to study animal locomotion in the wild that has wide applicability in field behavioral data collection. In this introductory chapter, I provide background information on gliding locomotion in general, an overview of *Draco* with a focus on morphology and behavior related to *Draco*, a description of the field site where the data for this dissertation were collected, and an overview of the field videography camera and kinematic data analysis methods that are common to Chapters 2-4.

1.1 What is gliding?

Gliding can be defined as a fluid-based form of locomotion in which the animal covers horizontal distance without generating power, and instead trades height (potential energy) for kinetic energy for movement [1]. A large and diverse assemblage of animals take to the air via gliding flight, with vertebrates represented by flying squirrels, flying lemurs, sugar gliders, gliding frogs, flying fish, and even flying snakes, among others [1]. Invertebrates are also

represented through gliding squid [2] and gliding ants, though the small body size typical of terrestrial invertebrates works against most aerodynamic performance attributes [3]. Gliding in terrestrial vertebrates including mammals, reptiles, and amphibians has evolved at least 30 times [4] and is actually a sophisticated adaptation that involves changes in anatomy, sensing, behavior, and judgement of the animal [5]. The motivation to glide by these individuals has been ascribed to a number of ecological roles that are essential for the individual's survival, including anti-predatory response, fall injury prevention, intraspecific interaction, expedited horizontal transit, and avoiding potential contact with surfaces [1].

Across all forms of gliding flight, terrestrial gliders have garnered considerable interest within the scientific community in three broad areas – the evolution of flight [4,6,7], gliding ecology [8–12], and mechanics of gliding [13–24]. The arguments put forth for the evolution of flight largely stem from fossil records and studies on the ecology and mechanics of gliding, making it especially important to study extant gliders. Studies on gliding ecology have been limited in number mostly because of the logistical difficulty of tracking animals in the wild. Conversely, the mechanics of gliding has been extensively studied due to the availability of lab specimens and advances in computer vision techniques to study motion. However, studies on gliding mechanics have been restricted to a few gliding taxa including flying squirrels, sugar gliders, and flying snakes. Nonetheless, each of the broad areas mentioned above provided key insights into the gliding behavior of animals. For example, flapping flight in bats has been shown to evolve from an arboreal gliding ancestor similar to extant gliding mammals [25]. Ecological studies on gliding have shown sex-specific behaviors such as territoriality in males of colugos and flying lizards and suggested that gliders might rarely reach terminal velocity for efficient gliding in their natural habitat. Studies on glide biomechanics have provided kinematic data for

various morphologies and described overall glide performance to draw comparisons with other biological flyers and engineered aircraft.

Two areas that have received relatively less attention are the use of computational techniques to model gliding flight and gliding performance studies in the animal's natural habitat. Both are important in understanding how gliders generate and control aerodynamic forces to stay aloft and how gliding performance varies in an ecological context. Current physical models of gliding behavior have treated gliders as static airfoils drawing parallels from fixed-wing aircraft (but see Yeaton et al. [26] and Willis et al. [27]). Such models are more relevant to describe equilibrium gliding where the animal descends at terminal velocity, and do not account for animals actively modulating their aerodynamic forces, as is imperative in controlling glide trajectory to navigate spatially cluttered environments. However, to develop and validate biologically relevant models, quantifying natural glide performance is necessary to provide crucial real-world data. Furthermore, studying natural gliding behavior provides the sensory, spatial, and behavioral framework that shapes the animals' glide performance landscape. That is, the performance envelope in which the glider operates, the influence of specific behaviors on glide performance, and the use of sensory information from the environment to control the glide trajectory, ultimately providing novel insights which are not possible in a lab setting.

1.1.1 Parts of a terrestrial glide

To glide and not fall, the animal must generate aerodynamic forces that will counter the pull of gravity and slow its descent. Simultaneously, the glider must actively control the direction and magnitude of the aerodynamic forces to safely descend and not crash into obstacles on the way or on the ground/landing tree. Most proficient gliders are also able to cover a substantial

amount of horizontal distance during the descent, order(s) of magnitude greater than their body length. The animal generates aerodynamic forces by combining surface area and speed, using its body to increase its surface area, and trading potential energy to acquire kinetic energy or speed. Together, this helps the animal generate lift and drag force which help partially counter the animal's body weight in air to slow its descent and cover horizontal distance.

So how does an animal execute a glide? In terrestrial vertebrates, a glide can be broken down into at least four parts. The first is the takeoff jump where the animal pushes itself from an arboreal substrate using its hindlimbs or posterior part of the body to gain initial speed. Once airborne, the animal deploys its wing membrane (patagium) or modifies its body shape to increase the surface area relative to the direction of motion to generate aerodynamic forces to slow its descent. During this morphological transition, the animal experiences a ballistic dive phase where the motion is dominated more by the animal's body weight rather than the aerodynamic forces produced by its airfoil. Once the animal gains sufficient flight speed, the glide trajectory transitions into a shallowing glide phase where the animal increases the horizontal distance traveled compared to the vertical height lost. Finally comes the landing maneuver in which the glider expends part of its kinetic energy in the form of drag to slow its descent and potentially gain some altitude. Previous studies have also noted a fifth part in glide execution which occurs after the shallowing phase and before the landing maneuver - the equilibrium glide phase. In this phase, the animal no longer accelerates in any direction, i.e., flight speed and direction are unchanging and the upward aerodynamic forces from the combination of lift and drag acting on the animal perfectly balance its weight. However, to achieve such a state, the animal would require a sufficiently long obstacle-free glide which is rarely possible in its natural habitat.

1.1.2 Aerodynamics

The aerodynamics of gliding is deceptively simple, and early efforts at understanding the aerodynamic characteristics and performance of gliding animals focused on so-called equilibrium gliding, the point at which a gliding animal or object no longer accelerates in any direction. While many descent angles can produce equilibrium gliding, the minimum descent angle is given by the maximum of the ratio of the coefficient of lift and coefficient of drag, non-dimensional numbers that quantify how effective the airfoil is at producing these forces and, when combined with air density, flight speed, and wing area, can be used to calculate the aerodynamic forces themselves. An equilibrium glide at the minimum descent angle provides the most horizontal transport for the least loss in height and therefore presents an attractive single number for comparing glide performance of animals and human-designed crafts ranging from flying snakes to sailplanes. However, a complicating factor is that there is little evidence that gliding animals commonly achieve equilibrium gliding. Instead, as described above, real-world glides contain several separate phases, none of which is necessarily equilibrium gliding. How various gliding animals combine these glide components while also maintaining aerial stability, maneuvering to avoid obstacles, selecting landing sites, and possibly tuning their aerodynamics to both travel the necessary distance to landing while also arriving with little remaining kinetic energy is unknown, especially in the context of a natural environment.

Figure 1.1 *Draco* in mid-glide phase. Note how the compliant wing results in a slightly convex curvature.

Biological airfoils also tend to differ in their mechanical and aerodynamic properties from their human-engineered counterparts. Human engineered airfoils are mostly rigid and have a fixed geometry, whereas biological airfoils are composed of compliant control surfaces that can be rapidly modified during the glide. For example, mammalian gliders and flying lizards have specialized wing membrane (patagium) which can be actively oriented to achieve different angles of attack (wing position with respect to relative motion) like a fixed-wing aircraft but can also actively change shape to operate at various degrees of camber (the curvature of the wing membrane) (Figure 1.1). The angle of attack is one of the simplest ways to increase overall lift

force in traditional airfoils, however, when traditional airfoils reach or cross a certain angle of attack (a typical value is 15°), there is airflow separation between the top and bottom surface of the airfoil leading to a drastic drop in lift and increase in drag, technically referred to as the onset of stall [28]. Gliding animals are also known to change their angle of attack to increase lift production and have to deal with extremely high angles of attack, especially during the landing maneuver (upwards of 40°) [19]. Surprisingly, gliding animals have not been observed to reach stall during the glide, a situation that can have dire consequences for the glider. It is hypothesized and shown by modeling [29] that gliding animals can use their compliant wings to reach higher lift and drag forces at relatively low angles of attack compared to similarly shaped rigid wings. Furthermore, they might use wing camber to delay the onset of stall at high angles of attack, allowing the animal to maintain sufficient lift while landing. Though such hypotheses are plausible, the implications of a compliant wing on the gliding performance of animals is unknown and requires a detailed experimental study of the aerodynamics of the complete glide trajectory of the animal.

1.1.3 Flying lizards of the genus Draco

The genus *Draco* of the family Agamidae is comprised of lizards capable of gliding flight. These lizards are often referred to as flying lizards, gliding lizards, or flying dragons, and are common in parts of Southeast Asia and southwest India [20]. The genus *Draco* is composed of at least 45 species with body mass varying between 3 gm to upwards of 22 gm and with a snout vent length ranging from 6 cm to 14 cm [30]. They are strictly arboreal except when females climb down to lay eggs on the ground [10]. Gliding flight is their primary mode of locomotion, used to move through their natural habitat consisting of mostly dipterocarp-dominated forests [20]. To glide, *Draco* use a unique primary wing design consisting of a

patagium supported by a set of 5-7 elongated ribs which are rotated laterally outwards to stretch the patagium and form an inverted delta wing.

Draco, though cryptic, can be recognized by the combination of a slender body with a patagium, throat fan (or dewlap) and a tail 1.5 to 2 times the snout vent length. The patagium remains tucked along the longitudinal axis when the *Draco* is on the tree and is occasionally partially opened by males and females during mating displays. In most *Draco* species there is female-biased dimorphism with females larger than males, especially in head and body width. Distinguishing the sexes is rather convenient, with male dewlap being almost two to three times longer than that of the females (Figure 1.2). Recently, it has been shown that male dewlaps are relatively translucent compared to that of females, making them more conspicuous in the day [31]. Sreekar et al. (2013) also showed that the number of blotches on the ventral surface of the patagium was significantly higher in females compared to males [32].

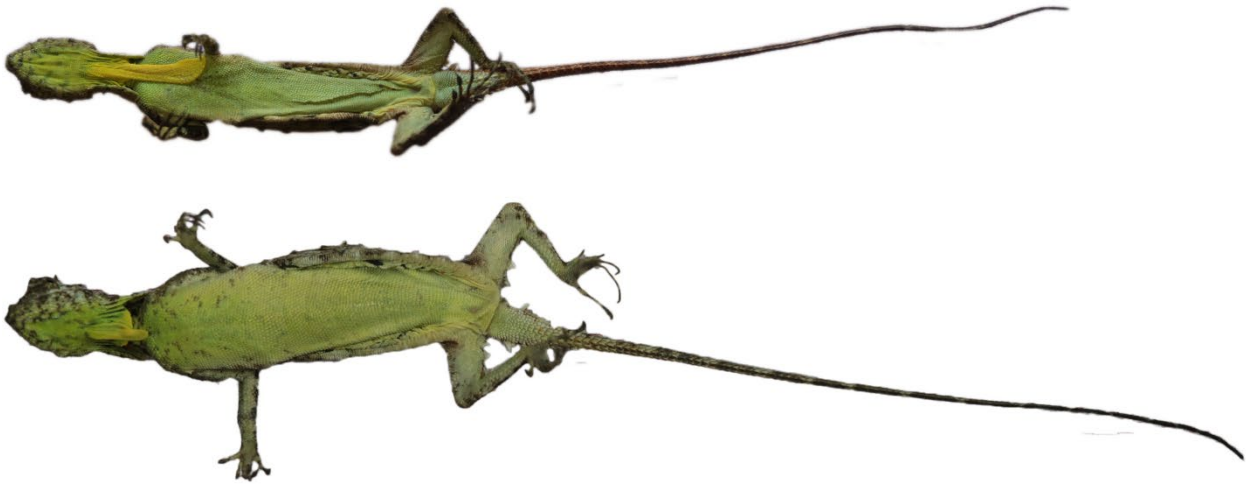

Figure 1.2 Ventral view of adult male (top panel) and female (bottom panel) lizard of the species *Draco dussumieri.* Males have significantly longer dewlaps; females are larger in body size.

1.1.4 Draco gliding apparatus

Unlike mammalian gliders, *Draco* possess a unique primary wing capable of active control during glide and unconstrained limb movement while climbing and during takeoff and landing. The primary wing consists of a patagium supported by elongated thoracic ribs and a specialized musculature [33–35]. The opening and closing of the patagium are controlled by the combination of highly modified external and internal intercostal muscles, external oblique muscles, and a system of ligaments spanning the individual elongated thoracic ribs [20]. The muscle actuation to rotate the ribs laterally is greatest for the first two anterior ribs. The large actuation to pull the first rib forward is achieved by the iliocostalis muscle extending far anteriorly to its insertion on the anterior ribs and vertebrae. The large length of the muscle is necessary to allow a degree of contraction sufficient to rotate the ribs far out to completely stretch the patagium [33]. The anteriorly located second rib has a similar but less extensive development of the intercostal muscle. The remaining ribs are pulled anteriorly more by the ligaments interconnecting the ribs and less by the musculature to complete the anterior extension of the ribs and consequently stretching the patagium open. The tension in the musculature is modulated to partially open the wings during mating displays and to completely open to glide. Just before touchdown from a glide, the tension on the ribs (and thus the patagium) is released by relaxing the strong iliocostalis muscles attached to the first two sets of ribs folding the wings back longitudinally [33]. Interestingly, due to the specialization of the intercostal muscle in *Draco* to deploy the primary wing, which otherwise is used for lung ventilation in other lizards, *Draco* rely on the pectoralis muscle to perform lung ventilation [34].

Finally, it should be noted that the patagium alone is not responsible for making *Draco* a proficient glider. Various other body parts of the *Draco*, including the head, lappets, and body

width along with a mostly flat body, are significant contributors, at least in increasing surface area of the overall gliding apparatus employed by *Draco* to glide. However, apart from an increase in surface area, it remains to be investigated if the other body parts have specific contributions towards controlling and/or stabilizing the glide trajectory. For example, it has been hypothesized that the lappets act as additional lift generating surfaces along with enhancing stability, much like canards on some fixed-wing aircraft [36]. Rapid tail movements during takeoff can be thought of as a mechanism to induce body roll without apparent spine bending as seen in flat-tailed house geckos [37]. Lastly, the forelimbs of the *Draco* might act as leading-edge slots to delay stall at high angles of attack during landing.

1.1.5 Behavior

Draco behavior can be categorized into foraging, evading predators, mate seeking, and territoriality. Foraging and evading predators are present throughout the life cycle of the individual whereas mate seeking, and territoriality are characteristic of the mating season. The mating season is likely species specific but has been poorly reported in the literature. Mating season in *Draco dussumieri* spans the month of February through May [10,38], and the season for *Draco v. sumatranus* has been previously reported to include at least December and January [9].

Foraging. All *Draco* primarily feed on ants [8,39,40] (Figure 1.3). However, John (1962) did report that a gravid female *Draco dussumieri* that was caught and placed in a cage to study egg-laying and hatching began to feed on small grasshoppers and other insects after refusing food for the first two days [41]. Furthermore, the availability of ants in the natural habitat has been reported to be in plenty and is not considered a defended resource, at least in *Draco v. sumatranus* [8].

Figure 1.3 Feeding and sleeping behavior in *Draco*. Left panel shows a female *Draco dussumieri* feeding on an ant on the areca nut tree at the field site. Right panel shows a male *Draco* sleeping on the tree.

Territoriality. Draco are known to actively defend their territories to get sole access to receptive females and increase their mating probability (Figure 1.4). Territorial displays include opening and folding the dewlap more frequently than normal, and at times extending and holding the dewlap such that it extends past the anterior tip along with partially opening the patagium ([9] and personal observation). Frequent territorial interactions also included males chasing each other up a tree, with the chase transitioning into multiple quick glides from one tree to the other (from personal observation and video footage).

Figure 1.4 Territoriality in males. Top panel sequence 1 to 4 shows a territorial fight between two male *Draco dussumieri*. In 1 the resident male (left) approaches the non-resident male (right), followed by biting the left lappet of the non-resident male in 2. In 3, both *Draco* lose balance and tumble (4), ultimately maneuvering and landing back lower on the same tree. The lower panel shows a separate *Draco* territorial fight where the resident male chased the non-resident male resulting in the resident male biting the left hindlimb of the non-resident mid-glide and both falling down to the ground. Both males were on the ground for more than 20 minutes without the resident male letting go of the other male.

Mating. Draco mating behavior has been described in [8–10], however, the most recent study was conducted by Mori et al. in 1994. Courtship behavior begins with the male gliding to the tree with a female. The male generally lands lower with respect to the female position on the tree and approaches the female from below. Once the male is relatively close to the female, the male lifts its body anteriorly, holding the dewlap at complete extension and with its stiff tail lifted circles around the female using a characteristic jerky gait. John (1967) had observed circling in the

clockwise direction in *Draco dussumieri* [10]; however, we did not see a preference for circling direction in the same species (Figure 1.5 shows circling in the anti-clockwise direction). The female partially extends its patagium during the courtship ritual. Mori et al. (1994) ascribed female wing opening to rejection and the male stopping its display [9]; however, we saw the male continuing its ritual even after the female partially extended its patagium. We did record male rejection where the female used its tail to push the male away when the male attempted to touch the pelvic region of the female (personal observation and video footage). At this point, the male glided away from the female, possibly in search of another female or to continue courtship at a later point.

Evading predators. Until now, there has not been documentation of predatory evasion using gliding in *Draco*. Snakes and birds are thought to be the main predators of *Draco*. On the contrary, high mortality rates have been attributed to females coming to the ground to oviposit and in males that exhibit territoriality [30]. John (1962) had noted *Draco dussumieri* to be relatively helpless on the ground in terms of their movement and agility [41]. Overall, previous observations suggest that *Draco* coloration and cryptic nature is the main way by which they evade predators.

Figure 1.5 A sequential shot of the mating behavior in *Draco dussumieri*. The male *Draco* lands on the tree with the female and approaches the female from below. The female partially opens her patagium in response to the male. The male keeps its dewlap extended and stiffens its tail circling around the female in sequences 2 to 6. The male can continue circling the female based on if the female is receptive or not.

1.1.6 Draco as a system to study gliding behavior

Studies in gliding behavior, like most locomotory behavior, make a tradeoff between the behavior and the resolution at which it can be captured. That is, locomotory behavior takes place in space, and is often constrained based on data collection techniques, typically either on-body sensors or motion capture systems. Aerial behavior deals with movement in three dimensions, further constraining the scope of the study. For example, bird migration has been studied using GPS data sampled at regular intervals in time, whereas bird takeoff has been investigated at high spatial and temporal resolution in a lab setting. Both present drastically different resolutions of data acquisition answering more specific to broader questions in locomotory behavior. Gliding behavior presents a more approachable case where the glide distance is limited by the height of takeoff, making it possible to collect data for the complete glide instead of parts of it. However, most gliding animals that have been studied, including gliding squirrels, sugar gliders, and colugos, are nocturnal making it difficult to collect data in the animal's natural habitat. Instead, these studies typically employ laboratory experiments to investigate certain aspects of the gliding behavior in detail. For example, takeoff and landing kinematics during a glide have been looked at independently and independent of the overall glide trajectory. Furthermore, such studies cannot link the behavioral context to the glide outcome. Many unanswered questions in gliding locomotion, including gliding performance in the wild, the link between behavior and performance, and variation in gliding behavior based on the intrinsic attributes of an individual like body mass and sex require high quality data collection in the animal's natural surroundings.

Following Krogh's principle, *Draco* fulfill the criteria of providing a system that can be used to answer some or all of the questions mentioned above. First, unlike mammalian gliders, *Draco* are diurnal, making it convenient to observe their behavior and use regular portable light

camera systems to record gliding locomotion. Second, *Draco* have distinct behaviors between males and females, making it possible to test hypotheses based on individuals rather than the entire species. Third, anthropogenic changes in the natural habitat over the past century have led to *Draco* inhabiting areca nut plantations making it possible to capture a wide variety of glide behaviors and intra-species interaction in the resident *Draco* population. Lastly, and potentially the most important aspect, *Draco* glide frequently during the day, especially males during the mating season, providing ample opportunities to collect high-quality data.

1.2 Camera methods

Throughout this study, we used field-portable, battery-powered, high-speed cameras to record flight behavior and reconstruct the 3D trajectory and kinematics of gliding *Draco* lizards. Cameras and 3D videography have a long history in the study of comparative biomechanics, in large part because they offer a non-invasive means for quantitative measurement of animal movement. Other methods such as on-animal inertial measurement units have also been applied to the study of locomotion and flight but were not considered appropriate here since the smallest units available at the time of this study were approximately 1 gram in mass, a substantial fraction of the 6 to 8 gram body mass of the lizards. Inertial measurement units also provide only a single point measurement and require the capture of the animal and recovery of the measurement unit before any data can be collected. In contrast, camera measurements can collect data from animals that are never handled by the researchers, can record multiple points on the body to measure pose and configuration, and also record other aspects of the context of the behavior such as the presence of other animal(s), location of nearby trees, and many other relevant factors in understanding behavior. For these reasons, cameras have been used as the primary measurement approach in most studies of gliding biomechanics. However, the application of multi-camera

videography and 3D kinematic reconstruction data in the field is challenging for many reasons. Most field sites lack access to power sources other than batteries (but see Bahlman et al. [23]), placing restrictions on the power available for cameras and making use of high-speed cameras designed for indoor, laboratory use impossible. However, recent and rapid increases in the capabilities of small, low power camera sensors driven by intensive efforts to improve the photography capabilities of mobile phones also resulted in the development of "action cameras" such as the GoPro series (The GoPro Inc.) which pair a small but high-quality camera sensor with a fixed lens, a battery, and hardware package designed to survive mistreatment and remain usable in outdoor environments. These cameras were ideal in many respects for recording *Draco* glides in the field, but also bring with them several challenges inherent in their design for consumer rather than laboratory use. These include challenges with inter-camera synchronization, lens distortion, and thermal management during recording stints.

The mathematics underlying reconstruction of a 3D location from the information in two or more 2D images requires that the 2D images be captured at the same instant in time. For this reason, cameras designed for laboratory use typically include specialized circuits and software for synchronizing their shutters. GoPros and other consumer cameras lack such features. Instead, we used a combination of audio tones and visual cues to identify the closest frames among a set of cameras, leaving a temporal uncertainty of ± 0.5 frames among the cameras. This degree of uncertainty increases the uncertainty in the 3D measurements, and in cases where this increase was detrimental to the analysis, we linearly interpolated the 2D time-series recorded from each camera to a virtual temporal offset of 0 frames before performing the 3D reconstruction step. GoPros and many other consumer video cameras also do not scan the entire imaging sensor at once. Instead, the top row of pixels is scanned before the bottom row, sometimes in a smooth

row-by-row linear fashion and sometimes in blocks of several rows together, depending on camera settings. The error associated with this is small since the scan requires much less than the duration of one frame but cannot be mathematically removed.

GoPro cameras and similar action cameras use a wide-angle lens that exhibits non-linear distortion. Unless accounted for, this distortion makes 3D reconstruction impossible. While more recent GoPro cameras have a hardware option to remove distortion, this also crops the view and partially defeats the point of using a wide-angle lens in the first place, which is to record a larger spatial volume. The GoPro Hero4 Black cameras that we used did not have this option, and instead we used the fisheye camera lens distortion approach described in [42,43] to model and remove the distortion.

Although designed for use outdoors, GoPro cameras turn out to overheat when run for more than a few minutes in temperatures of around 35° C or more without active cooling, especially when recording at relatively high video frame rate and resolution. Some examples of frame rate and resolution combination include 240 frames per second at 480p resolution and 120 frames per second at 1440p resolution. This random shutdown of cameras during recording was unexpected, though perhaps obvious in hindsight, but was accommodated by either designing recording methods that did not require the cameras to be left on for more than a few minutes or setting up active cooling with external, battery powered fans (see Chapter 2).

1.2.1 Camera calibration

Reconstructing 3D coordinates from multiple 2D camera images requires knowing the lens and sensor properties of the camera, information measurable under controlled circumstances in the lab, and knowing the relative position and orientation of the cameras in their field location. Determining this information is referred to as camera calibration [44]. We used the software

provided with the fisheye lens distortion model papers and the Argus suite of camera calibration software developed in the Hedrick lab to measure the lens and sensor properties [45]. We measured the relative position and orientation of the cameras using a structure-from-motion approach, which is to say the "structure" of the scene, or the camera positions and orientations, was recovered by tracking the motion of an object through the scene. The necessary information for such an approach is a large number of corresponding images where the pixel location of the object is known for all the cameras being calibrated. Depending on the distribution of known locations and the number of cameras anywhere from approximately 50 to several thousand corresponding pixel locations is required. We also enhanced this approach by simultaneously tracking two ends of a moving rod, adding the additional mathematical constraint that the distance between the two ends of the rod should remain constant throughout the scene. This information served as input to the open source sparse bundle adjustment library [46], so named according to the algorithm used to solve the calibration problem, using a MATLAB layer developed for community use by the Hedrick lab [47]. In the 2015 field season, we used these techniques to calibrate a set of three GoPro Hero4 Black cameras that were uniquely positioned for each naturally occurring glide event. In the 2017 field season, we used seven Hero4 Black cameras, positioned at mostly fixed locations in a flight arena constructed at the field site.

1.2.2 Scene alignment

Following camera calibration, it is possible to compute a 3D location from 2D observations in two or more cameras. However, the resulting 3D location, i.e. an [x,y,z] coordinate is not necessarily in a useful reference frame. Thus, we took a final calibration step of aligning the Z axis to gravity. In 2015, we used a tree trunk to identify this direction and in 2017 we made an alignment recording by tossing a ball into the air in the scene and computed the

second derivative of its trajectory, revealing the direction of gravitational acceleration and providing a measure of its magnitude to be compared to the known value of 9.81 ms^{-2}.

1.2.3 Kinematic data acquisition

Acquiring 3D kinematic data from video recordings means tracking the position of the object or feature of interest through the video sequence. We had hoped to use Deep Learning methods to train a neural network to identify the features we planned to track, thereby automating this otherwise tedious step. Unfortunately, the varied nature of the jungle forest scenes coupled with the small size of the *Draco* and its changing appearance with position and orientation with respect to the camera prevented current Deep Learning methods from producing sufficiently high-quality outputs. Instead, the video data were processed manually using a custom MATLAB software package developed in the Hedrick lab [48]. This package uses the camera calibration information, expressed as the epipolar lines, to aid in the data acquisition process. Marking a feature or location in one video defines a ray that passes through the camera sensor and the 3D location of the feature. This ray can then be visualized in other cameras that are part of the calibrated set, and this visualization is the epipolar line. For well-calibrated cameras, the epipolar line will pass through the feature being tracked, helping the user locate the feature in the other videos (Figure 1.6).

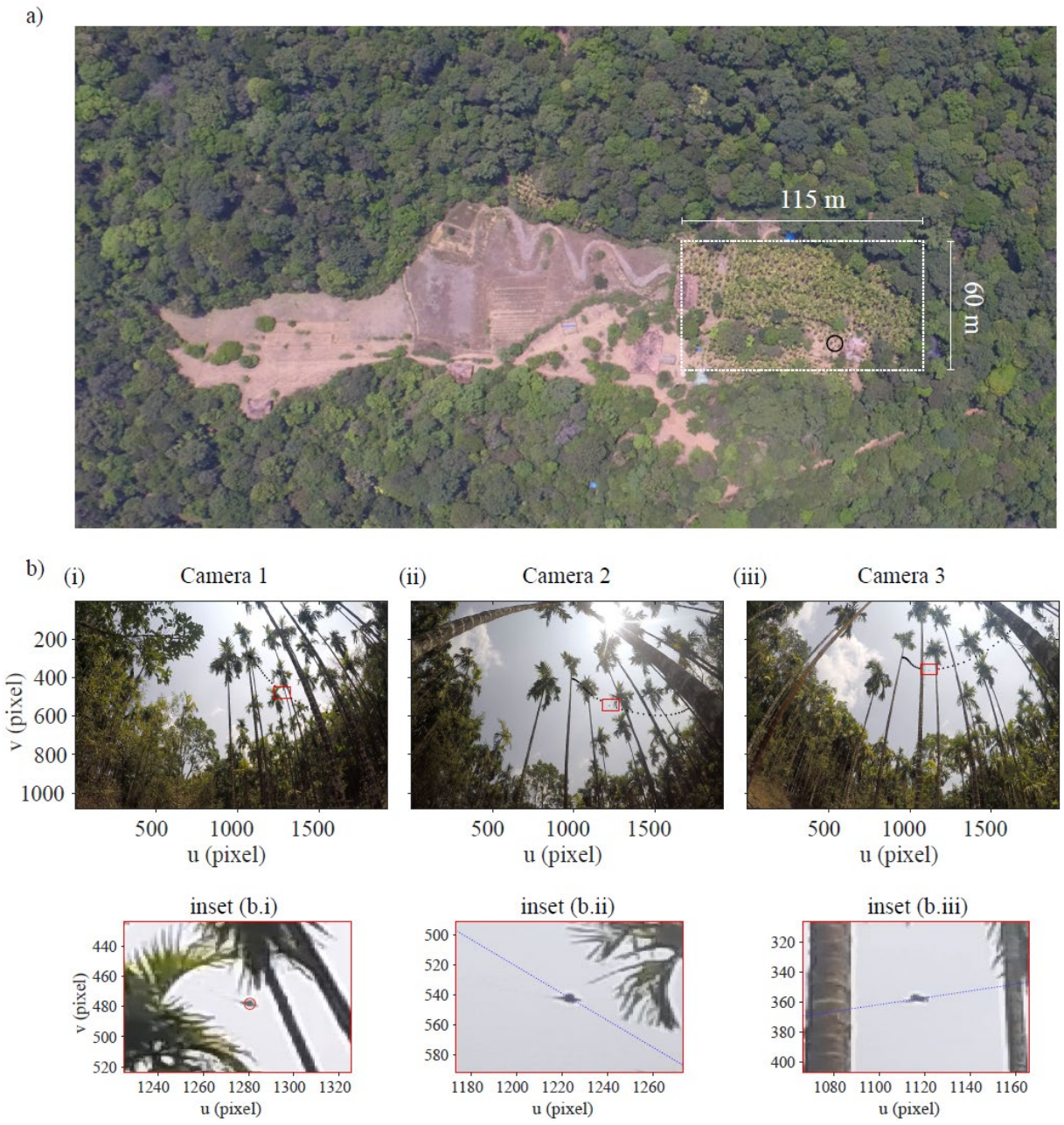

Figure 1.6 3D tracking of natural gliding behavior. (a) Overhead view of the Agumbe Rainforest Research Station (ARRS) showing the field site highlighted by the rectangular white box. The black circle (○) represents the location of the cameras for the recorded glide shown in panel (b) and insets. (b) Panel showing a snapshot of the lizard mid-glide across the three camera views. The dotted black line represents the complete glide track and the red rectangle shows the location of the lizard. *Insets.* Zoomed in views of the snapshots in panel b after scene calibration. (b.i) The lizard marked for 3D tracking in camera 1. (b.ii and b.iii) The marked lizard point in camera 1 defines the epipolar line shown in blue in the insets for cameras 2 and 3; this line is the ray from the camera 1 sensor passing through the clicked location as seen in cameras 2 and 3. A point marked on this ray in either camera 2 or 3 will have zero reconstruction error. However,

only one point (the lizard) will create a 3D coordinate with a 2D projection that falls on the lizard in all 3 camera views. After clicking the lizard in camera views 2 and 3, we get a reprojection error of ~0.30 pixels i.e., the difference between the marked camera points and the computed 3D point reprojected onto each 2D camera view.

1.2.4 Kinematic data smoothing

In a set of calibrated cameras, a 3D location can be thought of as the intersection of two or more epipolar lines. However, due to calibration uncertainties, the discretization of images into pixels, and other factors, the epipolar lines never precisely intersect. Instead, the 3D location is computed as the location that minimizes the distance to all the epipolar lines. The distance to the lines is a measure of the digitization error or uncertainty. We used this uncertainty to smooth the resulting time series of 3D position data. We first used a resampling approach to convert the pixel uncertainty given by the 3D reconstruction operation to uncertainty in the position of the [x,y,z] coordinate, providing a 95% confidence interval for the location of the 3D point. We then used a quintic smoothing spline to find the smoothest path through the time series that remained within the 95% confidence interval range for each point. In this case smoothest means the smallest value for the 3rd derivative of position with respect to time. Thus, the spline smoothing approach also provided the means to compute mutually consistent smoothed first and second derivatives of position with respect to time (i.e., velocity and acceleration) by differentiating the spline polynomial. These smoothed position, velocity and acceleration time-series were used as the basis for further kinematic analysis.

1.3 Field site

The field site was an abandoned areca nut plantation located within the premises of the Agumbe Rainforest Research Station (ARRS) in Karnataka, India (13°31’04” N, 75°05’18” E). The research station is located at an elevation of approximately 650 m above sea level within the central Western Ghats and has a distinctive tract of tropical moist evergreen forest. The areca nut

plantation was enclosed by open habitat on the east, and a mix of open habitat and tropical rainforest on the other sides. The site contained ~912 areca nut trees (~13 trees per 100 m^2) mixed with scattered local flora. The trees were ~10 cm to ~ 20 cm in diameter, ~5 m to ~23 m tall and had an inter-tree distance of ~1.5 m to ~8 m, providing areas of varying tree clutter. A population of flying lizards (*Draco dussumieri*) inhabited the plantation during the breeding season (February - May). Previous observations from the ARRS personnel at the field site described a sharp increase in the number of *Draco* sightings during the mating season. Potential reasons could include mating and territorial displays making lizards more conspicuous, and an untested hypothesis that the areca nut plantation provides relatively open spaces compared to dense surrounding forests, allowing male *Draco* to effectively display to attract females.

Overall, the flight arena provided a naturally constrained spatial setting with a consistent *Draco* population of male and female individuals to study the gliding behavior and biomechanics of flying lizards.

Ethics statement. The ARRS campus is privately owned and does not fall within a protected area, exempting us from requiring government permits. The study was conducted with permission from the local ARRS authorities and as per UNC Institutional Animal Care and Use Committee guidelines.

1.4 Concluding remarks

In the following chapters, I will describe detailed gliding aerodynamics in the flying lizard *Draco dussumieri*, behavior and body size effects on gliding performance, and how glides are executed in the animal's natural habitat.

Chapter 2 will describe in detail the aerodynamic performance envelope used by *Draco* while gliding. It will focus on the aerodynamic forces generated during the complete glide and the physical mechanisms by which they are produced. Chapter 3 will extend the performance analysis to an individual specific level and show how variation in body size and gliding motivations/behavior can manifest in the overall gliding performance. In Chapter 4, I will describe how *Draco* actually implement their previously described gliding ability (Chapter 2 and 3) in their natural habitat, focusing on the sensory and environmental context. Together, these chapters aim to provide a biologically relevant holistic understanding of gliding in *Draco* with applicability to other gliding taxa.

REFERENCES

1. Socha JJ, Jafari F, Munk Y, Byrnes G. 2014 How animals glide: From trajectory to morphology. *Can. J. Zool.* **93**, 901–924. (doi:10.1139/cjz-2014-0013)

2. O'Dor R, Stewart J, Gilly W, Payne J, Borges TC, Thys T. 2013 Squid rocket science: How squid launch into air. *Deep. Res. Part II Top. Stud. Oceanogr.* **95**, 113–118. (doi:10.1016/j.dsr2.2012.07.002)

3. Yanoviak SP, Dudley R, Kaspari M. 2005 Directed aerial descent in canopy ants. *Nature* **433**, 624–626. (doi:10.1038/nature03254)

4. Dudley R, Byrnes G, Yanoviak SP, Borrell B, Brown RM, McGuire JA. 2007 Gliding and the functional origins of flight: Biomechanical novelty or necessity? *Annu. Rev. Ecol. Evol. Syst.* **38**, 179–201. (doi:10.1146/annurev.ecolsys.37.091305.110014)

5. Alexander DE. 2015 *On the Wing: Insects, Pterosaurs, Birds, Bats and the Evolution of Animal Flight* .

6. Norberg UM. 1985 Evolution of vertebrate flight: an aerodynamic model for the transition from gliding to active flight. *Am. Nat.* **126**. (doi:10.1086/284419)

7. Chatterjee S, Templin RJ. 2007 Biplane wing planform and flight performance of the feathered dinosaur Microraptor gui. *Proc. Natl. Acad. Sci.* **104**, 1576–1580. (doi:10.1073/PNAS.0609975104)

8. Mori A, Hikida T. 1993 Natural History Observations of the Flying Lizard, *Draco Volans Sumatranus* (Agamidae, Squamata) From Sarawak, Malaysia. *Raffles Bull. Zool.* **41**, 83–94.

9. Mori A, Hikida T. 1994 Field observations on the social behavior of the flying lizard, Draco volans sumatranus, in Borneo. *Copeia* , 124–130. (doi:10.2307/1446678)

10. K.O. John. 1967 *Observations on the mating behaviour and copulation in Draco dussumieri Dum. & Bib. (Reptilia: Sauria)*. See https://www.biodiversitylibrary.org/item/186228.

11. Dudley R, DeVries P. 1990 Tropical Rain Forest Structure and the Geographical Distribution of Gliding Vertebrates. *Biotropica* **22**, 432. (doi:10.2307/2388564)

12. Klomp DA, Stuart-Fox D, Das I, Ord TJ. 2017 Gliding lizards use the position of the sun to enhance social display. *Biol. Lett.* **13**, 20160979. (doi:10.1098/rsbl.2016.0979)

13. Essner RL. 2002 Three-dimensional launch kinematics in leaping, parachuting and gliding squirrels. *J. Exp. Biol.* **205**, 2469–2477.

14. Bishop KL, Brim-Deforest W. 2008 Kinematics of turning maneuvers in the southern flying squirrel, Glaucomys volans. *J. Exp. Zool. Part A Ecol. Genet. Physiol.* **309**, 225–242. (doi:10.1002/jez.447)

15. Bishop KL. 2006 The relationship between 3-D kinematics and gliding performance in the southern flying squirrel, Glaucomys volans. *J. Exp. Biol.* **209**, 689–701.

(doi:10.1242/jeb.02062)

16. Holden D, Socha JJ, Cardwell ND, Vlachos PP. 2014 Aerodynamics of the flying snake Chrysopelea paradisi: How a bluff body cross-sectional shape contributes to gliding performance. *J. Exp. Biol.* **217**, 382–394. (doi:10.1242/jeb.090902)

17. Suzuki K, Asari Y, Yanagawa H. 2012 Gliding locomotion of Siberian flying squirrels in low-canopy forests: The role of energy-inefficient short-distance glides. *Acta Theriol. (Warsz).* **57**, 131–135. (doi:10.1007/s13364-011-0060-y)

18. Paskins KE, Bowyer A, Megill WM, Scheibe JS. 2007 Take-off and landing forces and the evolution of controlled gliding in northern flying squirrels Glaucomys sabrinus. *J. Exp. Biol.* **210**, 1413–1423. (doi:10.1242/jeb.02747)

19. Bishop KL. 2007 Aerodynamic force generation, performance and control of body orientation during gliding in sugar gliders (Petaurus breviceps). *J. Exp. Biol.* **210**, 2593–2606. (doi:10.1242/jeb.002071)

20. McGuire JA, Dudley R. 2011 The biology of gliding in flying lizards (genus draco) and their fossil and extant analogs. *Integr. Comp. Biol.* **51**, 983–990. (doi:10.1093/icb/icr090)

21. Byrnes G, Libby T, Lim NTL, Spence AJ. 2011 Gliding saves time but not energy in Malayan colugos. *J. Exp. Biol.* **214**, 2690–2696. (doi:10.1242/jeb.052993)

22. Socha JJ, O'Dempsey T, LaBarbera M. 2005 A 3-D kinematic analysis of gliding in a flying snake, Chrysopelea paradisi. *J. Exp. Biol.* **208**, 1817–1833. (doi:10.1242/jeb.01579)

23. Bahlman JW, Swartz SM, Riskin DK, Breuer KS. 2013 Glide performance and aerodynamics of non-equilibrium glides in northern flying squirrels (Glaucomys sabrinus). *J. R. Soc. Interface* **10**. (doi:10.1098/rsif.2012.0794)

24. Byrnes G, Lim NTL, Spence AJ. 2008 Take-off and landing kinetics of a free-ranging gliding mammal, the Malayan colugo (Galeopterus variegatus). *Proc. R. Soc. B Biol. Sci.* **275**, 1007–1013. (doi:10.1098/rspb.2007.1684)

25. Bishop KL. 2008 The evolution of flight in bats: Narrowing the field of plausible hypotheses. *Q. Rev. Biol.* **83**, 153–169. (doi:10.1086/587825)

26. Yeaton IJ, Ross SD, Baumgardner GA, Socha JJ. 2020 Undulation enables gliding in flying snakes. *Nat. Phys.* **16**, 974–982. (doi:10.1038/s41567-020-0935-4)

27. Willis D, Bahlman J, Breuer K, Swartz S. 2011 Energetically optimal short-range gliding trajectories for gliding animals. *AIAA J.* **49**, 2650–2657. (doi:10.2514/1.J051070)

28. Hull DG. 2007 *Fundamentals of airplane flight mechanics*. (doi:10.1007/978-3-540-46573-7)

29. Song A, Tian X, Israeli E, Galvao R, Bishop K, Swartz S, Breuer K. 2008 Aeromechanics of membrane wings with implications for animal flight. *AIAA J.* **46**, 2096–2106. (doi:10.2514/1.36694)

30. McGuire JA. 1998 Phylogenetic Systematics, Scaling Relationships, and the Evolution of Gliding Performance in Flying Lizards (Genus Draco). *Fac. Grad. Sch. Univ. Texas*

Austin

31. Klomp DA, Stuart-Fox D, Das I, Ord TJ. 2017 Gliding lizards use the position of the sun to enhance social display. *Biol. Lett.* **13**. (doi:10.1098/rsbl.2016.0979)

32. Sreekar R, Purushotham CB, Saini K, Rao SN, Pelletier S, Chaplod S. 2013 Photographic Capture-Recapture Sampling for Assessing Populations of the Indian Gliding Lizard Draco dussumieri. *PLoS One* **8**. (doi:10.1371/journal.pone.0055935)

33. Colbert EH. 1967 Adaptations for gliding in the lizard Draco. *Amer. Mus. Novitat.* **2283**, 1–20.

34. John KO. 1971 Caudal Musculature of the South Indian Flying Lizard Draco dussumieri Dum. and Bibr. *Acta Zool.* **52**, 249–255. (doi:10.1111/j.1463-6395.1971.tb00561.x)

35. Russell AP, Dijkstra LD. 2001 Patagial morphology of Draco volans (Reptilia: Agamidae) and the origin of glissant locomotion in flying dragons. *J. Zool.* **253**, 457–471. (doi:10.1017/S0952836901000425)

36. McGuire JA, Dudley R. 2011 The biology of gliding in flying lizards (genus draco) and their fossil and extant analogs. *Integr. Comp. Biol.* **51**, 983–990. (doi:10.1093/icb/icr090)

37. Jusufi A, Goldman DI, Revzen S, Full RJ. 2008 Active tails enhance arboreal acrobatics in geckos. *Proc. Natl. Acad. Sci. U. S. A.* **105**, 4215–4219. (doi:10.1073/pnas.0711944105)

38. Khandelwal PC, Hedrick TL. 2020 How biomechanics, path planning and sensing enable gliding flight in a natural environment. *Proc. R. Soc. B Biol. Sci.* **287**, 20192888. (doi:10.1098/rspb.2019.2888)

39. Inger RF. 2011 *Morphological and ecological variation in the flying lizards (Genus Draco) / Robert F. Inger.* (doi:10.5962/bhl.title.3131)

40. Reyes AY. 1968 Food habits of Draco volans Linnaeus. *Silliman J.* **15**, 353–356.

41. John KO. 1962 Notes on The. Bionomics of the Flying Lizard, Draco Dussumieri Dum. & Bib. *J. Bombay Nat. Hist. Soc.* **59**, 298–301.

42. Scaramuzza D, Martinelli A, Siegwart R. 2006 A toolbox for easily calibrating omnidirectional cameras. In *IEEE International Conference on Intelligent Robots and Systems*, pp. 5695–5701. (doi:10.1109/IROS.2006.282372)

43. Urban S, Leitloff J, Hinz S. 2015 Improved wide-angle, fisheye and omnidirectional camera calibration. *ISPRS J. Photogramm. Remote Sens.* **108**, 72–79. (doi:10.1016/j.isprsjprs.2015.06.005)

44. Hartley R, Zisserman A. 2004 *Multiple View Geometry in Computer Vision*. Cambridge University Press. (doi:10.1017/cbo9780511811685)

45. Jackson BE, Evangelista DJ, Ray DD, Hedrick TL. 2016 3D for the people: Multi-camera motion capture in the field with consumer-grade cameras and open source software. *Biol. Open* **5**, 1334–1342. (doi:10.1242/bio.018713)

46. Lourakis MIA, Argyros AA. 2009 SBA: A software package for generic sparse bundle

adjustment. *ACM Trans. Math. Softw.* **36**, 1–30. (doi:10.1145/1486525.1486527)

47. Theriault DH, Fuller NW, Jackson BE, Bluhm E, Evangelista D, Wu Z, Betke M, Hedrick TL. 2014 A protocol and calibration method for accurate multi-camera field videography. *J. Exp. Biol.* **217**, 1843–1848. (doi:10.1242/jeb.100529)

48. Hedrick TL. 2008 Software techniques for two- and three-dimensional kinematic measurements of biological and biomimetic systems. *Bioinspiration and Biomimetics* **3**, 034001. (doi:10.1088/1748-3182/3/3/034001)

CHAPTER 2: AERODYNAMICS OF GLIDING

2.1 Introduction

Gliding terrestrial locomotion is often considered a relatively simple form of aerial motion [1]. Unlike flapping flyers, gliding animals are incapable of muscle-powered flight and consequently cannot stay aloft for extended durations. They also use a mostly static airfoil with fewer degrees of freedom than the flapping wings of birds and bats. The airfoil is deployed after jumping and generates aerodynamic forces as the glider trades its height above the ground (i.e., potential energy) for kinetic energy and power to overcome drag. During the glide, the magnitude and direction of aerodynamic forces vary as the animal gains or loses speed but also may be actively modulated by the animal to control its trajectory and reach its desired target [1–3]. Aerodynamic control is critical in allowing the animal to execute a variety of glide trajectories, accommodating different goals and the habitat's spatial complexity [1,4], but the airfoil performance envelope used by gliders in their natural habitat remains unknown.

The first step towards understanding the physical limits governing the airfoil performance of the animal is quantification of the relationship between the non-dimensional coefficients of lift and drag with respect to one another and to the angle of attack (i.e., the angle between the airfoil surface and the airflow). The coefficients, in combination with knowledge of the airfoil speed and area, allow one to estimate the dimensional lift and drag forces and thus the real-world performance of the glider. Furthermore, the ratio of the two coefficients determines the equilibrium glide angle and the minimum amount of potential energy required to cover a given

horizontal distance. However, these coefficients are not a fixed property of the animal. Modulating angle of attack (AoA) is the simplest means for changing the aerodynamic performance of airfoils [5] and is accessible to animal gliders through mid-air changes to body orientation. Animal gliders also modify other aspects of their airfoil. For example, changing the curvature of the airfoil (i.e., camber), can directly change the coefficients of lift and drag [6,7]. Animals can also vary the dihedral angle, or the angle made by the airfoil above or below the horizontal plane, influencing the proportion of aerodynamic lift that is oriented in support of body weight [6]. Finally, animals may directly modify the effective area of the airfoil, thereby influencing dimensional lift and drag performance even if the underlying non-dimensional coefficients remain constant. For example, *Draco* extend their airfoil as they leap from a tree and begin to fold in the airfoil just before landing [4]. Mammalian gliders such as flying squirrels, sugar gliders, and the colugos have a patagium joining the forelimb and the hindlimbs which also permits area changes of the airfoil [8–10]. Gliding snakes flatten their body dorsoventrally, enhancing the surface area and altering airfoil camber [3,11]. All these examples demonstrate that gliding animals are well able to alter airfoil characteristics in mid-air to achieve different aerodynamic outcomes and vary their overall gliding performance.

Prior studies of gliding animals have taken a variety of approaches, all subject to some limitations that have hindered quantifying the aerodynamic performance envelope. The study of the gliding kinematics of live animals in the laboratory permits detailed quantification of aerodynamic performance, but not all gliding species are amenable to captivity, and the performance of captive animals may not be reflective of natural behavior due to changes in motivation and diet brought about by captive life. Furthermore, lab studies have been limited to quantifying parts of the glide and therefore may not be representative of the overall aerodynamic

performance of the animal. For example, lab studies on flying squirrels and sugar gliders have calculated the aerodynamic performance for a small continuous glide duration of 0.12 to 0.38 s for a glide distance of 4 to 4.5 m [9,10], but in the wild, flying squirrels are known to travel greater than 14 m on average in a single glide [12,13]. However, for limbless gliding, Yeaton et al. (2020) have performed high speed motion tracking of 11 to 17 landmarks on flying snake over complete glides to describe and model in detail the undulatory gliding motion [14].

Studies of live animals in the field have typically been handicapped by experimental design constraints such as a few low-resolution cameras or the use of on-animal technologies like accelerometers that can precisely record whole-animal trajectory kinematics but provide no other context for the measurements [8,15]. Bahlman et al. (2013) used a two camera system to record parts of a glide of wild flying squirrels departing from a feeder in a semi-natural setting but lacked multiple body point tracking to calculate metrics of camber and dihedral angle and morphometric data including mass, all essential for accurate aerodynamic performance measurements [2]. Overall, quantifying complete glide performance has been mostly limited to using average metrics for the whole glide such as speed, glide ratio, and glide angle [16]. These measures fail to capture the variety of aerodynamic and morphological modifications undertaken by the animal during the glide and, although they describe the observed glide performance, are an inadequate basis for revealing how an animal might use gliding to traverse varied natural environments.

Finally, physical models of gliding animals tested in a wind tunnel can also provide detailed information on aerodynamic performance, but such models are typically static and cannot probe all the means by which animals might modify or control their force production mid-air. Furthermore, absent a high-quality ground-truth dataset from live animal studies, it

remains uncertain how differences in material properties and other aerodynamic factors affect performance.

Here we address these questions by constructing a well-calibrated 7-camera gliding flight test arena in the animal's habitat and using it to record the 3D kinematics of complete glides of wild *Draco*. Gliding kinematics derived from 5 separate body landmarks allowed measurement of body orientation, wing orientation, and wing camber in addition to the overall glide trajectory. Furthermore, the measured glide trajectories along with known masses and surface areas of the individuals allowed calculation of instantaneous accelerations, aerodynamic forces, and lift and drag coefficients. Using these metrics, we tested the following hypotheses. We hypothesized that in *Draco* the relationship between the coefficient of lift, coefficient of drag and AoA follow those of a typical airfoil but operate closer to the range previously observed in mammalian gliders [2,5,10]. Overall, we expect that the highest lift to drag ratio (but smallest coefficient values) occur at low AoA and that the airfoil transitions to stall with an increasing coefficient of drag, and constant or declining coefficient of lift at higher angles of attack. Furthermore, we hypothesized that the lift to drag ratio is consistent with average whole-glide angles quantified here and previously reported by earlier studies of *Draco* [16]. Finally, the *Draco* wing anatomy restricts wing movement outside the sagittal plane of the body and the maximum possible wing area due to the orientation and extension of the intercostal musculature. Therefore, we hypothesized that in *Draco*, the aerodynamic forces are primarily controlled by varying the body orientation (i.e., body pitch) and consequently the AoA to enable a high lift to drag ratio during the mid-glide to cover horizontal distance, and high lift and drag forces at landing to enable minimal loss of elevation while also reducing kinetic energy before landing.

2.2 Materials and Methods

2.2.1 Field Site and Motion capture arena

The field site was an abandoned areca nut plantation located within the Agumbe Rainforest Research Station campus (ARRS), Karnataka, India (13°31'04" N, 75°05'18" E) and previously described in Khandelwal et al. 2020 (also see Chapter 1) [4]. We conducted our field data collection from February to April 2017 during which we uniquely identified 33 individuals (16 males and 17 females) inhabiting the plantation. The sexes were identified based on their dewlap length (see section 1.1.3). Glide data from these individuals was collected by setting up a motion capture arena in the plantation.

The motion capture arena was constructed on an approximately 6 m x 7 m patch of the plantation containing two areca nut trees 5.5 m apart (Figure 2.1a and 2.1c). The patch was selected to represent the average glide distance (~5 m) observed in our previous study describing natural gliding behavior at the field site [4]. The patch was enclosed by a mix of shrubs and rainforest on the south and areca nut trees on all other sides. The two trees within the patch were designated as the takeoff and landing tree for glide recordings. The arena was constructed by cordoning off the two trees from the rest of the plantation using white sheets on all sides except the south. The white sheets spanned almost the entire tree height and were also spread on the ground between the takeoff and the landing tree. The sheets encouraged the lizard to glide towards the designated landing tree by eliminating other tree options and provided a high contrast background for video recording and 3D motion tracking. We used an array of seven GoPro Hero4 Black cameras (GoPro, Inc) in wide field of view (FOV) mode, which together recorded the complete glide of the lizard between the takeoff and landing tree. The seven cameras were categorized into three groups based on their position between the takeoff and the

landing tree. The camera mounted on the takeoff tree and on the pole adjacent to the takeoff tree formed the takeoff camera group. They were used to record close-up recordings of the takeoff phase. Three cameras on the ground recorded the glide between the takeoff and landing tree and formed the glide camera group. The camera mounted on the landing tree along with the one placed adjacent to it formed the landing camera group. They were used for close-up recordings of the landing phase. Reconstructing 3D kinematics required that the animal be seen simultaneously by at least two cameras.

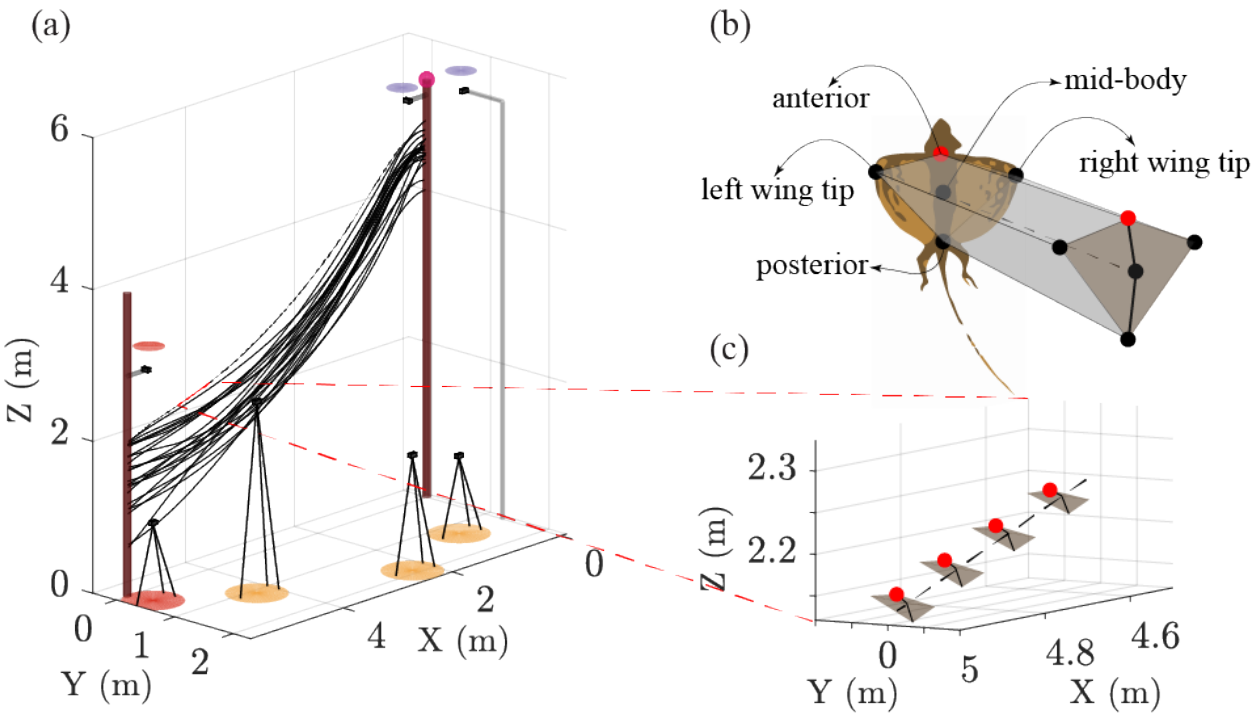
(a)
6
4
2
0
Z (m)
0
1
2
Y (m)
0
2
4
X (m)
(b)
anterior
mid-body
left wing tip
right wing tip
posterior
(c)
2.3
2.2
Z (m)
0
5
Y (m)
4.8
4.6
X (m)

(c)


1
2
3
4
5
6
7

Figure 2.1 Motion capture arena set up in the areca nut plantation at ARRS. (a) A scaled illustration of the motion capture arena showing 23 glides and seven cameras used to collect 3D kinematic data. The seven cameras are divided into three groups (color coded) based on the part of the glide they record. The takeoff cameras are marked by purple discs, glide cameras with orange and landing cameras with red. (b) Illustration showing the body points tracked per frame for each glide. The mid-body point was used as a proxy for center of mass and whole glide kinematic calculations including velocity and acceleration. (c) Enlarged view of one glide closer to the landing tree showing the tracked 3D points in space. (d) Side view photograph of the motion capture arena in the field with all seven cameras marked. The tree adjacent to camera 1 is the takeoff tree and the tree adjacent to camera 7 is the landing tree. Cameras 1 and 2 formed the takeoff group, cameras 3, 4 and 5 formed the glide group, and cameras 6 and 7 formed the landing group.

Takeoff camera group. The group consisted of two cameras. One was mounted close to the top of the takeoff tree looking downwards towards the ground and capturing close-up top view recordings of the takeoff phase. The second camera was mounted on a pole adjacent to the takeoff tree and a similar height as the first camera. The second camera was tilted at an angle to capture the side view of the takeoff phase. Both cameras recorded video at 240 frames per second (fps) and 480p resolution (purple discs in Figure 2.1a and cameras 1 and 2 in Figure 2.1c; also see Figure 2.2b).

Glide camera group. The group consisted of three cameras placed on the ground in a staggered formation between the takeoff and landing tree. The first camera was placed closer to takeoff tree looking upwards with part of the sky as the backdrop. The FOV captured the complete glide. The second camera was placed approximately midway between the takeoff and landing tree and had the white sheets as the backdrop. It also captured the complete glide. The last camera was placed closer to the landing tree and captured part of the mid-glide phase and the complete landing phase. All three cameras recorded at 120 fps and 1080p resolution (orange discs in Figure 2.1a and cameras 3, 4, and 5 in Figure 2.1c).

Landing camera group. The group consisted of two cameras. The first camera was mounted on the landing tree looking downwards towards the ground. This allowed close-up recordings of the top view of the landing maneuver. The second camera was placed adjacent to the landing tree on the ground and provided a side view of the landing phase. Both cameras recorded at 120 fps and 1080p resolution (red discs in Figure 2.1a and cameras 6 and 7 in Figure 2.1c; also see Figure 2.2c).

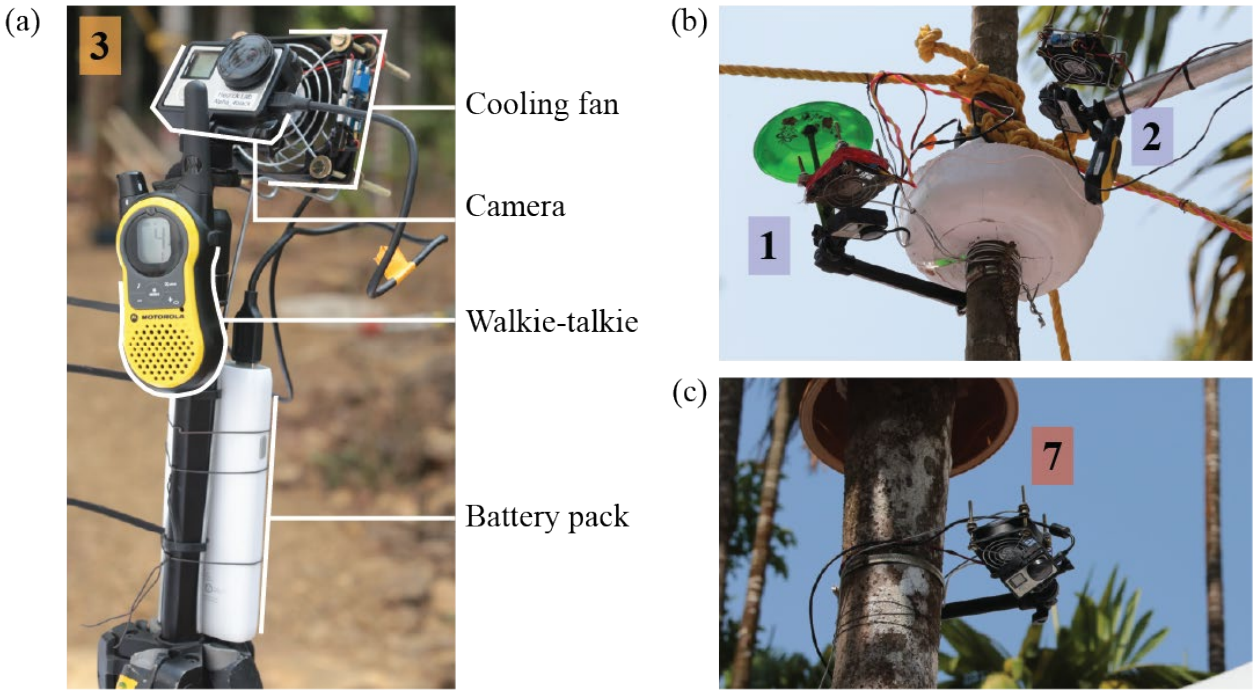

Figure 2.2 Close-up view of the camera setup. (a) Close-up view of camera 3 in the motion capture arena. Each camera was equipped with a cooling fan and battery pack to prevent overheating and enable day long recording. The walkie-talkie was used for temporal alignment of video frames and taking audio field notes. (b) Close-up view of the takeoff cameras 1 and 2. Camera 1 was mounted on the takeoff tree and camera 2 was on a L shape pole erected next to the takeoff tree. A cooling fan was mounted at the back of both cameras and a single walkie-talkie was used for both. (c) Close-up view of camera 7 mounted on the landing tree. The camera at the back of the camera was equipped with an external power switch which allowed us to turn off the fan as soon as the *Draco* landed to prevent any injury to the lizard.

Each of the seven cameras was accompanied by an 80 mm cooling fan, a walkie talkie, and a 20000 mAh external battery pack (Figure 2.2a). The cooling fan was mounted

approximately 8 cm away from the back of the camera using a wire frame to damp vibrations during recording. The airflow was towards the camera and prevented it from overheating. The external battery charged the camera and powered the cooling fan during the recording duration. The walkie talkie was used to receive audio notes and beeps that were used for temporal alignment of the video frames from all cameras for 3D reconstruction. All seven cameras were connected to a Wi-Fi remote to start and stop recording.

2.2.2 Data collection

Prior to data collection, from 24 February until 8 March 2017, an extensive tree and *Draco* survey was carried out at the field site to uniquely identify individuals and their spatial distribution (see Chapter 3 for details). During the survey, all *Draco* lizards spotted in the plantation were captured, marked with a unique number, measured, and immediately released on the same tree from which they were caught.

Glide data collection was performed from 9 March to 21 April 2017, during the *Draco* mating season. Four data collection breaks of two days each were uniformly interspersed during the data collection period to potentially reduce the influence of our presence on *Draco* behavior at the field site. Glides were recorded between 9 am and 4 pm each day based on previous observations of lizard activity at the field site [4]. A complete glide recording began with capturing a lizard from the plantation and releasing it at the bottom of the takeoff tree in the motion capture arena (Fig. 2.1c). After the lizard voluntarily climbed on top of the takeoff tree, all seven cameras were triggered to start video recording. Each recording duration ranged from ~3 min to ~10 min, based on the time taken by the lizard to perform a voluntary glide. The glide event was followed by triggering 10 audio beeps on the walkie talkie and a scene calibration procedure of moving a wand of known length (1.04 m) through the common camera viewing

volume between the takeoff and the landing tree. The wand was constructed using a pipe of 1.8 cm diameter and 1.04 m in length. Three distinct colored balls were placed on the wand. Orange ball on one end and red on the other end. A green ball was placed 26 cm from the red ball. The red and orange ball helped easily identify the two ends of the wand and the green ball was used to distinguish between the two ends for consistent digitization for scene calibration. Finally, a tennis ball was tossed upward and allowed to fall in the motion capture arena; this trajectory was used to align the vertical (Z) axis with gravity during 3D reconstruction of the glide and validate the camera calibration accuracy. After completion of the recording, the lizard was placed back on the takeoff tree or, if the individual already had three recordings on the same day, then it was ready to be released back on the tree from which it was captured. Before setting the lizard free, the mass of the lizard was measured on a digital balance (resolution +- 0.01 gm) and was followed by taking images of the lizard on a graph paper for morphometric measurements (see Chapter 3 for details). No lizard was held captive for more than the duration of the recording on a single day. If the *Draco* captured for recording was unmarked, the lizard was marked after completing all the glide recordings for that day to ensure that the fresh marking did not affect the gliding behavior in the arena.

2.2.3 Data processing

3D position data ([x,y,z] coordinate) was obtained using the MATLAB (The MathWorks, Natick, MA, USA) package DLTdv [17]. Because the lizards were unmarked, we chose five locations on the dorsal side of the *Draco* for manual digitization in each frame of the complete glide (Figure 2.1b). The anterior point was identified as the place where the head of the lizard connected to the body. The posterior point was identified as the place where the tail joined the body. The left- and right-wing tips were the two extremities of the wing, clearly demarcated as

the two end points of the *Draco* along the lateral axis. The mid-body point was roughly the mid-point between the anterior and posterior body point and corresponded to a distinct pattern on the dorsal side of the lizard. Each of the five body points were digitized in all camera views in which they were visible (at least two or more views for each frame throughout the complete glide). Therefore, each of the five body points resulted in five tracks corresponding to the complete glide trajectory. Each track was smoothed using a smoothing quintic spline weighted by the 95% confidence intervals of the 3D reconstruction uncertainty. There were no missing points or gaps in the digitized tracks used for data analysis. Each glide was rotated and translated to place the takeoff tree on the origin and the landing tree on the positive X axis. Glides were divided into phases (takeoff, mid-glide, and landing) based on criteria established for glides from freely behaving lizards (see Chapter 4). Briefly, the end of takeoff was marked by the momentary alignment of the resultant aerodynamic force vector with the velocity vector leading to a minimum in the centripetal acceleration curve. The start of the landing phase corresponded to the decrease in the horizontal speed of the *Draco* (Figure 2.3b and 2.3e).

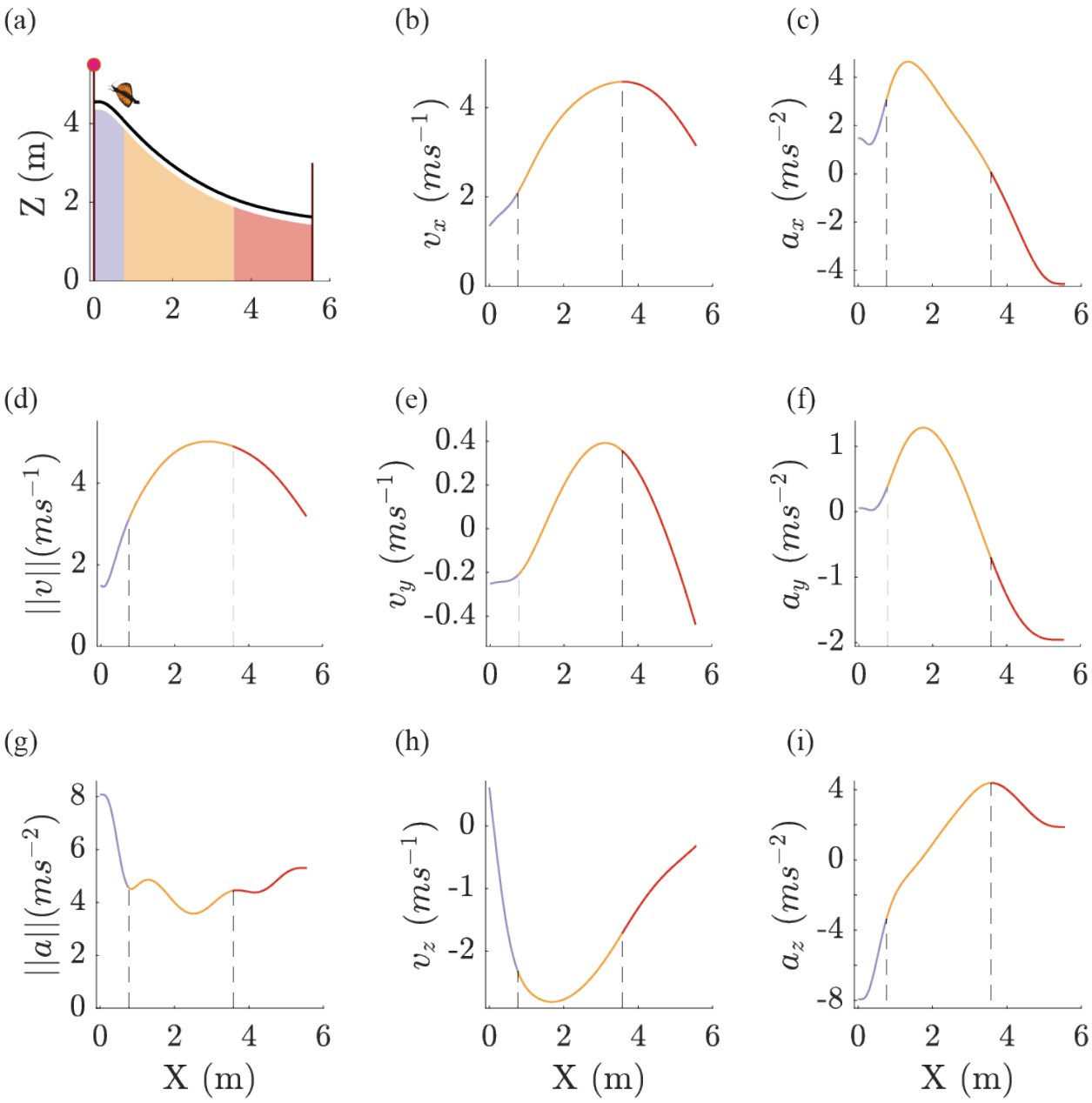

Figure 2.3 Kinematics of single *Draco* glide. Panels (a), (d), and (g) show the side view profile of one of the 23 glides recorded along with the total speed and acceleration magnitude. The glide trajectory is divided into takeoff, mid-glide and landing phases based on the definitions followed in Khandelwal et al (2020) [4]. Panels (b), (e), and (h) show the x, y, and z components of the velocity vector during the glide. Note the drop in v_x marking the start of the landing phase. Panels (c), (f), and (i) show the x, y, and z components of the acceleration vector during the glide. Note the start value of a_z close to 9.81 ms^{-2} indicating the ballistic dive phase of the takeoff.

2.2.4 Kinematic and aerodynamic parameters

Yaw angle (°). The angle made by the line joining the anterior and posterior point (longitudinal axis) with the positive X axis at every instant of time (Figure 2.4b and 2.5a).

$$yaw = tan^{-1}\left(\frac{anterior_y - posterior_y}{anterior_x - posterior_x}\right)$$

where $anterior$ and $posterior$ refer to the tracked points on the *Draco*'s body.

Pitch angle (°). The angle made by the line joining the anterior and posterior points (longitudinal axis) on the lizard with the horizontal X-Y plane at each instant of time. A positive pitch angle raises the anterior point of the lizard and lowers the posterior point (Figure 2.4e and 2.5d).

$$pitch = tan^{-1}\left(\frac{anterior_z - posterior_z}{anterior_x - posterior_x}\right)$$

Roll angle (°). The angle made by the line joining the left-wing tip and right-wing tip (parallel to the lateral axis) with the horizontal X-Y plane at each instant of time. A positive roll angle raises the left-wing tip and lowers the right-wing tip (Figure 2.4g and 2.5g).

$$roll = tan^{-1}\left(\frac{anterior_y - posterior_y}{anterior_x - posterior_x}\right)$$

Instantaneous glide angle (θ, °). The angle defined by the inverse tangent of the ratio of the vertical component of velocity (v_z) to the horizontal component of velocity (v_x).

$$\theta = tan^{-1}\left(\frac{v_z}{v_x}\right)$$

Angle of attack (°). The difference between the pitch angle and the instantaneous glide angle at each instant of time (Figure 2.4c and 2.5b).

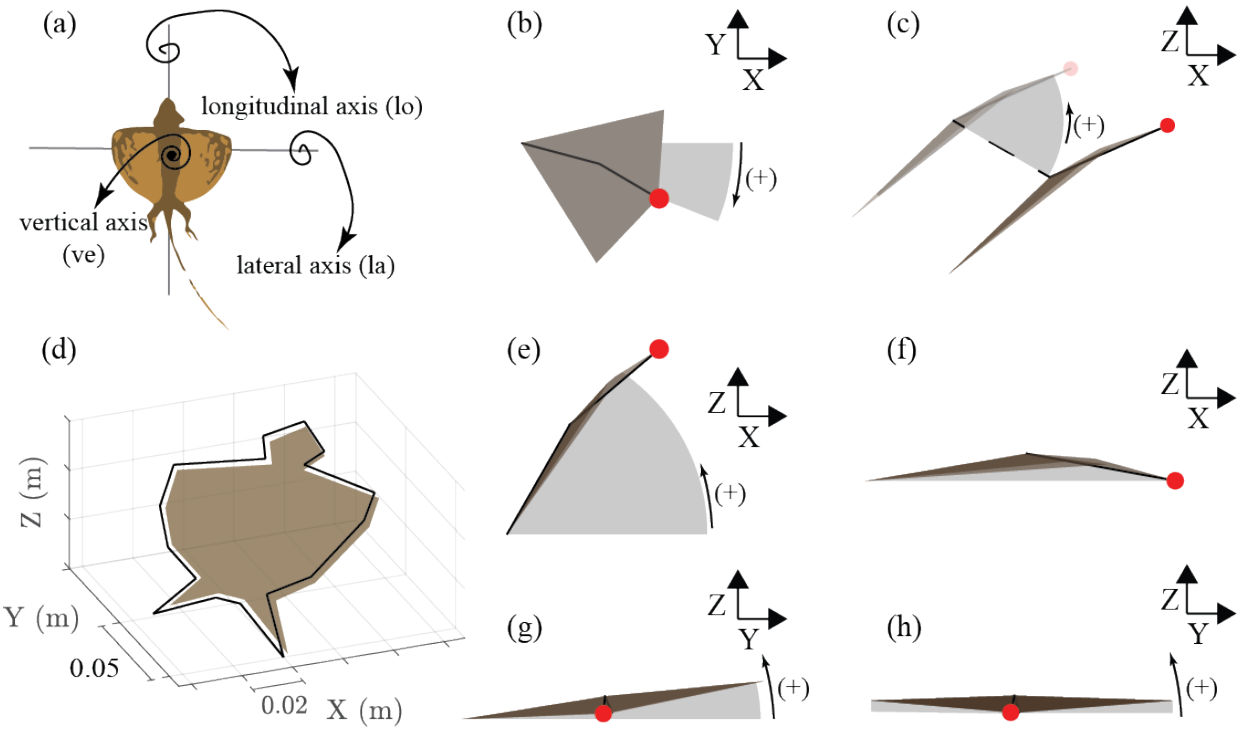

Figure 2.4 An overhead view illustration of the axes of flight and aerodynamic parameters calculated for each glide (a) The three axes about which the lizard can move in flight. Longitudinal axis (**lo**) about which the lizard rolls. Lateral axis (**la**) about which the lizard pitched. Vertical axis (**ve**) about which the lizard changed its yaw. (b) Yaw angle is the rotation about the **ve** from the X-Z plane, positive yaw is to the lizard's right. (c) Angle of attack (AoA) is the angle made by the airfoil surface relative to the direction of motion (airflow). (e) Pitch angle is the rotation about the **la** from the X-Y plane, positive pitch raises the head upward. (f) Camber is the convexity of the airfoil from the leading to the trailing edge. (g) Roll angle is the rotation about the **lo** from the Z-Y plane, positive roll raises the left-wing tip. (h) Dihedral angle is the average of the upward angle made by either side of the wing with the X-Y plane. (d) Illustration showing the airfoil area used to calculate the aerodynamic force coefficients. The area was calculated by fitting a plane to the 17 3D points tracked around the lizard.

percentage camber. The ratio of the perpendicular distance of the mid-body point from the longitudinal axis to the distance between the anterior and posterior body point (chord length). The ratio is multiplied by 100 to give the percentage camber (Figure 2.4f and 2.5e).

Dihedral angle (°). After correcting for pitch and roll, the average of the angle made by the line joining the mid-body point to the left- and right-wing tip with the horizontal X-Y plane. A

positive dihedral angle raises the left- and right-wing tip above the horizontal X-Y plane (Figure 2.4h and 2.5h).

Airfoil area (m^2). A single video frame from the complete glide trajectory was used to calculate airfoil area. The frame corresponded to the *Draco* in glide when the patagium was completely stretched open. A total of 17 points were 3D tracked around the body periphery and included the head, lappets and the hindlimbs but excluded the tail. These 17 points were used to define an airfoil representing the total body surface area used to generate aerodynamic forces (Figure 2.4d).

Lift and Drag (N). Aerodynamic lift and drag were calculated using the angle (φ) between the drag vector, i.e. opposite to the velocity vector ($\boldsymbol{V}$), and the resultant aerodynamic force vector ($\boldsymbol{R}$) [9].

$$\boldsymbol{R} = a_x + a_y + (a_z + 9.8)$$

$$\varphi = cos^{-1}\left(\frac{-\boldsymbol{V}.\boldsymbol{R}}{|\boldsymbol{V}||\boldsymbol{R}|}\right)$$

The components of $\boldsymbol{R}$ perpendicular and opposite to the *Draco*'s direction of travel were multiplied by the *Draco*'s mass (m) to give the normalized lift and drag force, respectively.

$$L = |\boldsymbol{R}|sin\varphi.m; D = |\boldsymbol{R}|cos\varphi.m$$

Coefficients of lift and drag (n.d.). Instantaneous coefficients of lift and drag (i.e., C_L and C_D) were calculated from the kinematic and airfoil data from the following equations:

$$C_L = L\left(\frac{1}{2}\rho S v^2\right)^{-1}$$

$$C_D = D\left(\frac{1}{2}\rho S v^2\right)^{-1}$$

where ρ is air density (1.225 kg m^{-3}), S is the airfoil area (Figure 2.4d), v is instantaneous airspeed (Figure 2.3d), and L and D are the normalized lift and drag forces, respectively. Note that S is assumed to be constant at the measured fully open value, so these instantaneous calculations will not produce accurate results for the beginning and end of the glide when the *Draco* patagium is incompletely deployed or being retracted (Figure 2.5c, 2.5f and 2.5i).

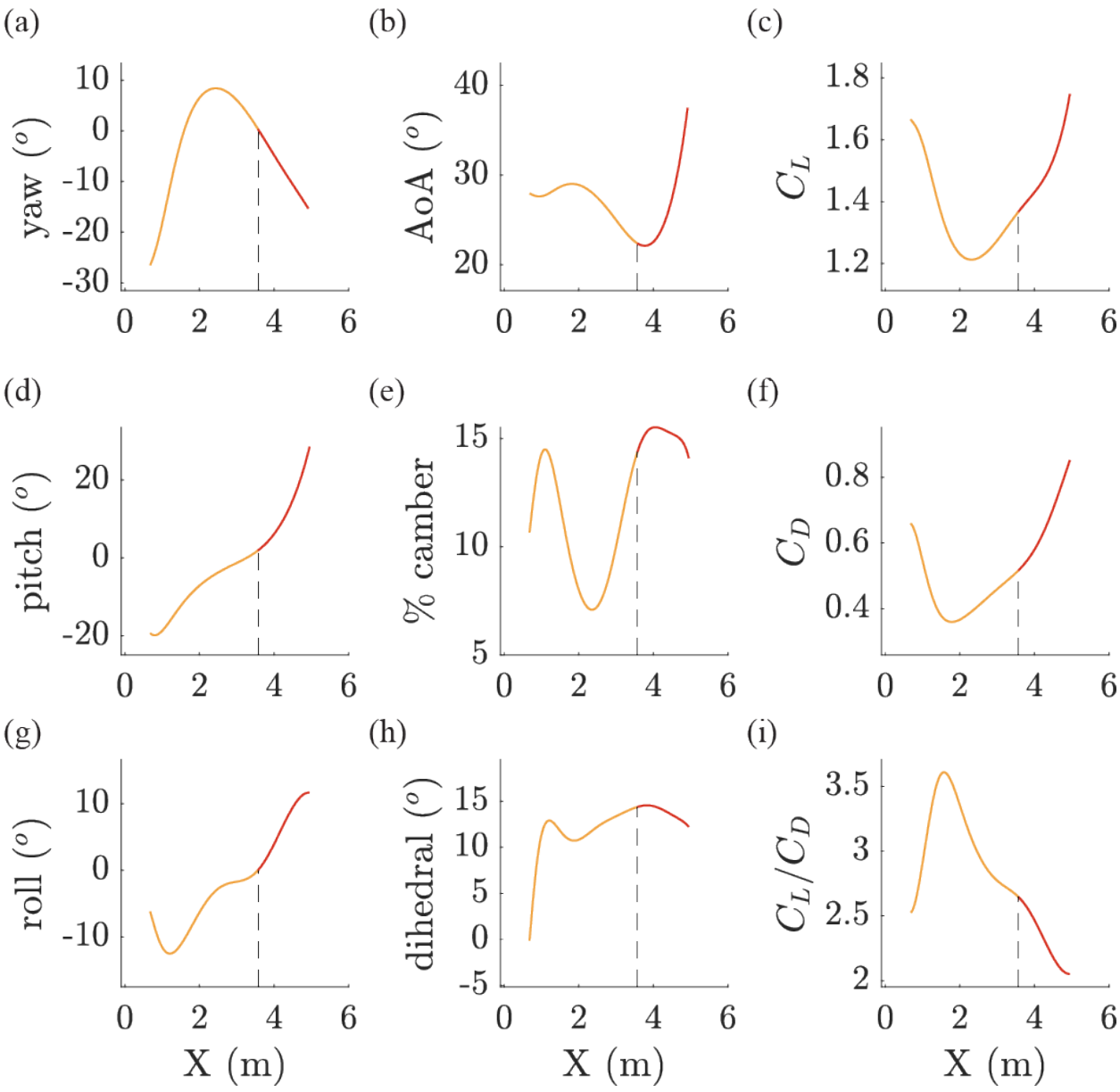

Figure 2.5 *Draco* orientation and aerodynamic parameters for a representative glide during the mid-glide and part of the landing phase. The takeoff phase and end of the landing phase was not considered since the *Draco* rapidly changes its orientation and wing shape during that time. Panels (a), (d), and (g) show the *Draco* orientation in flight. Panels (b), (e), and (h) show angle of attack (AoA), percentage camber, and dihedral angle, all parameters that are directly relevant for aerodynamic force generation. Panels (c), (f), and (i) show the variation in C_L and C_D and their ratio with glide progression.

C_L and C_D polar plot. The set of corresponding values for C_L, C_D, and AoA were determined as follows from the instantaneous values by a sliding window approach applied to C_D from 0.35 to

2.0 in increments of 0.1 (Figure 2.9). For each window mid-point, we identified all instantaneous C_D values from the mid-point ± the increment of 0.1. Within this data subset we calculated the average C_D, C_L and AoA for each individual *Draco* represented. From this set of individual means we calculated the inter-individual mean, inter-individual standard deviation, and standard error at each of the C_D window mid-points. Note that the values contributing to each mid-point overlap by 50%, for example, the mid-points at 0.35 includes the range from 0.25 to 0.45 while the mid-point at 0.45 includes the range from 0.35 to 0.55. The sliding window approach was performed to lessen the effect of the artificial and arbitrary window size on the resulting glide polar. Finally, instantaneous values from the first 50 (0.42 s) and last 20 (0.17 s) frames were not included in these calculations because the *Draco* patagium was typically seen to be incompletely extended during those intervals.

Average glide parameters. The fixed takeoff and landing tree distance of 5.5 m established by the motion capture arena allowed us to quantify the behavior of each kinematic and aerodynamic parameter as the *Draco* moved towards the landing tree. To quantify the range of values used by the *Draco*, we used a sliding window of 0.1 m starting from 0.6 m to 5.2 m along the +X axis and identified all values for each parameter within each step of 0.1 m increment (Figure 2.6). For each window, the mean and standard deviation for each parameter was calculated. The first 0.6 m and the last 0.3 m of the glide were excluded because they corresponded to the first 50 and last 20 frames of glide recording which were removed from the analysis as mentioned previously.

2.2.5 Statistical methods

In addition to the preceding calculations, univariate linear regression (ULR) and generalized linear mixed-effects models (GLME) were used to examine the data for significant

relationships among the individual *Draco* averages for coefficients of lift and drag, lift-to-drag ratio, camber, AoA and dihedral. These and all other calculations were performed in MATLAB version r2020a.

2.3 Results

A total of 23 glides from 7 different males and 6 different females were used for kinematic and aerodynamic analysis. Since the glides were recorded in the motion capture arena, the glide distance between the takeoff and the landing tree was fixed at 5.5 m. The average glide duration from the takeoff to the landing tree was 1.69 ± 0.06 s (mean ± std, n = 23). Lizards reached a maximum speed of 5.06 ± 0.32 ms^{-1} with an average overall glide angle of -28.86 ± 2.91°, corresponding to a theoretical equilibrium glide with a lift to drag ratio of approximately 1.8. However, none of the glides reached equilibrium; all showed continuous changes in acceleration in the X, Y and Z directions. For analysis, each glide was divided into takeoff, mid-glide and landing phases. The duration, distance covered, and the average glide angle observed for each phase is described in Table 2.1.

Table 2.1 Duration, distance, and average glide angle for each glide phase across all 23 glides. The values reported are mean ± std.

	Takeoff	**Mid-glide**	**Landing**
Duration (s)	0.43 ± 0.03	0.75 ± 0.08	0.52 ± 0.10
Horizontal distance (m)	0.79 ± 0.10	2.72 ± 0.29	2.00 ± 0.30
Glide angle$_{avg}$ (°)	-35.84 ± 3.88°	-36.18 ± 3.17°	-13.35 ± 4.35°

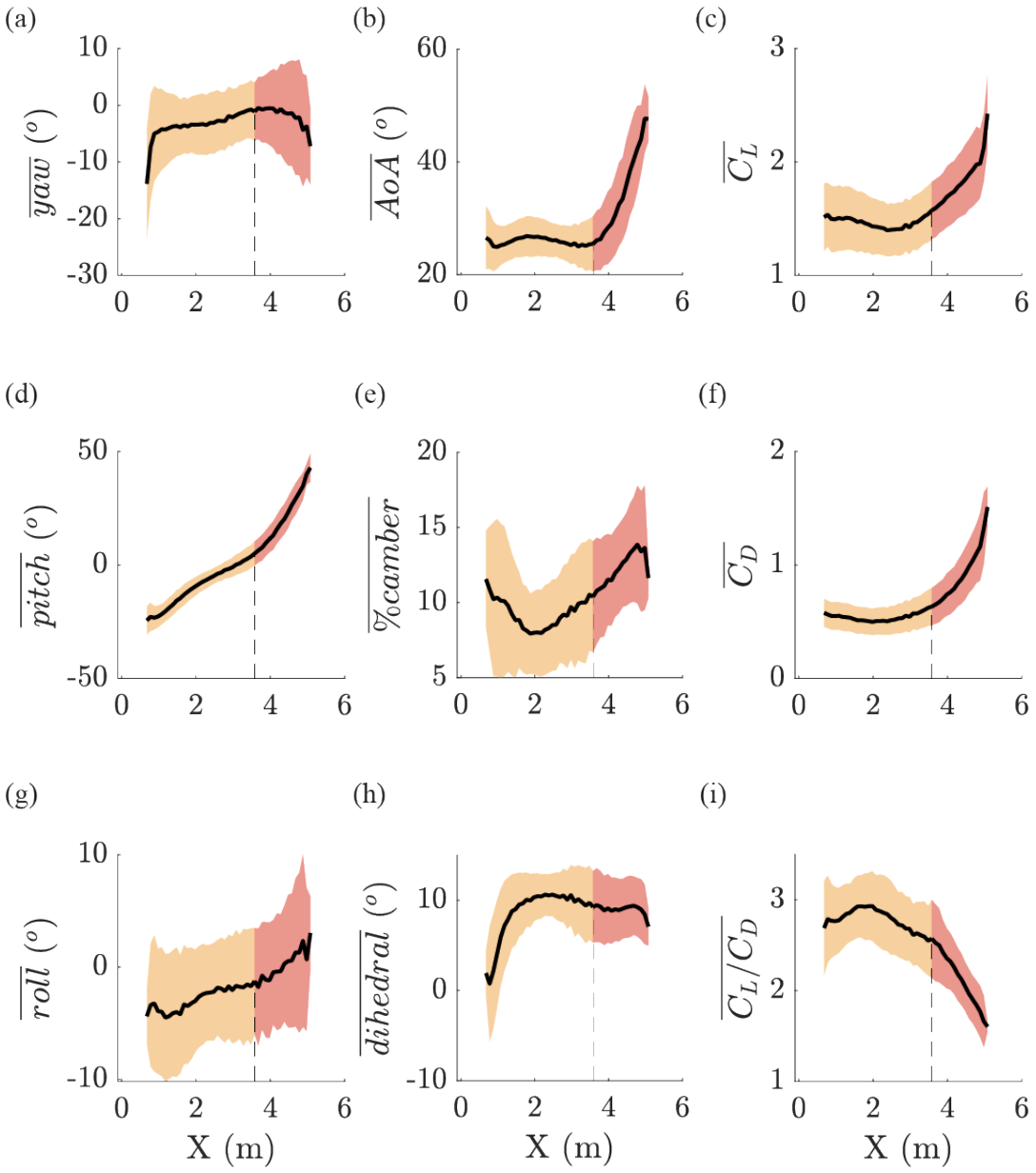

Figure 2.6 Parameter behavior for a horizontal glide distance of 5.5 m for all 23 glides performed in the flight arena. The solid black line shows the average value, and the shaded area shows the standard deviation. The orange shaded region represents the average mid-glide phase, and the red shaded region represents the average landing phase excluding the last 0.3 m of glide distance. The vertical dashed line denotes the start of the landing phase calculated as the average of start of landing phase for all glides. Panels (a), (d) and (g) show the overall variation in yaw, pitch, and roll angle. Yaw and role angle showed a variation of approximately 15° while pitch showed a narrow variation and a continuous increase as the glide progressed. Panels (b), (e) and (h) show the variation in angle of attack, percentage camber and dihedral angle. Note the sharp increase in angle of attack in the landing phase. Panels (c), (f) and (i) show the change in average force coefficients and their ratio with glide progression. Note the steep drop in lift-to-drag ratio during the landing phase.

2.3.1 Variation in roll, pitch, and yaw angle

The first 50 frames (0.42 s) and the last 20 frames (0.17 s) of the glide were not considered for aerodynamic analysis since these instances corresponded to rapid changes in *Draco* posture, wing shape, and size. Yaw and roll angles were highly variable across glides, and the pitch angle increased at an average rate of $10.3 \pm 0.2°\ m^{-1}$ (ULR, $R^2 = 0.99$, $p < 0.001$) with the *Draco* transitioning into a more upright pose, with a more rapid increase of $26.1 \pm 0.9°\ m^{-1}$ (ULR, $R^2 = 0.98$, $p < 0.001$) at the end of the glide during the landing maneuver (Figure 2.6a, 2.6d and 2.6g).

2.3.2 Variation in angle of attack, camber, and dihedral angle

During the mid-glide, *Draco* used a percentage camber of 9.35 ± 3.62 and a dihedral angle of $8.7 \pm 3.7°$, i.e., the patagium was convex upwards with the camber height being approximately 10% of the chord length and the wing tips elevated at approximately 9° with respect to the body midpoint (Figure 2.6e and 2.6h). The AoA was held mostly constant at $25.9 \pm 3.7°$ during the mid-glide phase despite the continuous increase in body pitch angle at a rate of $10.3 \pm 0.2°\ m^{-1}$ (Figure 2.6b). The AoA then increased rapidly at a rate of $16.8 \pm 0.8°\ m^{-1}$ (ULR, $R^2 = 0.97$, $p < 0.001$) towards the end of the glide during the landing maneuver. Furthermore, the landing phase saw a steady increase in percentage camber with little variation in the dihedral angle. Overall, the *Draco* modulated its percentage camber and AoA during the glide with a steady dihedral angle of approximately 9° to cover a horizontal glide distance of 5.5 m.

2.3.3 *Aerodynamic force coefficients*

Overall, *Draco* generated more lift than drag, C_L was always greater than C_D (Figure 2.6c and 2.6f, and Figure 2.9b). During the mid-glide phase, *Draco* used a C_L of 1.47 ± 0.25 (mean ± std, n = 30) and C_D of 0.55 ± 0.13. In the landing phase, the lift and drag coefficients both increased, but the rate of increase was higher for the drag coefficient at 0.53 ± 0.05 m^{-1} (ULR, R^2 = 0.90, $p < 0.001$) compared to 0.45 ± 0.05 m^{-1} (ULR, R^2 = 0.85, $p < 0.001$) for the lift coefficient, leading to an overall decrease in the lift-to-drag ratio. The average maximum C_L was 2.42 ± 0.33 and the average maximum C_D 1.51 ± 0.18; both these maxima occurred near the end of the landing phase after approximately 5.2 m of horizontal translation (0.3 m from the landing tree). However, the aerodynamic analysis could produce higher maximum C_L and C_D values than those reported here if the last 0.3 m of glide distance were included. The average maximum C_L to C_D ratio was 2.93 ± 0.38 and peaked early in the glide at around 2.1 m of horizontal travel (Figure 2.6i).

2.3.4 *Effect of angle of attack and percentage camber on aerodynamic force coefficients*

We fit three separate generalized linear mixed effects models with the coefficient of lift, coefficient of drag, and the lift-to-drag ratio as the outcome variable, with fixed effects of AoA and percentage camber, and an uncorrelated random effect of AoA and percentage camber grouped by position. Since the underlying data were generated by binning successive *Draco* measurements by horizontal position between the takeoff and landing tree, we included horizontal position (X) as the grouping variable in an attempt to remove any spatial association between the fixed effects and the outcome variable.

In the mid-glide phase, percentage camber was significantly and positively correlated with the aerodynamic force coefficients, whereas AoA was not significantly correlated with them

and was approximately 26° throughout mid-glide (Table 2.2, Figure 2.7a and 2.8). However, AoA (and not percentage camber) was a significant and positive predictor of the lift-to-drag ratio during the mid-glide, though the small range of variation in AoA (25° to 27°) means that the overall effect on the lift to drag ratio was small (Table 2.2).

During landing, both AoA and percentage camber were significantly correlated with the aerodynamic force coefficients. AoA was positively correlated and percentage camber was negatively correlated to each of the force coefficients (Table 2.3 and Figure 2.8). Like the mid-glide phase, the landing phase showed a negative correlation of angle of attack with the lift-to-drag ratio and non-significant relationship with percentage camber. However, it should be noted that towards the end of the observed landing phase, there is a steep drop in percentage camber as the *Draco* begins to position itself for tree contact that could lead to the negative non-significant effect on the lift-to-drag ratio (Table 2.3).

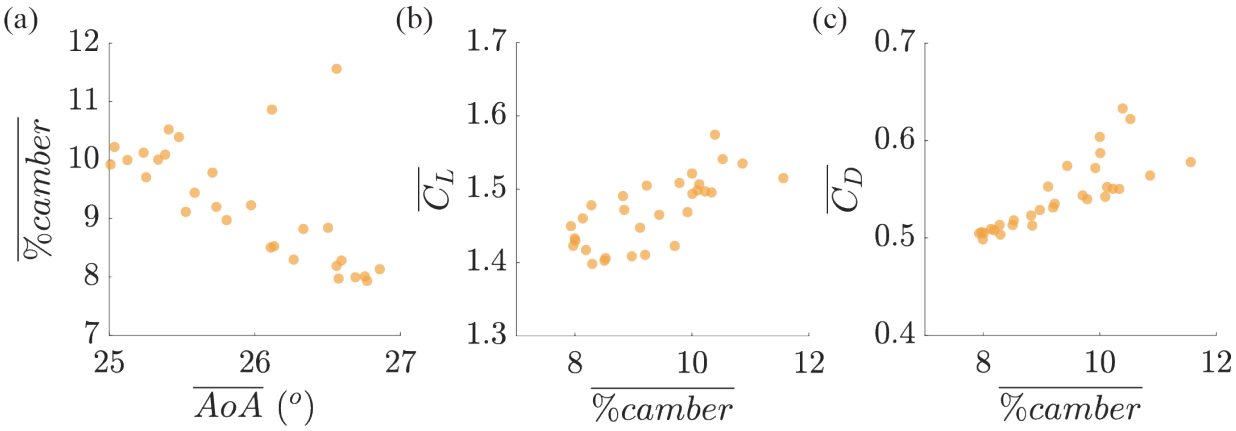

Figure 2.7 Effect of average percentage camber in mid-glide phase for all glides. (a) *Draco* use a narrow range of AoA of approximately 2° but vary their percentage camber in mid-glide. (b) and (c) show average force coefficients increasing with increase in percentage camber during mid-glide.

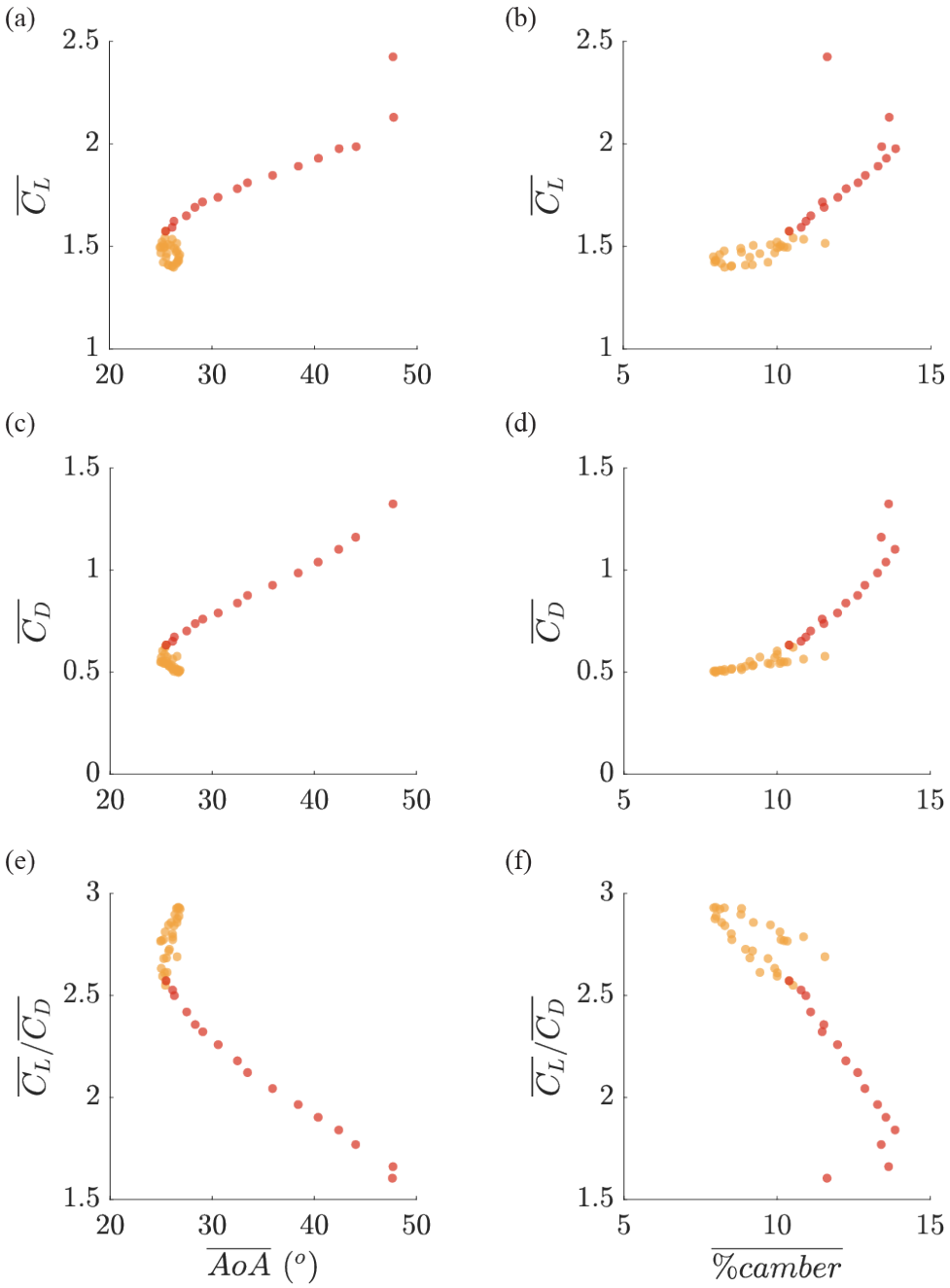

Figure 2.8 Variation of lift and drag coefficients with angle of attack and percentage camber. The orange markers denote values from the average mid-glide phase and the red markers represent values from the average landing phase. Panels (a), (c), and (e) show that *Draco* operate within a narrow range of approximately 2° angle of attack during the mid-glide phase but use a larger range during landing. Panels (b), (d), and (f) show that unlike the AoA, *Draco* use a range of percentage camber values throughout the mid-glide and the landing phase. The variation follows the expected trend of force coefficients individually increasing with percentage camber but their ratio decreasing with an increase in percentage camber.

Table 2.2 Generalized linear mixed effects for aerodynamic force coefficients and their ratio in the mid-glide phase. The significant effects are highlighted in bold.
Model fit: Intercept + AoA + Camber + (AoA|X) + (Camber|X)

		Estimate	SE	95% CI		t	p	SD (random effect)
				Lower	Upper			
Coefficient of Lift	Intercept	0.42	0.41	-0.43	1.27	1.01	0.32	
	AoA	0.02	0.01	-0.00	0.05	1.78	0.09	$< 10^{-5}$
	Camber	0.04	0.01	0.03	0.06	5.31	$< 10^{-4}$	0.00

		Estimate	SE	95 % CI		t	p	SD (random effect)
				Lower	Upper			
Coefficient of Drag	Intercept	0.64	0.25	0.13	1.15	2.56	0.02	
	AoA	-0.01	0.01	-0.03	0.00	-1.53	0.14	$< 10^{-6}$
	Camber	0.02	0.00	0.01	0.04	4.69	$< 10^{-4}$	0.00

		Estimate	SE	95% CI		t	p	SD (random effect)
				Lower	Upper			
Lift-to-drag ratio	Intercept	0.24	0.96	-1.72	2.20	0.25	0.80	
	AoA	0.11	0.03	0.04	0.17	3.52	<0.01	<0.0001
	Camber	-0.03	0.02	-0.07	0.01	-1.71	0.10	0.01

Table 2.3 Generalized linear mixed effects for aerodynamic force coefficients and their ratio in the landing phase. The significant effects are highlighted in bold.
Model fit: Intercept + AoA + Camber + (AoA|X) + (Camber|X)

		Estimate	SE	95% CI		t	p	SD (random effect)
				Lower	Upper			
Coefficient of Lift	Intercept	1.38	0.15	1.06	1.70	9.36	$< 10^{-6}$	
	AoA	0.03	0.00	0.03	0.04	11.63	$< 10^{-7}$	0.00
	Camber	-0.06	0.02	-0.10	-0.02	-3.28	<0.01	$< 10^{-6}$

		Estimate	SE	95% CI		t	p	SD (random effect)
				Lower	Upper			
Coefficient of Drag	Intercept	0.39	0.08	0.22	0.56	4.95	< 0.001	
	AoA	0.04	0.00	0.04	0.04	29.76	$< 10^{-12}$	<0.001
	Camber	-0.07	0.01	-0.09	-0.05	-7.75	$< 10^{-5}$	$< 10^{-6}$

		Estimate	SE	95% CI		t	p	SD (random effect)
				Lower	Upper			
Lift-to-drag ratio	Intercept	3.71	0.11	3.46	3.96	32.29	$< 10^{-13}$	
	AoA	-0.04	0.00	-0.04	-0.03	-18.92	$< 10^{-10}$	<0.001
	Camber	-0.02	0.01	-0.05	0.01	-1.70	0.11	$< 10^{-6}$

2.3.5 Lift-drag polar

The polar plot derived from the *Draco* glide data reveals a slightly concave downwards relationship between lift and drag, such that the highest lift to drag ratio occurred at low values of the observed coefficients (Figure 2.9a). Coefficient values at $C_D > 1.6$ vary widely, with substantial differences in C_L between individual lizards producing large standard errors. Taken as a whole (along with the large standard errors), the data show little change in C_L for $C_D > 1.6$. Variation in C_L and C_D with respect to AoA show a well-resolved middle range from AoA of approximately 26° to 45° where both coefficients increase steadily with increasing AoA. At the high AoA extreme, values are disorganized and typically represented by few data, both within and among individuals. *Draco* typically used these high AoA values during the landing phase (Fig. 2.9b), which is brief compared to the mid-glide. The low AoA extreme (< 25°), also exhibits an unusual pattern with an overlapping of C_L and C_D results suggesting wide variation in aerodynamic performance with minimal change in AoA (Figure 2.8a, 2.8c and 2.8e). These AoA values were used in the transition from takeoff to mid-glide and are also sparsely represented in the overall dataset. The highest lift-to-drag ratio was achieved at approximately 26° which corresponded to the steady AoA held by the *Draco* during the mid-glide phase (Figure 2.9c).

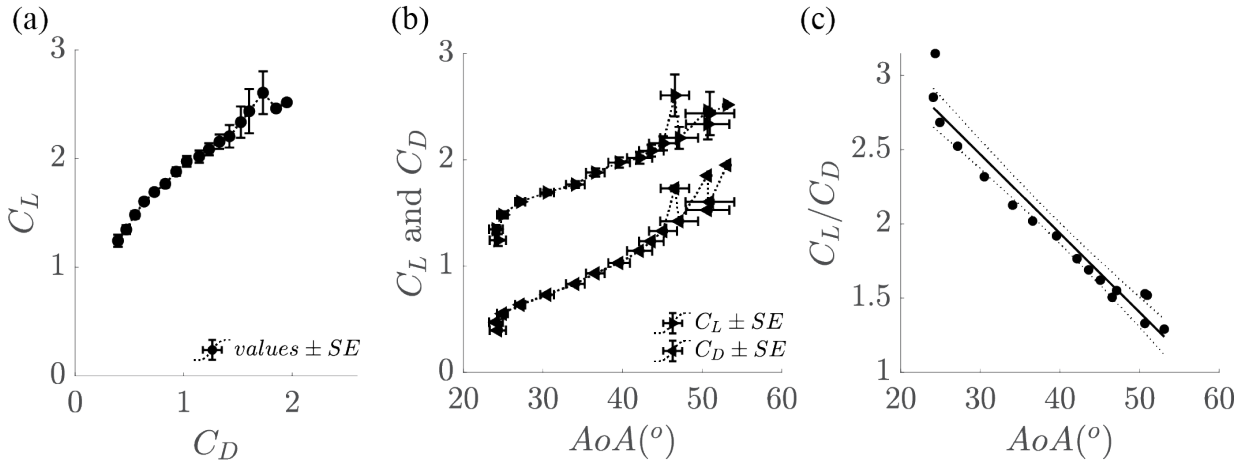

Figure 2.9 Aerodynamic force coefficients. (a) A polar plot of the aerodynamic force coefficients; (b) their variation with the angle of attack. Note the expected gradual increase in the each of the force coefficients with the increase in angle of attack up to a value of approximately 45^{o} (c) the ratio of C_L and C_D with respect to angle of attack shows a strong negative correlation (ULR, $R^2 = 0.94$, $p < 0.001$).

2.4 Discussion

Our study provides the first real-world insight into how *Draco* actively modulate their orientation and posture to control aerodynamic forces to achieve near-optimal gliding performance in their natural environment. In doing so, we present the highest quality dataset of real-world aerodynamic performance currently available for complete glides in any gliding animal, which may serve as an input for detailed modeling of the behavioral and locomotor options available to *Draco* and other gliding species in complex natural environments.

In our field flight arena, we saw that wild-caught *Draco* used an aerodynamic strategy that maintained their AoA at approximately 26° during mid-glide to achieve their maximum lift-to-drag ratio while modulating camber to use different combinations of the coefficients of lift and drag. In landing, *Draco* rapidly increased their AoA in excess of 40° without stalling, allowing them to minimize altitude loss while decelerating to land safely.

2.4.1 Aerodynamic performance envelope

Gliding animals need to produce aerodynamic forces to move in the air. These forces are generated and controlled by the intrinsic properties of the animal's airfoil (coefficient of lift and drag) as well as the airfoil interaction with the surrounding medium (speed, orientation, exposed surface area, shape). Mammalian gliders, including gliding squirrels and sugar gliders, have been shown to glide at an average AoA of 42.5° and 44.2°, producing lift-to-drag ratios of 2.26 and 1.39, respectively [9,10]. However, these measurements relate to a small portion of the entire

glide and represent an airfoil with a smaller aspect ratio (i.e., ratio of the wing span to mean chord length) of approximately 1 [7] compared to the *Draco* airfoil with an average aspect ratio of 1.42 (n = 23).

We hypothesized that the relationship between the *Draco* coefficient of lift, coefficient of drag, and AoA would follow those of a typical airfoil but operate at higher ranges of AoA, with low values for coefficients but high lift to drag ratio at low AoA. Furthermore, the aerodynamic force coefficients would increase with increasing AoA and eventually reach a stall point where the coefficient of drag would continue to increase with increasing AoA, but the coefficient of lift would remain steady or decline. This hypothesis was supported, with *Draco* airfoil characteristics broadly matching our prediction, although *Draco* were not observed to glide at AoA lower than approximately 20° so the polar plot of results does not include any coefficient data near zero (Figure 2.9a). The absence of AoA below 20° could be an artifact of the flight arena setup with the takeoff height of the *Draco* restricted by the placement of the takeoff camera. In the flight arena, the observed takeoff heights varied between 4 to 5 m above the ground.

Our data showed the expected distinction between the *Draco* data and typical engineered airfoil results – *Draco* operated at much higher angles of attack, apparently without stalling, than might naively be expected. For instance, the airfoil based on an albatross wing section [18] and simulated in [19] has a peak lift-to-drag ratio at an AoA of around 1° and experiences stall at AoA above 10°. In contrast, the *Draco* operated with an AoA of 20° to 55°, with stall like characteristics beginning to appear at 45° to 50° (Figure 2.9b). Our results are consistent with other gliding animals and the flapping wings of insects [20], all of which also use high angles of attack and only appear to stall at 40° or higher. This highlights the differences in fluid dynamics

between low Reynolds number biological airfoils and those of larger and higher Reynolds number human engineered systems. Additionally, we saw that *Draco* achieve higher lift-to-drag ratios between 2.5 and 3 (Figure 2.9c), greater than those seen in mammalian gliders and likely due to the higher aspect ratio of *Draco* airfoil, but similar to the lift-to-drag ratio measured in a model of flying snakes [21]. Finally, even above 50° of AoA we did not see clear stalling behavior (Figure 2.9b), implying that *Draco* can induce a soft stall (i.e., C_L is maintained but does not increase while C_D decreases), potentially through other physical mechanisms such as a compliant wing membrane [7] and/or by the position of their forelimbs at the leading edge of their patagium to form a leading edge slot [5].

A related observation from our study is that the calculation of the coefficients of lift and drag depends on the area of the airfoil. This is of course a simple mathematical statement, but it raises practical problems when applied to gliding animals that have small wings but may use much of their body surface in gliding. During initial analyses of our dataset, we used only the area of the patagium, extracted by hand during morphometric data collection, as the airfoil area. This resulted in implausibly high values for the coefficients, leading us to shift to using the planform area of the entire *Draco*, including head, body, patagium and proximal portions of the limbs for aerodynamic coefficient calculations, approximately doubling the area compared to the patagium alone. Comparison between this dataset and other studies of animal gliding should keep this methodological distinction of airfoil area in mind; it strongly influences the value of C_L and C_D but not their ratio since in that case the area terms cancel. Furthermore, this result emphasizes the significant contribution of the mostly flat body parts of the glider, apart from the primary wing surface, towards generating aerodynamic forces.

2.4.2 Compliant wing membrane

Draco have a unique primary airfoil design where the aerodynamic surface is formed by rotating the ribs laterally outwards and stretching the patagium to form an inverted delta wing. The wing membrane is not rigid and adopts a cambered shape under aerodynamic load. Furthermore, a positive dihedral angle throughout the mid-glide implies that the tip of the *Draco* wing is held higher than the root of the wing where it extends from the body (Figure 2.6h). Song et al. (2008) showed that for a rectangular latex wing membrane of aspect ratio 1.4, camber induced by aerodynamic loading resulted in a significant enhancement in lift at low AoA compared to rigid wings and exhibited a soft stall at AoA of over 40° [7]. Our results show surprisingly similar characteristics for the *Draco* airfoil with an average aspect ratio of 1.41. In the mid-glide phase, we observed a significant rise in coefficient of lift at low AoA with percentage camber varying between 8 and 10 (Figure 2.7a) and a dihedral angle of approximately 9°. The coefficients of lift and drag were significantly correlated with percentage camber and increased both coefficients as expected (Table 2, Figure 2.7b and 2.7c). We believe this is the first demonstration of gliding animals modulating camber to influence aerodynamic force production. During the landing phase, the results are more difficult to interpret, with percentage camber, AoA and the aerodynamic coefficients all varying simultaneously and camber decreasing rapidly near the end of the landing. In our linear mixed-effects analysis of these results, percentage camber is significantly but negatively associated with the aerodynamic coefficients (Table 2.3). The negative relationship between percentage camber and aerodynamic coefficients may be an artifact of the multiple-linear analysis of non-linear results, or due to the dip in camber at the end of landing, or due to the post-stall aerodynamic regime reached at the end of the landing phase.

The proximity in position between the tip and the root of the wing also suggests the presence of tip vortices and their influence on the inboard portion of the wing [22]. In a low aspect ratio wing like *Draco*, the tip vortices can cover most of the wing area creating a low-pressure region above the wing. Overall, these flow structures can play a role similar to the tip vortices on a delta wing providing vortex lift [22]. Such a characteristic allows for an increase in maximum lift force and lift coefficient, and a delay of stall at higher AoA. We see *Draco* exhibiting similar features showing the importance of a compliant wing and allowing *Draco* to have at its disposal a range of AoA and lift-to-drag ratios based on the demands of the habitat and behavior.

2.4.3 Aerodynamic gliding strategy

A favorable gliding strategy for an animal would be to operate at their maximum lift-to-drag ratio to maximize their range and minimize energy losses during glide because the lift force is produced with minimal drag losses [23]. We saw strong support for such a strategy and for our hypothesis that *Draco* would vary their body orientation during the glide to enable a high lift to drag ratio during mid-glide and high lift and drag forces at landing. *Draco* steadily pitched upward throughout mid-glide, on average moving from a pitch orientation of -24° to 5° from beginning to end of mid-glide. In contrast, average AoA – the crucial parameter for determining airfoil performance – ranged between 25° to 27° during this portion of the glide. Lift to drag ratio was found to peak for *Draco* at about 26° (Figure 2.9c), implying that the in-air change in body orientation during mid-glide serves to keep the lizard at a nearly optimal configuration for maximizing glide distance. *Draco* were also found to pitch up sharply during the landing maneuver, reaching an average AoA of 35°; according to the aerodynamic analysis this approximately doubles the coefficient of drag and increases the coefficient of lift by 50%

compared to the 26° mid-glide AoA. These high coefficients along with the shallowing glide trajectory correspond to large upward and rearward forces, removing kinetic energy from the lizard through drag losses and by conversion of kinetic energy to potential energy and thus reducing the amount of remaining kinetic energy that would need to be absorbed by the body at landing.

2.4.4 Average gliding mechanics

We hypothesized that the lift to drag ratio revealed in the airfoil analysis would be consistent with the overall glide performance of *Draco*, recorded here and elsewhere. This hypothesis was also supported, in that the peak lift to drag ratio identified here was 2.9 whereas the average lift to drag ratio implied by the whole glide performance was 1.8. Because the whole glide includes the takeoff and landing maneuvers which we found were performed either without a fully extended airfoil, or while the lizard was pitching up to a landing position, or both, it is expected that the whole glide performance is less than the theoretical maximum performance. McGuire et al. (2005) reported an average glide angle range between 18° to 30° for 11 species of *Draco* for a glide distance of 9.3 m [16]. This corresponds to an average lift-to-drag ratio between 1.5 and 3 which is consistent with our results for a glide distance of 5.5 m. Bahlman et al. (2013) have reported lift-to-drag ratios in flying squirrels as high as 5 at glide distance of 15 m, however, they caution on the measurement uncertainty since the cameras were placed at the beginning of the glide, producing much uncertainty in the overall distance measurement. For glide distances between 5 and 10 m, they reported a lift-to-drag ratio of approximately 2, similar to our study [2].

2.5 Conclusion

In summary, our study of the aerodynamic performance envelope of wild-caught *Draco* lizards revealed a drag polar consistent with the whole-glide performance of *Draco* and other gliding animals and with airfoil characteristics similar to more well understood human-engineered airfoils in some respects and startlingly distinct in others. The overall shape of the drag polar was similar to engineered airfoils but occurred at much higher AoA. The magnitude of the force coefficients was high, reaching approximately 2 for lift before any indication of stall, but the maximum lift to drag ratio of approximately 2.9 was low by aircraft standards. These properties are shared with many low Reynolds number biological airfoils, including those of other gliding animals. *Draco* were found to use a broad aerodynamic performance envelope during even this limited and standardized field recording environment. Coefficients of lift and drag varied by a factor of 1.5 to 2 during each glide while AoA varied from approximately 25° to upwards of 50°. *Draco* proved unexpectedly adept at managing AoA during the glide, keeping it close to the 26° optimal value for horizontal transport throughout the mid-glide phase by changing body pitch to compensate for changes in flight direction. Finally, we showed support for *Draco* airfoil as a compliant wing revealing the likely role of airfoil camber on aerodynamic performance in a gliding animal.

REFERENCES

1. Socha JJ, Jafari F, Munk Y, Byrnes G. 2014 How animals glide: From trajectory to morphology. *Can. J. Zool.* **93**, 901–924. (doi:10.1139/cjz-2014-0013)

2. Bahlman JW, Swartz SM, Riskin DK, Breuer KS. 2013 Glide performance and aerodynamics of non-equilibrium glides in northern flying squirrels (Glaucomys sabrinus). *J. R. Soc. Interface* **10**. (doi:10.1098/rsif.2012.0794)

3. Socha JJ, Miklasz K, Jafari F, Vlachos PP. 2010 Non-equilibrium trajectory dynamics and the kinematics of gliding in a flying snake. *Bioinspiration and Biomimetics* **5**. (doi:10.1088/1748-3182/5/4/045002)

4. Khandelwal PC, Hedrick TL. 2020 How biomechanics, path planning and sensing enable gliding flight in a natural environment. *Proc. R. Soc. B Biol. Sci.* **287**. (doi:10.1098/rspb.2019.2888)

5. Hull DG. 2007 *Fundamentals of airplane flight mechanics*. (doi:10.1007/978-3-540-46573-7)

6. Thomas ALR, Taylor GK. 2001 Animal flight dynamics I. Stability in gliding flight. *J. Theor. Biol.* **212**, 399–424. (doi:10.1006/jtbi.2001.2387)

7. Song A, Tian X, Israeli E, Galvao R, Bishop K, Swartz S, Breuer K. 2008 Aeromechanics of membrane wings with implications for animal flight. *AIAA J.* **46**, 2096–2106. (doi:10.2514/1.36694)

8. Byrnes G, Libby T, Lim NTL, Spence AJ. 2011 Gliding saves time but not energy in Malayan colugos. *J. Exp. Biol.* **214**, 2690–2696. (doi:10.1242/jeb.052993)

9. Bishop KL. 2006 The relationship between 3-D kinematics and gliding performance in the southern flying squirrel, Glaucomys volans. *J. Exp. Biol.* **209**, 689–701. (doi:10.1242/jeb.02062)

10. Bishop KL. 2007 Aerodynamic force generation, performance and control of body orientation during gliding in sugar gliders (Petaurus breviceps). *J. Exp. Biol.* **210**, 2593–2606. (doi:10.1242/jeb.002071)

11. Socha JJ, O'Dempsey T, LaBarbera M. 2005 A 3-D kinematic analysis of gliding in a flying snake, Chrysopelea paradisi. *J. Exp. Biol.* **208**, 1817–1833. (doi:10.1242/jeb.01579)

12. Vernes K. 2001 Gliding performance of the northern flying squirrel (Glaucomys sabrinus) in mature mixed forest of eastern Canada. *J. Mammal.* **82**, 1026–1033. (doi:10.1644/1545-1542(2001)082<1026:GPOTNF>2.0.CO;2)

13. Suzuki K, Asari Y, Yanagawa H. 2012 Gliding locomotion of Siberian flying squirrels in low-canopy forests: The role of energy-inefficient short-distance glides. *Acta Theriol. (Warsz).* **57**, 131–135. (doi:10.1007/s13364-011-0060-y)

14. Yeaton IJ, Ross SD, Baumgardner GA, Socha JJ. 2020 Undulation enables gliding in flying snakes. *Nat. Phys.* **16**, 974–982. (doi:10.1038/s41567-020-0935-4)

15. Byrnes G, Lim NTL, Spence AJ. 2008 Take-off and landing kinetics of a free-ranging gliding mammal, the Malayan colugo (Galeopterus variegatus). *Proc. R. Soc. B Biol. Sci.* **275**, 1007–1013. (doi:10.1098/rspb.2007.1684)

16. McGuire JA, Dudley R. 2005 The cost of living large: Comparative gliding performance in flying lizards (Agamidae: Draco). *Am. Nat.* **166**, 93–106. (doi:10.1086/430725)

17. Hedrick TL. 2008 Software techniques for two- and three-dimensional kinematic measurements of biological and biomimetic systems. *Bioinspiration and Biomimetics* **3**, 034001. (doi:10.1088/1748-3182/3/3/034001)

18. Ananda GK, Selig MS. 2018 Design of bird-like airfoils. In *AIAA Aerospace Sciences Meeting, 2018*, (doi:10.2514/6.2018-0310)

19. Waldrop LD, He Y, Hedrick TL, Rader JA. 2020 Functional Morphology of Gliding Flight I: Modeling Reveals Distinct Performance Landscapes Based on Soaring Strategies. *Integr. Comp. Biol.* **60**, 1283–1296. (doi:10.1093/icb/icaa114)

20. Dickinson MH, Lehmann FO, Sane SP. 1999 Wing rotation and the aerodynamic basis of insect right. *Science (80-.).* **284**, 1954–1960. (doi:10.1126/science.284.5422.1954)

21. Holden D, Socha JJ, Cardwell ND, Vlachos PP. 2014 Aerodynamics of the flying snake Chrysopelea paradisi: How a bluff body cross-sectional shape contributes to gliding performance. *J. Exp. Biol.* **217**, 382–394. (doi:10.1242/jeb.090902)

22. Torres GE, Mueller TJ. 2004 Low-aspect-ratio wing aerodynamics at low reynolds numbers. *AIAA J.* **42**, 865–873. (doi:10.2514/1.439)

23. Willis D, Bahlman J, Breuer K, Swartz S. 2011 Energetically optimal short-range gliding trajectories for gliding animals. *AIAA J.* **49**, 2650–2657. (doi:10.2514/1.J051070)

CHAPTER 3: INDIVIDUAL VARIATION IN GLIDING BIOMECHANICS AND BEHAVIOR DUE TO BODY SIZE AND SEX

3.1 Introduction

Body size has a pervasive influence on the biomechanics of flying such that an increase in body size comes with the baggage of overcoming greater gravitational pull to stay aloft. Aerodynamic forces are produced through the interaction of the animal's body surfaces with the surrounding fluid, air, and therefore the forces increase in proportion to the surface (wing) area [1,2]. However, in the absence of positive allometric change in wing area, an increase in body size can create a scaling mismatch such that, larger animals must support themselves in the air with relatively smaller wings, potentially compromising aerodynamic performance. This is in fact the case in powered flight, where isometric scaling of wing area with body mass is observed. Mechanical power required to stay aloft in flapping flyers is determined by muscle force output and contraction frequency which scales nearly independent of body mass ($M^0 – M^{1/6}$), but available power scales negatively to the one-third body mass ($M^{-1/3}$) [3,4]. The tradeoff between the two scaling relationships sets an upper bound to the largest mass (12 – 14 kg) that a flapping flyer can attain to stay aloft under wing isometry. Thus, the overall flight performance of large birds is constrained by the limited power available for flight compared to smaller flyers that have a larger range of power output at their disposal, translating into greater flight capabilities [3].

However, because aerodynamic forces also depend on the square of airspeed [2], trade-offs due to scaling mismatch can be circumvented by increasing flight speed. This is especially applicable for gliding animals since they may not be as strongly influenced by scaling effects as

flyers that support their weight in the air through muscle-powered wing flapping. In fact, the expected aerodynamic performance of a glider, expressed as its theoretically optimal descent angle (i.e., glide angle), is determined only by the ratio of two non-dimensional aerodynamic coefficients, the coefficient of lift and the coefficient of drag, and glide performance need not suffer at all from relatively smaller wings [1]. However, although going faster preserves aerodynamic performance, it carries consequences of its own. Faster moving animals have greater kinetic energy that must be dissipated at landing, potentially increasing the chance of injury; for this reason, larger animals might use less performant aerodynamics by operating at lower lift to drag ratios to fly more slowly and avoid hard landings. Achieving higher speeds also takes time, so larger gliders that require faster speeds may exhibit lower overall performance, especially over short distances where takeoff and landing phase are larger fractions of the overall glide duration.

A single study on *Draco* by McGuire et al. (2005) has shown body size/mass to negatively affect glide performance [5]. However, these findings are based on three glide performance metrics, including maximum glide speed, average glide angle, and the total height lost for a fixed glide distance of 9.3 m. Though the results presented show strong support for larger sized *Draco* performing steeper glides, it did not show a significant relationship between glide speed and body size. Furthermore, it can be argued that total height lost and the average glide angle are two variations of the same metric. Over a fixed glide distance of 9.3 m, the average glide angle is equal to $\tan^{-1}\left({}^{9.3}/_{\text{height lost}}\right)$. Therefore, it remains unclear if a larger body size negatively affects other gliding performance metrics and if its effect varies during the glide in the takeoff, mid-glide, and landing phase. Moreover, it is unknown if larger individuals

show a difference in glide behavior and use higher aerodynamic force coefficients to compensate for their increased body mass but still achieve similar glide performance.

Aside from effects due to the confluence of aerodynamics and scaling, the locomotor performance of animals can also be influenced by external selective pressures such as predation or environment (e.g., tree density, temperature) as well as intrinsic factors such as sex of the individual [6,7]. The latter is exemplified by the disparity seen in the energetic cost of rearing young between sexes [8]. In most species, females have a higher parental investment in their offspring in terms of bearing eggs and development, whereas male fitness is solely based on the number of receptive females they have access to. Similarly, in gliding, different locomotor strategies are seen to increase fitness during the mating season, particularly with males gliding more often, or covering larger areas to increase their probability of encountering females and establish territoriality [9,10]. Brynes et al. (2011) used sensors placed on wild colugos to show that daily gliding frequency in males was double that of females and that the mean glide distance was independent of body size and sex, even though female colugos are approximately 30% larger than males [7]. Furthermore, they reported that 60% of female glides resulted in foraging bouts compared to just 36% in males, with males using 45% of the glides merely as transit points. These results strongly suggest different selective pressures to glide between sexes. However, it remains unknown if and how behavioral differences between males and females can manifest as sex-specific differences in gliding performance.

We test the effects of body size, behavior, and sex on gliding performance through a survey of the *Draco* lizards at the field site and by examining the aerodynamic performance dataset, described in Chapter 2. First, based on previous behavioral observations in *Draco* ([9,11,12] and personal observations), we hypothesize that the spatial distribution of male *Draco*

in the plantation would indicate territoriality compared to the spatial distribution in females. Second, we hypothesize that within the constraints of geometric isometric wing area scaling with body mass, larger *Draco* will glide faster, but with the same lift and drag coefficients as smaller lizards and will do so by undertaking a steeper takeoff dive to rapidly gain speed. Alternatively, if larger lizards glide at the same speed as smaller lizards, they should do so with higher lift and drag coefficients and a lower lift to drag ratio. Finally, independent of effects of body size, male *Draco* employ a shallower overall glide angle than females based on the behavioral demands of seeking mates and establishing territories.

3.2 Materials and Methods

3.2.1 Tree marking

During the survey period from 24 February until 8 March 2017, all trees in the areca nut plantation were marked with a unique letter and number combination (Figure 3.2a inset). The letters were the rows (short side of the plantation) and the numbers were the columns (long side of the plantation), together forming a grid like pattern. The markings were made with dark red ink on the tree and placed approximately 40 cm from the ground to reduce any potential influence that the markings might have on the behavior of animals in the vicinity. A total of 912 trees were marked spanning the entire length and width of the plantation resulting in a tree density of approximately 13 trees per 100 m^2.

3.2.2 Draco marking

Along with tree marking, *Draco*(s) spotted in the plantation were captured using a contraption. The contraption was made of a long aluminum pole (6 m) with a horseshoe shaped wire attached to a pliable tong at one end which was wrapped with a thick, soft padding and cloth hanging from it. The horseshoe shaped wire could be wrapped around the tree trunk above

the *Draco* and motivated the lizard to climb down on the tree or glide to a nearby tree. Once within reach, the *Draco* was caught by hand, and the tree location on which it was captured was recorded. The captured *Draco* was marked by painting a unique number using white correction ink (Kores Eraz-ex Aqua Fast Dry Correction Fluid) on the ventral side (Figure 3.1b). This was followed by measuring the mass of the lizard on an electronic balance (Figure 3.1a) and placing the lizard on a graph paper and recording images for morphometric measurements. For morphometric measurements, multiple images of the lizard were taken from the ventral and dorsal sides, with the limbs and tail almost flat on the graph paper (Figure 3.1b) and the camera lens mirror positioned parallel to the graph paper. An image was also taken with the wings spread for wing area calculations (Figure 3.1c). The lizard was then released on the same tree from which it was captured.

During the course of the entire field season, there were instances when certain *Draco* had almost lost their markings over time or due to shedding of their skin. On such occasions, the *Draco* was recaptured and given the same unique number as before. The field study resulted in a total of 33 marked individuals consisting of 16 males and 17 females.

3.2.3 Glide data collection

The glide data were recorded as previously described in Chapter 2. After completing the glide recording for a *Draco* and before releasing it back on the tree from which it was captured, mass and images were taken for morphometric analysis.

There were a few occasions when the *Draco* escaped the motion capture arena after completing a glide, and in those cases, we were not able to take morphometric measurements. In such cases, for data analysis, we took the measurements from the same *Draco* from another day which was closest to the day of the recording with the missing measurement.

3.2.4 Morphometrics

A custom MATLAB GUI was used to take multiple 2D measurements from the images of the *Draco* on the graph paper. The measurements included head width, snout-vent length, hindlimb length, tail length, body width, and wing area. Each image in the set of clicked images was calibrated by scaling the pixel distance with the real-world distance (1 x 1 cm grid) on the graph paper. Following calibration, relevant images for each measurement were chosen, and consistent markers were identified for each measurement (Figure 3.1b and 3.1c).

Head width. The distance between the two widest points on the head gave the head width measurement.

Snout-vent length. A polyline (path consisting of a series of connected segments) was used to track the length from the anterior tip of the head, following the mid-line to the beginning of the tail marked by where the hindlimbs join the body.

Hindlimb length. A two-part line was used to track the start of the hindlimb from the body to the hindlimb joint and until the ankle joint.

Tail length. A polyline was used to track the length of the tail from the vent at the posterior end of the *Draco* to the tail tip.

Body width. The widest two points in the body, excluding the head, was used for the body width measurement.

Wing area. A polyline was used to track the boundary of the stretched wing and form a closed area. The area included the body of the *Draco* but excluded the head, limbs, and tail.

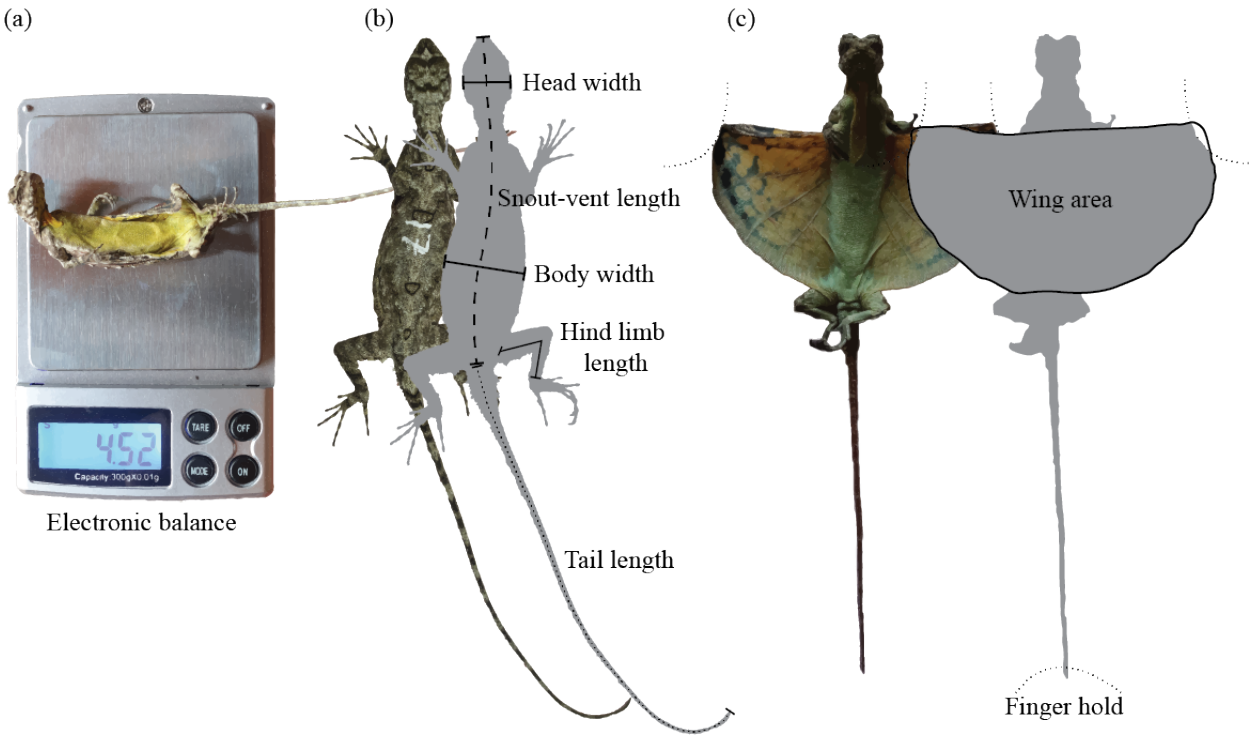

Figure 3.1 *Draco* morphometric measurements. (a) *Draco* when placed on their dorsal side, lay still. This allowed for convenient measurement of their mass using an electronic balance (resolution +- 0.01 gm). (b) and (c) Images of *Draco* on a graph paper were used to measure head width, snout-vent length, body width, hind limb length, tail length, and wing area as shown. (b) also shows one of the unique number IDs given to each *Draco* using white correction ink.

3.2.5 Territory identification

During the period from 6 March to 21 April 2017, *Draco* sightings were recorded every day between 4 pm and 6 pm. This daily time window corresponded to when the lizards were least active and potentially present in their respective territories. We ran multiple transects parallel to the long edge of the plantation covering the width of the plantation. Using binoculars, the *Draco* ID was recorded along with its location (tree ID) and activity/behavior. *Draco* sightings were not uniform during the field season with most individuals not sighted every day. *Draco* with a single sighting were removed from the territory analysis resulting in a territory dataset from 13 males and 12 females out of a total of 33 individuals.

Territories for each *Draco* were calculated by superimposing the *Draco* sighting locations on the tree distribution in the plantation. For each *Draco*, the territory was described by a circle with the center as the median of all the X and Y positions of the individual sightings. The radius of the circle or territory size was determined by fitting a kernel distribution of bandwidth 5 m to the distance of all *Draco* sightings from the territory center. From these territory centers and diameters, for each individual *Draco* we calculated the distance to the territory of the closest other same-sex individual and the number of same-sex individuals with overlapping territories.

3.2.6 Statistical methods

Univariate linear regression model (ULR) on log-transformed data was used to investigate the scaling relationship between various morphometric measurements and body size (i.e., mass). Morphometric measurements and spatial distribution across males and females were compared using a non-parametric Mann-Whitney U-test (MWU) to check for sexual dimorphism and territoriality, respectively.

A generalized mixed-effects model (GLME) approach was used to investigate the effects of body size (i.e., mass) and behavior (sex) on various performance metrics. For each performance metric, we fit three separate GLME corresponding to fixed effects of mass, sex, and the interaction between the two, and an uncorrelated random effect of intercept grouped by individual (*Draco* ID). The model with the least AIC score was selected as the appropriate model for each performance metric.

All statistical tests and calculations were performed in MATLAB version 2020a (The MathWorks, Natick, MA, USA).

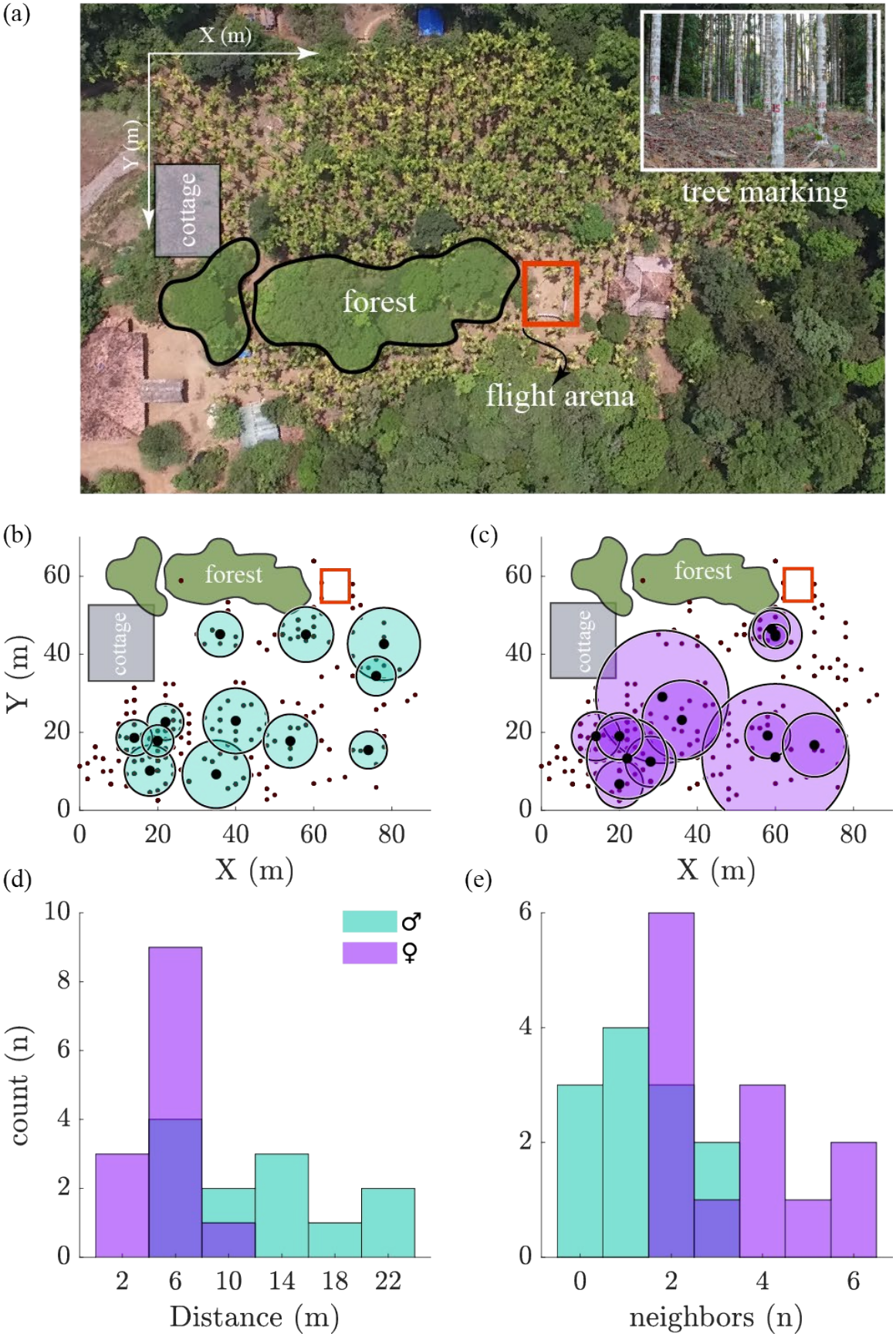
(a)
X (m)
Y (m)
cottage
forest
flight arena
tree marking
(b)
forest
cottage
Y (m)
X (m)
(c)
forest
cottage
X (m)
(d)
♂
♀
count (n)
Distance (m)
(e)
neighbors (n)

Figure 3.2 *Draco* distribution in the areca nut plantation between 6 March to 21 April 2017. (a) Top view of the field site showing the location of the cottage, forest distribution within the plantation, and the flight arena location. Inset shows the unique alphabet-number marking for each areca nut tree which was used to map the plantation and track individual *Draco* location each day. (b) Male *Draco* distribution of 12 individuals in the plantation. (c) Female *Draco* distribution of 13 individuals in the plantation. (d) Bar plot showing the frequency of the closest distance between the territory centers of the same-sex *Draco* (MWU, male – female, $p < 0.01$). (e) Bar plot showing the frequency of territory overlap between *Draco* of the same sex (MWU, male - female, $p< 0.01$).

3.3 Results

3.3.1 Draco spatial distribution

Male *Draco* (n = 12) were more spatially distanced than females (n = 13) in the areca nut plantation (Figure 3.2b, 3.2c and 3.2d). Closest neighbor distance, calculated using the territory center, ranged between 6 m to 22 m in males with a median distance of 11.51 m, and only 4 out of 12 individuals occupying territories within 6 m of each other. In females, the closest neighbor distance ranged between 2 m to 10 m with a median of 6 m, and 9 out of 13 individuals were located at a distance of 6 m from each other.

Overlapping territories was used as another metric to examine the degree of spread across individuals within the same sex (Figure 3.2b, 3.2c and 3.2e). Male territory overlap was significantly lower than females and peaked with four individuals having a territory overlap with one other individual and three individuals having no overlap. All females showed territory overlap, with six females having territory overlap with two neighbors to a maximum of two females having territory overlap with six other individuals.

3.3.2 Morphometric measurements

Morphometric comparison between males and females was performed using two sample sizes. The first (Table 3.1) represented the individuals used in the performance metric analysis (23 glides, 7 males and 6 females) and the second (Table 3.2) represented the complete set of 33

individuals sampled at the field site (16 males and 17 females). Across both samples, males and females differed in dewlap length, head width, and body width, with males having longer dewlaps and females having a wider head and body. For the smaller sample, mass and wing area were marginally significant, with females being heavier and having larger wings than males. However, the complete dataset of all males and all females captured at the site did not show sexual size dimorphism in body mass or wing area.

Table 3.1 Morphometric measurements (mean ± s.d.) of males and females and their comparison using a non-parametric Mann-Whitney U-test. The dataset used here included 13 individuals, 7 males and 6 females, which were used in the glide performance analysis presented in Chapter 3 and Chapter 4. The measurements in bold show measurements that are larger in females compared to males.

Morphometric measurement	**Males** ♂	**Females** ♀	**p**
Dewlap (cm)	2.17 ± 0.09	0.86 ± 0.13	< 0.01
Mass (gm)	5.68 ± 0.63	8.62 ± 2.52	0.05
Snout-Vent (cm)	7.92 ± 0.19	8.36 ± 0.83	0.23
Head width (cm)	1.06 ± 0.05	1.24 ± 0.10	< 0.01
Body width (cm)	1.23 ± 0.09	1.65 ± 0.23	< 0.01
Hind limb (cm)	2.31 ± 0.13	2.35 ± 0.34	0.84
Tail (cm)	11.73 ± 1.37	12.91 ± 1.52	0.14
Wing area (cm^2)	21.39 ± 1.47	27.96 ± 8.16	0.05

Table 3.2 Morphometric measurements (mean ± s.d.) of all males and females and their comparison using a non-parametric Mann-Whitney U-test. The dataset used here included 33 individuals, 17 males and 16 females, which were marked and measured during the field season. The measurements in bold show measurements that are larger in females compared to males.

Morphometric measurement	**Males** ♂	**Females** ♀	**p**
Dewlap (cm)	2.24 ± 0.19	0.81 ± 0.13	10^{-5}
Mass (gm)	5.86 ± 0.99	7.95 ± 3.23	0.16
Snout-Vent (cm)	7.81 ± 0.52	7.99 ± 0.97	0.98
Head width (cm)	1.10 ± 0.07	1.20 ± 0.13	0.02
Body width (cm)	1.24 ± 0.11	1.46 ± 0.27	0.01
Hind limb (cm)	2.14 ± 0.16	2.12 ± 0.24	0.92
Tail (cm)	12.24 ± 0.83	12.12 ± 1.60	0.58
Wing area (cm^2)	24.00 ± 4.25	25.14 ± 8.05	0.79

3.3.3 Scaling with body size

All 33 individuals were used to examine scaling relationships of various morphometric measurements with mass (body size). Isometric scaling was observed for wing area with body mass (Table 3.3). Head width and hind limb length showed strong negative allometry with mass. Tail length and snout-vent length showed slight negative allometry and body width had a slight positive allometry with mass. The dewlap is characteristically longer in males compared to females and had no relation with body mass overall but showed an isometric increase with respect to body mass within sexes.

Table 3.3 Scaling relationship (log-log) of various morphometric measurements with body size (mass). The dataset used includes all 33 individuals identified and measured at the field site. ≈ indicates isometry between the morphometric measurement and body size. ↑ indicates positive allometry and ↓ indicates negative allometry of the measurement with body size. * Dewlap showed isometry within sexes.

Morphometric measurement	**Estimate**	**SE**	**for isometry (≈)**	
Dewlap (cm)	-0.44	0.29	0.33	*
Snout-Vent (cm)	0.27	0.02	0.33	↓
Head width (cm)	0.22	0.03	0.33	↓↓
Body width (cm)	0.40	0.05	0.33	≈
Hind limb (cm)	0.19	0.04	0.33	↓↓
Tail (cm)	0.28	0.03	0.33	≈
Wing area (cm^2)	0.64	0.07	0.67	≈

3.3.4 Body mass effects

For many performance measures, the AIC indicated the data were best explained by a model with only mass as a fixed effect. Heavier and larger *Draco* used a higher average coefficient of lift and coefficient of drag during mid-glide but a lower lift-to-drag ratio for the flight arena glide distance of 5.5 m (Table 3.4, Figure 3.3a, 3.3b and 3.3c). They covered this horizontal distance using a steeper overall glide angle. Furthermore, heavier *Draco* entered the

mid-glide phase at higher speeds, attained marginally higher maximum glide speed, and transitioned into the landing phase at slightly higher speeds compared to smaller *Draco* (Table 3.4). Interestingly, the speed at touchdown was independent of body mass ($p = 0.38$) and sex ($p = 0.55$) of the individual. The average AoA during mid-glide phase was 25.6 ± 2.9° (n = 23 glides) and consistent with the observation of *Draco* maintaining an AoA of approximately 26° to maximize their lift-to-drag ratio (see Chapter 2) but was very slightly higher for larger *Draco*. The AoA at the beginning of the landing phase was significantly higher for heavier *Draco* compared to smaller ones (Table 3.4).

Table 3.4 Performance metrics with body mass as a significant predictor. The table shows the output from a GLME with body mass as a fixed effect and uncorrelated random effect of intercept grouped by individual.
Model fit: Intercept + Mass + (Intercept|Draco ID)

Metric	Estimate	SE	95% CI		t	p	SD (random effect)
			Lower	Upper			
$\overline{\boldsymbol{\theta}}$ (°) **Average glide angle**	-0.78	0.23	-1.27	-0.30	-3.34	<0.01	1.37
$\overline{\boldsymbol{C_L}}$ **Mid-glide**	0.07	0.02	0.04	0.12	4.71	<0.001	$<10^{-4}$
$\overline{\boldsymbol{C_D}}$ **Mid-glide**	0.05	0.01	0.03	0.07	5.32	$<10^{-4}$	0.02
$\overline{\boldsymbol{C_L}}/\overline{\boldsymbol{C_D}}$ **Mid-glide**	-0.07	0.02	-0.12	-0.02	-2.76	0.01	0.16
$\|\|\mathbf{v}\|\|$ (ms^{-1}) **End of takeoff**	0.05	0.02	0.01	0.08	2.88	<0.01	$<10^{-4}$
$\|\|\mathbf{v}\|\|_{max}$ (ms^{-1}) **Mid-glide**	0.06	0.03	$<-10^{-4}$	0.11	2.08	0.05	0.07
$\|\|\mathbf{v}\|\|$ (ms^{-1}) **Start of landing**	0.05	0.02	0.00	0.10	2.19	0.04	0.06
$\overline{\boldsymbol{AoA}}$ (°) **Mid-glide**	0.58	0.28	-0.01	1.16	2.04	0.05	1.75
$\boldsymbol{AoA}$ (°) **Start of landing**	1.32	0.31	0.67	1.96	4.22	<0.001	1.69

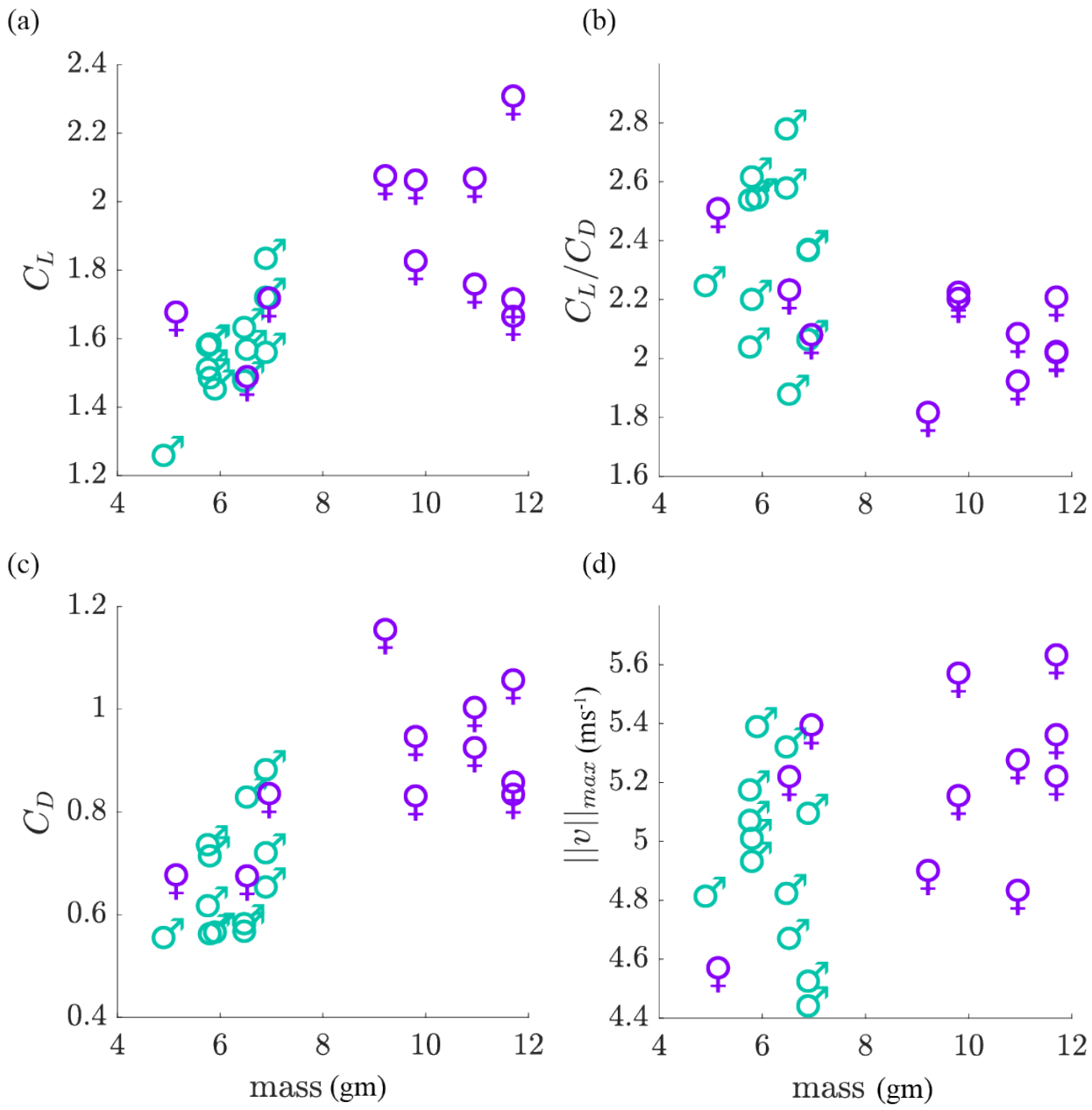

Figure 3.3 Scatter plot of aerodynamic force coefficients and maximum speed variation with mass for all 23 glides. Males are denoted by ♂ and females by ♀. (a) and (c) show a positive correlation of coefficient of lift and coefficient of drag with an increase in body size. (b) Lift-to-drag ratio decreases with an increase in body size. (d) shows a marginal positive association between with the maximum speed attained in the mid-glide phase with body size.

3.3.5 Sex specific effects

For some performance measures, the AIC indicated the data were best explained by a model with only sex as a fixed effect. Females performed a steeper dive resulting in a steeper average takeoff phase angle compared to males (Figure 3.4a). The steeper takeoff angle transitioned into females entering the mid-glide phase at higher overall acceleration compared to males (Figure 3.4b). Interestingly, the speed and acceleration at takeoff were independent of mass and sex of the individual. Finally, the touchdown height on the landing tree was lower for females compared to males but had a larger variation than males (Table 3.5, Figure 3.4c).

Table 3.5 Performance metrics with sex as a significant predictor. The table shows the output from a GLME with sex, categorized as '1' for males and '0' for females, as a fixed effect and uncorrelated random effect of intercept grouped by individual.
Model fit: Intercept + Sex + (Intercept|Draco ID)

Metric	**Estimate**	**SE**	**95% CI**		**t**	**p**	**SD** (random effect)
			Lower	Upper			
$\overline{\boldsymbol{\theta}}$ (°) **Takeoff**	3.48	1.56	0.23	6.72	2.23	0.04	1.95
$\|\|\mathbf{a}\|\|$ (ms^{-2}) **End of takeoff**	-0.55	0.21	-1.00	-0.11	-2.62	0.02	<0.001
Height (m) **touchdown**	0.41	0.16	0.07	0.74	2.52	0.02	0.22

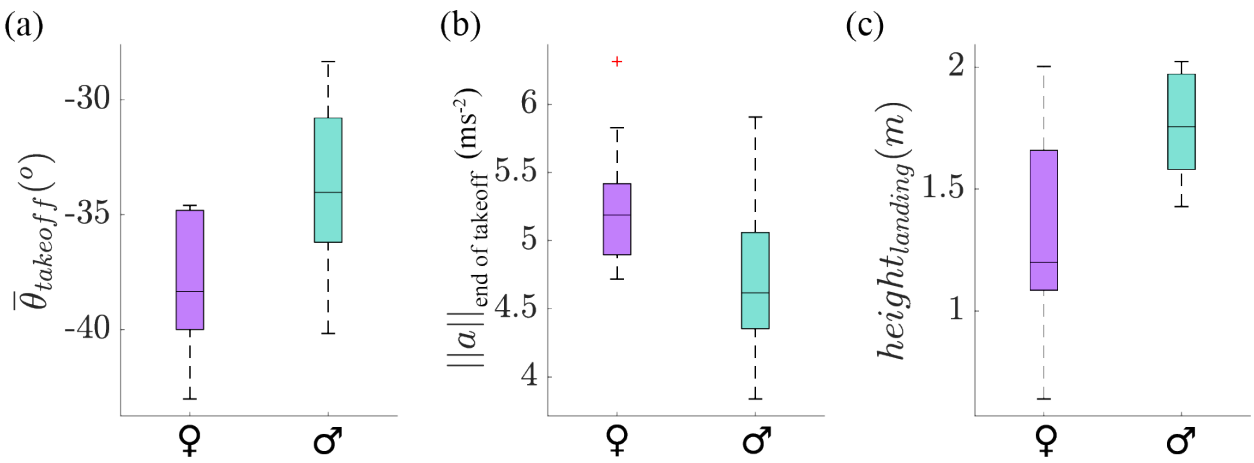

Figure 3.4 Performance metric comparison between sexes. (a) Males had shallower average takeoff angles compared to females. (b) Females entered the mid-glide phase with higher acceleration compared to males. (c) Males consistently landed higher on the landing tree within a small range of values compared to females.

3.3.6 Sex and body mass effects

For some performance measures, the AIC indicated the data were best explained by a model with only a sex*mass interaction as a fixed effect or indicated a combination of several fixed effects. Mid-glide phase showed an interesting relationship within sexes. Across sexes, males performed shallower mid-glides than females. However, within females, heavier individuals showed a steeper average mid-glide angle compared to smaller and lighter females but, in males, the relationship was inverted with larger and heavier males performing shallower mid-glides compared to smaller sized males (Table 3.6).

In the landing phase, males used a shallower approach angle for landing compared to females, but within males and females, heavier individuals displayed steeper average landing angles compared to smaller individuals (Table 3.6).

Table 3.6 Performance metrics with mass-sex interaction term as the significant predictor. Table shows the output from a GLME with mass and sex interaction as a fixed effect and uncorrelated random effect of intercept grouped by individual.
*Model fit: Intercept + Mass*Sex + (Intercept|Draco ID)*

Metric	Effect	Estimate	SE	95% CI		t	p	SD (random effect)
				Lower	Upper			
$\overline{\theta}$ (°) Mid-glide	Intercept	-31.83	2.89	-37.88	-25.78	-11.02	$<10^{-8}$	<0.001
	Sex	-17.60	7.08	-32.43	-2.78	-2.48	0.02	
	Mass	-0.65	0.30	-1.29	-0.01	-2.13	0.05	
	Sex:Mass	3.17	1.14	0.78	5.55	2.78	0.01	
$\overline{\theta}$ (°) Landing	Intercept	-10.34	4.22	-19.17	-1.50	-2.45	0.02	1.24
	Sex	21.60	10.29	0.07	43.12	2.10	0.05	
	Mass	-0.57	0.45	-1.52	0.38	-1.26	0.22	
	Sex:Mass	-3.26	1.66	-6.74	0.23	-1.95	0.06	

3.4 Discussion

We hypothesized that although body size has a pervasive effect on the biomechanics of flight, individual differences in body size would have a limited effect on glide performance such that larger individuals would glide faster, but otherwise with similar aerodynamic performance. This hypothesis was partially supported in that larger individuals did glide faster, but a number of other effects were identified that act against this outcome (see below). We also hypothesized that differences between sexes in territoriality and behavior during the mating season would be reflected in differences in gliding behavior and biomechanics that would be better explained by sex than by body size, even in the presence of sexual dimorphism. This was also supported in part as described below.

3.4.1 Morphometric scaling of Draco with respect to body mass

Draco have been previously reported to follow isometric scaling of patagium area with body size/mass. This was extensively shown by McGuire (1998) by analyzing body size data from 886 specimens representing 29 species of *Draco* [13]. Our hypotheses relating size to

gliding performance assumed isometric scaling, which predicted that larger individuals have relatively smaller wings and, therefore, should have decreased glide performance [5]. *Draco* wing area was found to scale isometrically with body mass; however, during our aerodynamic analysis (Chapter 2) we realized that using the complete airfoil area which includes the head, lappets, and the hindlimb is a more appropriate estimation of the aerodynamic surface for glide performance calculations. Therefore, we investigated scaling relationships of head width, body width, snout vent length, hind limb length and for completeness included tail length. Though wing area, body width and tail length followed isometry, snout-vent length, head width and hind limb showed negative allometry with body size (Table 3.3), suggesting that the overall lifting surface of the *Draco* could exhibit slightly negative allometry even though the patagium itself scales isometrically. In our data set of 13 individuals for glide performance, a log-log ULR of airfoil area with body mass gave a regression coefficient of 0.43 ± 0.20 (slope ± s.d., $n = 13$) which is significantly smaller than 0.67, the expected slope for isometry. However, this deviation from expectations does not conflict with any other predictions, since in either scenario, isometry or slightly negative allometry, larger *Draco* have relatively smaller lifting surfaces.

It should be noted that our scaling analysis did not consider *Draco* age and the study population may include juveniles and subadults along with adults. This does not affect the overall interpretation since ontogenetic area-mass relationship in *Draco* has been previously reported in [5] and was shown to be consistent with isometry scaling of patagium area with body mass. Nonetheless, it does raise an interesting question – do adults behaviorally compensate for the expected improved gliding performance of juveniles and subadults?

3.4.2 Male territoriality and female home range

Individual territory is defined as a spatial region that is defended against conspecifics for the purpose of using resources and access to mating opportunities [14]. A key indication of territoriality within a species can be the spatial separation of individuals in their natural habitat and the lack of spatial overlap of their territories. Territoriality in male *Draco* has been reported on several occasions; however, it has been limited to behavioral observations and to a few individuals [9,12,15]. For example, Mori et al. (1994) observed that few males (*Draco Sumatranus)* formed territories consisting of one to three adjacent trees and where one to three females were found to coexist [12]. We attempted to quantify, for the first time, territoriality in *Draco* and showed that indeed, males tend to occupy territories minimizing their spatial overlap with each other. The closest neighbor distance in males was twice that of females (Figure 3.2d) and males had reduced territory overlap with a maximum of 3 males having overlapping territories compared to 6 in females. In contrast to previous observations, we saw that *Draco* territory can span multiple trees (up to 12), but this observation might be unique to our field site since previous studies lack information on tree density for comparison.

Females, as expected, were not observed to form territories based on our criteria and instead formed a home range with some home ranges having complete spatial overlap with other females. Each female home range could be associated with at least one male territory with a maximum number of 3 females seen within a single male territory. From personal observation, the male territory with 3 females was adjacent to the flight arena, and the male could be seen actively chasing away males throughout the field season; at times, voluntarily gliding to the takeoff tree in the flight arena to chase the male captured by us for video recordings. Four out of

12 male territories did not overlap with any female home range suggesting that these males could be ‘non-residents’ in search of a territory [9].

Quantifying territory size is an important first step to test the hypothesis based on the sexual selection model, which predict that smaller male size provide a locomotor performance advantage compared to larger males while defending territories and/or larger male size might provide increased bite force advantage during male-male competition [15]. Though our data does not show a correlation of male territory size with *Draco* size (body mass and head width), or locomotor performance (observed maximum glide speed in the flight arena), we believe our study lays the groundwork to test such a hypothesis using a more robust and direct measurement.

3.4.3 Effect of body mass on glide performance

Due to isometric and/or negative allometric scaling of airfoil area with body mass, aerodynamic theory dictates that larger individuals are poor gliders compared to smaller individuals [1]. That is, larger individuals would have less surface area available per unit mass to generate lift forces to stay aloft [13]. Therefore, it is reasonable to expect, in the absence of behavioral or physiological compensation, larger *Draco* would perform less well over a fixed glide distance [5].

McGuire et al. (2005) showed that for a fixed glide distance of 9.3 m, larger *Draco* performed steeper glides, lost more height, and achieved higher maximum glide speed compared to smaller sized *Draco* [5]. Though this study showed larger individuals performing less favorable steeper glides, it lacked the resolution to investigate performance changes of body size with glide progression, aerodynamic performance, and variation in fundamental factors that influence aerodynamic performance such as AoA and camber.

Somewhat counter-intuitively, heavy gliders do not necessarily have worse aerodynamic performance than lighter gliders because the most common single expression for glide performance, the minimum glide angle (mathematically determined by the maximum lift to drag ratio) does not vary with size. However, to achieve this performance, heavier gliders must fly faster than lighter gliders [1] or undertake behavioral changes to affect other performance trade-offs. We saw a combination of both strategies at play. Larger *Draco* attained higher speed during the transition from takeoff to mid-glide phase (Table 3.4). Since the speed and acceleration immediately after the takeoff jump was independent of body size, a higher speed at the end of takeoff could be achieved from a steeper ballistic dive or delaying wing opening to maintain a more streamlined body while using similar takeoff angles. It should be noted that both strategies are likely to lower the overall glide angle even while preserving mid-glide performance. Though we saw sex to be a better predictor for takeoff angles (Table 3.5), i.e., females performed steeper takeoff than males, we believe this also indicates that larger *Draco* undertake a relatively steeper takeoff since females did cover the upper end of the body mass spectrum in our data set. Furthermore, preliminary data on wing deployment timings in males and females indicated that females might actually achieve complete wing extension marginally before males, further supporting the idea of larger *Draco* using relatively steeper takeoff angles.

In the mid-glide phase, as expected, the flight speed continued to increase, but surprisingly the maximum glide speed achieved was only marginally higher in larger *Draco* compared to smaller ones ($p = 0.05$), suggesting a potential behavioral compensation undertaken by larger *Draco*. We identified highly significant increases in the coefficient of lift and coefficient of drag with increasing body mass (Table 3.4). These effects act to increase the aerodynamic forces produced per unit airfoil area and allow larger individuals to support their

weight in the air at slower flight speeds. However, an increase in the lift and drag coefficients is also expected to decrease their ratio, an effect also significantly present in our data, along with a significant increase in AoA for larger individuals that explains how they might produce the higher force coefficients.

Finally, larger *Draco* entered the landing phase at significantly higher AoA compared to smaller individuals (Table 3.4). Aerodynamic theory shows that at higher AoA, the coefficient of drag increases rapidly compared to the coefficient of lift [16] (also see Chapter 2). This translates to an overall lower lift-to-drag ratio with slower flight speeds and steeper descents (see discussion on mass and sex interaction). Interestingly, we saw touchdown speed to be independent of body size, potentially a consequence of larger *Draco* using higher AoA during landing and suggesting that landing safely may therefore be more of a constraint than expected on *Draco* glide performance. Previously, we had shown that *Draco* touchdown speed was independent of gliding distance [17] (also see Chapter 4). A similar observation was also noted by Byrnes et al. (2008) where they saw the landing force and the landing impulse duration in colugos to be independent of glide duration, suggesting that colugos modulate their aerodynamic forces prior to landing to have a safe impact [18].

Thus, we find evidence that not only does increasing body size have the expected aerodynamic effect of increasing flight speed, but this effect also appears to produce a secondary response where larger *Draco* use higher but less optimal force coefficients to fly more slowly than their size would otherwise demand, potentially to land safely.

3.4.4 Sex related effects on Draco glide performance

Although our analysis of *Draco* territoriality supports the underlying reasoning for our hypotheses of differing glide behavior and biomechanics associated with sex, in practice few of

these metrics were most strongly associated with sex. This may be due in part to the trend toward female-biased dimorphism in our species of *Draco* [19]; because females are larger than males and because body size has pervasive effects on the biomechanics of flight it may be difficult to statistically support sex-related effects on top of the physically necessary size-related effects. Nevertheless, we saw that females used slightly steeper takeoff angles compared to males, which resulted in a significantly higher acceleration at the start of the mid-glide phase (Table 3.5). Intuitively, it makes sense to relate higher acceleration to higher overall glide speed. However, we saw that body mass was a better predictor of flight speed at the beginning of the mid-glide phase compared to sex. Such an effect may be attributed to sexual size dimorphism with females being heavier in our data set of 13 individuals used for glide performance analysis (Table 3.1).

During mid-glide, males performed shallower glides than females, further corroborating our intuition that gliding performance might be linked to the behavioral outcomes of the individual. That is, a shallower and therefore more efficient glide will facilitate males performing glides more frequently to seek mates and defend territories [12], which has also been hypothesized as one of the many reasons for the evolution of female-biased dimorphism in *Draco* [9,21]. Surprisingly, we saw a body size effect within sexes where body size was negatively correlated with average mid-glide angle in males but positively correlated in females. That is, bigger males performed shallower mid-glides than smaller males, but larger females performed steeper mid-glides than smaller females (Table 3.6). Though our inferences are drawn from a small sample size, it raises a few interesting insights which are worth pursuing in the future.

First, since male body mass in our analysis data set ranged between 4.6 gm to 6.6 gm (5.68 ± 0.63 gm, mean ± s.d., n = 7) and female body mass was between 4.8 gm to 11.5 gm (8.62

± 2.52, mean ± s.d., n = 6), it is reasonable to expect that our sample size did include at least subadults if not juveniles. An opposite correlation between sexes for mid-glide angle with body mass might suggest that adult males behaviorally overcompensate, operating at higher AoA and flight speed than similarly sized females. Second, our finding may represent sex-specific ontogenetic variation in behavioral responses with body size; smaller (juveniles/subadults) males showing poorer behavioral response than larger males (adults) towards modulating glide performance. An alternate perspective is that our observations relate to the fundamental behaviors of foraging, mating, evading predators and territoriality in gliding animals [20]. For example, there may be selection for adult males to better compensate for large body size, allowing them to effectively seek mates and defend territories. On the other hand, females do not glide to actively seek mates ([11] and personal observation) and do not form territories ([9,11,12] and Figure 2), therefore not showing any behavioral overcompensation in their gliding performance.

Finally, in the landing phase, we saw males using shallower average landing angles compared to females and in both sexes, larger individuals showed slightly steeper average landing angles. The height at touchdown was higher and less variable for males (1.75 ± 0.15 m, n = 7) compared to females (1.36 ± 0.38 m, n = 6). Although the higher landing height in males is a consequence of the physics of gliding, the smaller variation in landing height might imply that males prefer to land higher which will ultimately reduce their climbing and transition time into the next glide. The small variation in male landing height is in contrast with the findings of McGuire et al. (2005) which showed that smaller individuals had larger variation in landing heights, with the rationale that smaller individuals have greater flexibility with respect to glide performance compared to larger individuals for a given glide distance [5]. However, it should be

noted that McGuire et al. (2005) did not consider the sex of the individual and used only adult *Draco* in their study.

3.5 Conclusion

Overall, our study presents a compelling case for body size, behavior, and sex simultaneously influencing gliding performance in *Draco*. We show that gliding performance is driven by the evolutionary pressures acting on the individual while also operating within the individual's physical limits dictated by aerodynamic theory. For example, we show that territoriality and mating behavior potentially lead to males performing shallower mid-glide and landing phases than females, but the overall glide angle is still influenced by the physics of scaling in both sexes, with larger individuals exhibiting steeper glides overall. We show that larger individuals compensate for the reduced glide performance by using higher AoA in combination with marginally higher flight speeds to operate at higher coefficients of lift and drag but lower lift-to-drag ratio. Moreover, adult males potentially overcompensate for their size compared to similarly sized females and outperform smaller males in the mid-glide phase, demonstrating the selective pressures that shape an individual's locomotor performance. Finally, we hope that our study shows the importance of studying animal performance within the ecological and biomechanical context in which it resides.

REFERENCES

1. Norberg UM. 1990 *Vertebrate flight: mechanics, physiology, morphology, ecology and evolution*. (doi:10.5860/choice.28-0296)
2. In press. The Simple Science of Flight | The MIT Press. See https://mitpress.mit.edu/books/simple-science-flight (accessed on 23 December 2020).
3. Dial KP. 2003 Evolution of Avian Locomotion: Correlates of Flight Style, Locomotor Modules, Nesting Biology, Body Size, Development, and The Origin of Flapping Flight. *Auk* **120**, 941–952. (doi:10.1093/auk/120.4.941)
4. Ellington CP. 1991 Limitations on Animal Flight Performance. *J. Exp. Biol.* **160**.
5. McGuire JA, Dudley R. 2005 The cost of living large: Comparative gliding performance in flying lizards (Agamidae: Draco). *Am. Nat.* **166**, 93–106. (doi:10.1086/430725)
6. Irschick DJ, Higham TE. 2016 *Animal Athletes*. Oxford University Press. (doi:10.1093/acprof:oso/9780199296545.001.0001)
7. Byrnes G, Lim NTL, Yeong C, Spence AJ. 2011 Sex differences in the locomotor ecology of a gliding mammal, the Malayan colugo (Galeopterus variegatus). *J. Mammal.* **92**, 444–451. (doi:10.1644/10-MAMM-A-048.1)
8. Fokidis HB, Risch TS. 2008 The burden of motherhood: Gliding locomotion in mammals influences maternal reproductive investment. *J. Mammal.* **89**, 617–625. (doi:10.1644/07-MAMM-A-116R1.1)
9. Mori A, Hikida T. 1993 Natural History Observations of the Flying Lizard, *Draco Volans Sumatranus* (Agamidae, Squamata) From Sarawak, Malaysia. *Raffles Bull. Zool.* **41**, 83–94.
10. Socha JJ, Jafari F, Munk Y, Byrnes G. 2014 How animals glide: From trajectory to morphology. *Can. J. Zool.* **93**, 901–924. (doi:10.1139/cjz-2014-0013)
11. K.O. John. 1967 *Observations on the mating behaviour and copulation in Draco dussumieri Dum. & Bib. (Reptilia: Sauria)*. See https://www.biodiversitylibrary.org/part/152900.
12. Mori A, Hikida T. 1994 Field observations on the social behavior of the flying lizard, Draco volans sumatranus, in Borneo. *Copeia* , 124–130. (doi:10.2307/1446678)
13. McGuire JA. 1998 Phylogenetic Systematics, Scaling Relationships, and the Evolution of Gliding Performance in Flying Lizards (Genus Draco). *Fac. Grad. Sch. Univ. Texas Austin*
14. Potts JR, Lewis MA. 2014 How do animal territories form and change? lessons from 20 years of mechanistic modelling. *Proc. R. Soc. B Biol. Sci.* **281**, 20140231. (doi:10.1098/rspb.2014.0231)
15. Husak JF, Mcguire JA. 2014 Does ‘gliding while gravid’ explain Rensch’s rule in flying lizards? *Biol. J. Linn. Soc.* **113**, 270–282. (doi:10.1111/bij.12319)

16. Hull DG. 2007 *Fundamentals of airplane flight mechanics*. (doi:10.1007/978-3-540-46573-7)

17. Khandelwal PC, Hedrick TL. 2020 How biomechanics, path planning and sensing enable gliding flight in a natural environment. *Proc. R. Soc. B Biol. Sci.* **287**. (doi:10.1098/rspb.2019.2888)

18. Byrnes G, Lim NTL, Spence AJ. 2008 Take-off and landing kinetics of a free-ranging gliding mammal, the Malayan colugo (Galeopterus variegatus). *Proc. R. Soc. B Biol. Sci.* **275**, 1007–1013. (doi:10.1098/rspb.2007.1684)

19. John KO. 1962 Notes on The. Bionomics of the Flying Lizard, Draco Dussumieri Dum. & Bib. *J. Bombay Nat. Hist. Soc.* **59**, 298–301.

20. Socha JJ, Jafari F, Munk Y, Byrnes G. 2014 How animals glide: From trajectory to morphology. *Can. J. Zool.* **93**, 901–924. (doi:10.1139/cjz-2014-0013)

21. Shine R, Keogh S, Doughty P, Giragossyan H. 1998 Costs of reproduction and the evolution of sexual dimorphism in a 'flying lizard' Draco melanopogon (Agamidae). *J. Zool.* **246**, 203–213. (doi:10.1111/j.1469-7998.1998.tb00149.x)

CHAPTER 4: HOW BIOMECHANICS, PATH-PLANNING AND SENSING ENABLE GLIDING FLIGHT IN A NATURAL ENVIRONMENT[1]

Gliding animals traverse cluttered aerial environments when performing ecologically relevant behaviors. However, it is unknown how gliders execute collision-free flight over varying distances to reach their intended target. We quantified complete glide trajectories amid obstacles in a naturally behaving population of gliding lizards inhabiting a rainforest reserve. In this cluttered habitat, the lizards used glide paths with fewer obstacles than alternatives of similar distance. Their takeoff direction oriented them away from obstacles in their path and they subsequently made mid-air turns with accelerations of up to 0.5 g to reorient towards the target tree. These maneuvers agreed well with a vision-based steering model which maximized their bearing angle with the obstacle while minimizing it with the target tree. Nonetheless, negotiating obstacles reduced mid-glide shallowing rates, implying greater loss of altitude. Finally, the lizards initiated a pitch-up landing maneuver consistent with a visual trigger model, suggesting that the landing decision was based on the optical size and speed of the target. They subsequently followed a controlled-collision approach towards the target, ending with variable impact speeds. Overall, the visually guided path-planning strategy that enabled collision-free gliding required continuous changes in the gliding kinematics such that the lizards never attained theoretically ideal steady state glide dynamics.

[1] This chapter previously appeared as an article in the Proceedings of the Royal Society B. The original citation is as follows: Khandelwal Pranav C. and Hedrick Tyson L. 2020 How biomechanics, path planning and sensing enable gliding flight in a natural environment. Proc. R. Soc. B.28720192888
http://doi.org/10.1098/rspb.2019.2888

4.1 Introduction

Terrestrial habitats are complex spatial structures, frequently traversed by animals to perform behaviors essential for their survival. Different modes of locomotion necessitate that animals use varied biomechanical strategies and sensory inputs to precisely navigate their environment while maintaining physical stability and speed. For example, on land, scrub lizards normally use quadrupedal running but reduce their sprint speed to negotiate obstacles with occasional switches to bipedal running [1]. Cockroaches use a mechanically mediated strategy, taking advantage of their body shape and mechanical feedback from the environment to reorient their body while moving through clutter [2]. Unlike terrestrial locomotion, volant taxa have an added constraint of maintaining minimum lift to stay aloft, either from flapping and/or maintaining forward speed. To maneuver, flying birds reduce forward speed and increase flapping frequency to perform turns mid-air [3]. Altogether, such strategies involve generating directional forces, along with propulsive forces, to alter the animal's path to either negotiate an obstacle or reorient towards the desired target. Gliding animals power flight by trading altitude for kinetic energy to ultimately generate lift for locomotion, facing the additional constraint of a finite energy supply for powering maneuvers. Furthermore, gliding taxa often have simpler wing anatomy with fewer degrees of freedom than flapping flyers such as birds or bats. Despite such limitations, gliders like colugos, squirrels, snakes, and lizards thrive in dense forests presenting complex 3D spatial geometries. They frequently glide to forage, seek mates, defend territories and avoid predators [4], behaviors that have direct fitness consequences. Collision-free flight is key to their survival, yet how animals execute such glides in their natural habitat remains unclear.

Among gliding terrestrial vertebrates, laboratory studies have described the mechanics of parts of the glide in detail, including takeoff and landing in flying squirrels and sugar gliders [5–9]. These studies produced high-resolution kinematic data of the animal but lacked information of the behavioral context and entirety of the glide which might be crucial to understanding the observed outcomes. Additionally, captivity and a laboratory setting might limit or influence the animal's behavior. Field studies have explored gliding behavior using animal-borne data loggers in colugos, providing takeoff and landing kinematics [10] and energetic costs of gliding [11]. Field recordings on flying lizards have described simple glide metrics such as glide angle and ratio in 2D along with speed and acceleration estimates [12]. Non-equilibrium gliding biomechanics of wild flying squirrels and snakes has been studied while departing from a single takeoff location with limited landing options [13,14]. While data loggers do not capture body shape changes undertaken by the animal or the environmental context, video recordings limit the spatial scale at which gliding can be observed. Furthermore, observational studies on Siberian flying squirrels have shown gliding patterns to be related to the forest structure, capturing the environmental context but lacking kinematic details [15,16]. Thus, the above studies look at specific aspects of the glide, but none offer a holistic view of gliding biomechanics in the animal's natural habitat. We used an ultra-portable 3D stereo videography setup to study locomotory strategies employed by wild, freely behaving flying lizards (*Draco dussumieri*) traversing a naturally cluttered habitat. This video tracking approach captured the lizard's motion covering the entire takeoff to landing duration along with the environmental features which it might have encountered while gliding. The resulting dataset incorporated the combined effect of behavior and the environment on the gliding biomechanics of the animal, allowing us to address the following hypotheses.

We hypothesized that in a natural environment, flying lizards would use a glide profile including a ballistic descent to gain speed followed by a non-equilibrium mid-glide to cover distance and negotiate obstacles, and finally a swoop-up landing maneuver to decelerate and reduce the energy dissipated at impact. Our expectation of non-equilibrium glide kinematics is in contrast to previously reported equilibrium glides in *Draco* between fixed takeoff and landing poles [12], but similar to observations in flying squirrels [4,13]. Next, a cluttered environment may present obstacles that will require flying lizards to execute lateral maneuvers. Producing such maneuvers requires either a reduction in upward force or an increase in total lift, both leading to a greater loss of altitude (energy) for a given glide distance. Hence, we hypothesized that lizards would preferentially use a path planning strategy to minimize the energetic losses due to maneuvering. Alternatively, lizards may simply avoid glides that require them to fly around an obstacle, restricting them to glide distances similar to the average spacing between trees in their habitat. Lastly, we assumed vision to be the primary sensory modality used by *Draco* to navigate their natural habitat. In this case, the spatial uncertainty of environmental features (obstacles and targets) increases with glide distance. Thus, we hypothesized that lizards control their heading direction based on an existing vision-based obstacle-avoidance steering model [17], but may reactively respond to potential obstacles mid-air during longer glides. Furthermore, we assumed that lizards use their optical flow field to derive the distance and approach speed to the landing tree. Therefore, we predicted that they initiate their landing approach based on a critical value of the optical size and speed of the target as described by the 'relative retinal expansion velocity (RREV)' model, as has been previously reported in groups as diverse as fruit flies and birds [18–20].

4.2 Methods

4.2.1 Field site

The field site was a ~115 x ~60 m abandoned areca nut (*Areca catechu*) plantation located within the Agumbe Rainforest Research Station (ARRS) campus, Karnataka, India (13°31'04" N, 75°05'18" E). The site was enclosed by open habitat on the east, and a mix of open habitat and tropical rainforest on the other sides. The site contained ~912 areca nut trees (~13 trees per 100 m^2) mixed with scattered local flora. The trees were ~10 cm to ~ 20 cm in diameter, ~5 m to ~23 m tall and had an inter-tree distance of ~1.5 m to ~8 m, providing areas of varying tree clutter. A population of flying lizards (*Draco dussumieri*) inhabited the plantation during the breeding season (February - May). The number of lizards at the field site during data collection was unknown, but a study at this site in 2017 identified 33 individuals (16 males), i.e. ~4.7 lizards per 1000 m^2 [21].

4.2.2 Animals

Our study species *Draco dussumieri* is a medium-sized flying lizard (max snout-vent length = 9.7 cm [22]), endemic to the Western Ghats region of southern India. They are found inhabiting plantations, secondary, and evergreen forests ranging from 80 to 1300 m elevation above sea level [23]. The lizards are diurnal and use gliding as the main mode of locomotion to traverse among trees in their natural habitat [24]. Unlike other gliding animals, *Draco* glide using a unique primary wing composed of membrane attached to a set of 5-7 elongated ribs on either side [25]. When gliding, the wings are stretched open by rotating the ribs laterally. Secondary force-generating structures include lappets on the lateral margins of the head along with almost planar fore and hind limbs. During the landing phase of the glide, the ribs collapse medially, folding the wings and facilitating movement on trees. Frequent glides can be observed by lizards

during the mating season (Feb-May) as the lizards forage, defend territories (male-male encounters) or seek mates (male-female encounters).

4.2.3 Data collection

Glides were recorded from freely behaving lizards moving about an abandoned plantation (Figure 4.1a). A stereo videography technique was used to record 33 voluntary glides from 10th to 14th March 2015 (9 am until 5 pm daily). Active lizards were identified, and their glide direction and timing were predicted based on their movement on a tree, dewlap activity, and presence of conspecifics in the vicinity. Male and female gliding lizards were identified based on their dewlap size, with males having longer dewlaps than females [1]. Three cameras (GoPro Hero4 Black, GoPro, Inc.) were placed in a staggered orientation with overlapping fields of view (diagonal FOV = 133.6^{o}) covering the expected glide location of active lizards (Figure 4.1a). Recording durations ranged from ~1 min to ~9 min depending on how soon the glide was performed. The glide recording was followed by a scene calibration procedure of moving a wand of known length (0.97 m) through the common camera viewing volume to set the scale of the scene and measure the extrinsic camera parameters [2]. The trees or the corner of the cottage (Figure 4.1a) located on the field site were used to align the scene with gravity such that the Z axis was antiparallel to gravity. Finally, an audio synchronization tone was recorded to temporally align the individual camera frames [3]. We used a range of the possible temporal and pixel resolutions available in the cameras while seeking the best possible combination; glides were recorded at 120 fps (1920x1080p) on day 1, 80 fps (1920x1440p) on day 2 and 3, followed by 60 fps (2704x1520p) on day 4 and 5. The camera recording rate had no effect on the calculated maximum acceleration values (Wilcoxon rank sum test, $p > 0.3$).

4.2.4 Data processing and analysis

3D data ([x,y,z] coordinates) for each glide were obtained by manually digitizing the body midpoint (Figure 4.2a) of the lizards using the MATLAB (The MathWorks, Natick, MA, USA) package DLTdv [4]. The glide tracks were smoothed and interpolated using a smoothing quintic spline weighted by their 95% confidence intervals. The interpolated points accounted for a total of 6.42% of the total clicked points (171 out of 2664 points). The 95% confidence intervals themselves were computed from the reprojection error of the 3D point with respect to the measured 2D points; the median confidence intervals for the x, y and z directions were 0.0069, 0.0097 and 0.0108 m. The first and second derivatives with respect to time were computed by differentiating the spline polynomials. The smoothed digitized glide track was used to identify and mark surrounding treetops along the glide path. We overlaid the manually digitized glide track on top of the video from each camera. By visualizing the environment along with the complete glide track for each camera view, we were able to identify the trees along the glide path. The treetops of the identified trees were then tracked across all camera views to reconstruct the treetop point in 3D. The 3D points of all the identified treetops were used to identify the obstacle tree (based on the obstacle tree criteria) and also calculate the height of the tree. The [x,y] tree coordinates specified the location of the tree, and the [z] coordinate corresponded to the tree height. Each glide along with its surrounding trees was rotated and translated to place the takeoff tree on the origin and the landing tree on the positive X axis. The [x,y,z] track coordinates were used to calculate kinematic parameters of the glide including velocity, acceleration, instantaneous radius of curvature and centripetal acceleration. Basic glide metrics such as glide distance, glide ratio, average glide angle ($\bar{\theta}$) and instantaneous glide angle

(θ) were also calculated (Figure 4.2a). These metrics and others reported in the supplementary table were defined as follows –

Average glide angle (°). The angle made with the horizontal in the X-Z plane, from the start to the end of each phase. A more negative glide angle corresponded to a steeper section of the glide along the vertically downward direction.

Instantaneous glide angle (°). The angle made with the horizontal in the X-Z plane at every instant of time.

Glide distance (m). The distance along a straight path in the X-Y plane, joining the takeoff and landing tree.

Glide ratio. The ratio of the glide distance with loss in altitude for the complete glide. For example, a glide ratio of 2 would imply that the glider covers 2 units of distance for a loss of 1 unit in altitude.

Obstacle angle. The absolute angle made by the obstacle tree with the takeoff tree in the X-Y plane.

4.2.5 Glide phases

We developed consistent definitions for dividing complete glides into takeoff, mid-glide and landing phases based on characteristic changes in centripetal acceleration and horizontal speed (Figure 4.1b).

Takeoff consisted of jumping from the takeoff tree followed by wing deployment. These morphological adjustments resulted in an increase in aerodynamic lift force with lizards transitioning from a mostly downwards to mostly forward motion. During this transition, the resultant aerodynamic force vector momentarily aligned with the velocity vector of the lizard, leading to a minimum in the centripetal acceleration curve. We used this centripetal acceleration

minima in each glide track to mark the end of takeoff. *Mid-glide* followed takeoff as the lizard proceeded towards the eventual landing tree. The mid-glide phase usually consisted of the highest overall glide speed and a continuously shallowing instantaneous glide angle. The end of the mid-glide phase was marked by the instant at which the lizard began to decelerate in the horizontal plane. *Landing* began with a decrease in horizontal speed and ended when the lizard reached the target tree. During landing, lizards continuously increased their body pitch and, just before contact, moved their forelimbs forward, their head back relative to their spine, and collapsed their wings.

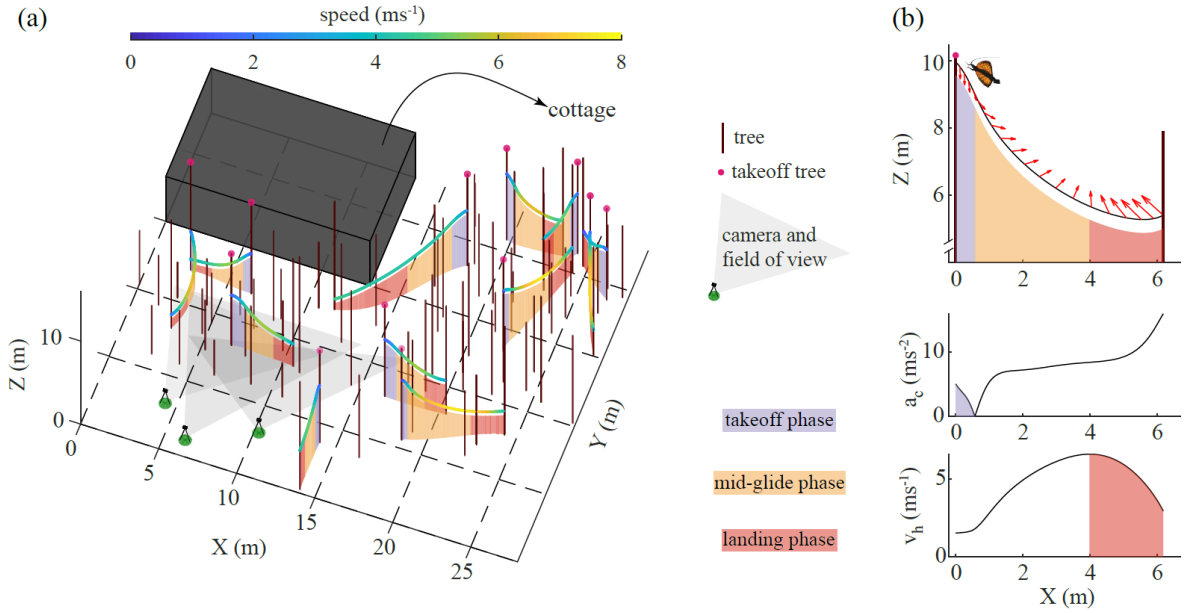

Figure 4.1 A scaled illustration of part of the field site, trajectories and glide phases. (a) An overview of part of the field site showing the distribution of trees and the trajectories of 11 out of 26 glides along with a sample camera array and a schematic of the field site cottage. Each glide is color-coded based on the speed of the lizard and divided into takeoff, mid-glide and landing phases. (b) Panel shows the side profile of a representative glide along with the behavior and use of the kinematic parameters to divide each glide into takeoff, mid-glide and landing phases. The red arrows show the acceleration vectors in the X-Z plane at various instants of time along the glide path, transitioning from an almost vertically downwards (takeoff) to nearly horizontal in the forward direction (mid-glide) to vertically backwards for landing. The first minima in the centripetal acceleration (a_c) curve corresponds to the end of the takeoff phase where the acceleration vector aligns with the velocity vector. The landing phase begins with deceleration in horizontal speed (v_h). The part of glide between takeoff and landing forms the mid-glide phase.

4.2.6 Environmental effects - obstacles

The surrounding trees along the glide path were analyzed as obstacles to locomotion. To simplify the analysis and modelling, the tree with the smallest orthogonal distance (d_y) from a straight path between the takeoff and landing tree was defined as the obstacle for that glide (Figure 4.2c). The obstacle was quantified by defining the absolute angle (γ) subtended by the obstacle tree on the takeoff tree in the horizontal plane, as shown in Figure 4.2c. The effect of the obstacle on the lizard's trajectory was quantified via takeoff direction (β, Figure 4.2c) and the lateral acceleration (a_y) while passing the obstacle (a_{yO}), each calculated in the horizontal plane. Furthermore, we modelled the lizard as a simple fixed-wing glider to calculate the roll angle (Equation 1) required to generate the observed a_{yO} and thus infer losses in the aerodynamic lift force due to obstacles (Figure 4.2d).

$$Roll\ angle = tan^{-1}\left(\frac{a_{yO}}{a_{zO}+9.81}\right) \quad \text{.....(1)}$$

where at the instant of passing the obstacle, a_{yO} is the observed lateral acceleration and (a_{zO} + 9.81) is the upward acceleration after accounting for body weight.

Lastly, to understand the influence of γ on landing tree choice, we simulated a forest with a tree distribution representative of the field site and calculated γ's for all possible combinations of takeoff and landing trees having a glide distance of less than 12 m. We then compared the recorded γ with the median of the simulated γ distribution for the observed glide distances to check for landing tree preferences in flying lizards.

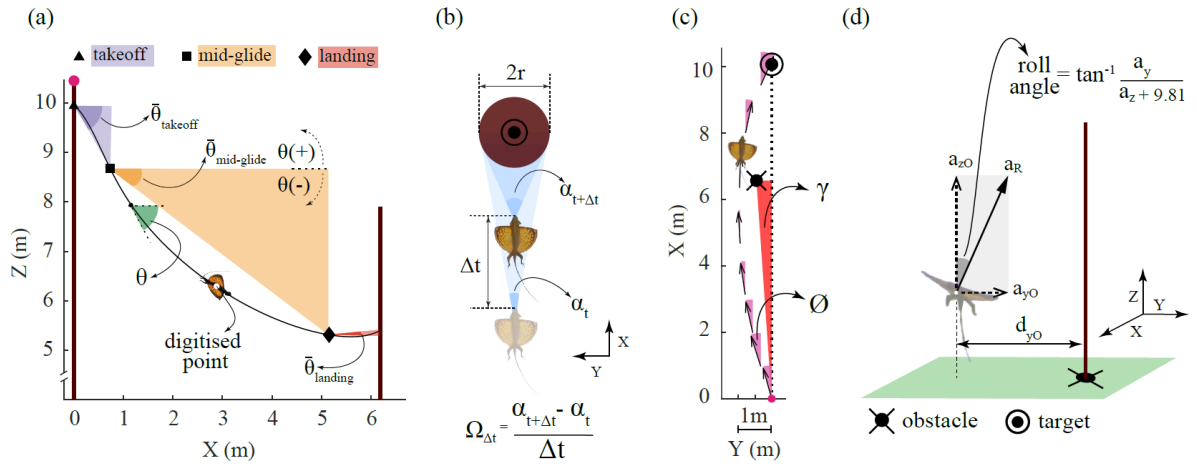

Figure 4.2 An illustration of the calculated glide parameters. (a) Calculation of the average takeoff ($\bar{\theta}_{takeoff}$), mid-glide ($\bar{\theta}_{mid\text{-}glide}$) and landing ($\bar{\theta}_{landing}$) angle. The instantaneous glide angle (θ) was used to calculate the shallowing rate of the mid-glide phase. (b) Overhead view (X-Y plane) of lizard approaching the target tree of radius 'r' at two instants of time separated by Δt. The retinal size of the target changes from α_t to $\alpha_{t+\Delta t}$ such that the retinal expansion velocity is $\Omega_{\Delta t}$ at time instant (t + Δt). (c) Overhead view (X-Y plane) showing the calculation of obstacle angle (γ) and the instantaneous heading angle (ϕ). (d) Front view (Y-Z plane) of the lizard at the instant of crossing the obstacle, showing the calculation of the modelled roll angle and the orthogonal distance (d_{yO}) from the obstacle tree.

4.2.7 Visual landing control

We used the RREV model, also known as the τ strategy, to predict the initiation of a landing response during the glide [19,20]. This model suggests a critical value of the ratio of retinal expansion velocity (Ω) to the retinal size (α) of the landing tree where lizards initiate a deceleration response. The required quantities were calculated as follows [20],

$$RREV = {}^{\Omega}/_{\alpha} = {}^{1}/_{\tau} \quad \text{.....(2)}$$

$$\alpha = 2sin^{-1}\left({}^{r}/_{d}\right) \quad \text{.....(3)}$$

$$\Omega = \frac{d\alpha}{dt} = \frac{-2v_h(r/d^2)}{\sqrt{1-(r/d)^2}} \quad \text{.....(4)}$$

where r = 0.10 m (assumed radius of the landing tree), d is the distance of the lizard from the landing tree in the horizontal plane and v_h is the horizontal speed (Figure 4.2b).

We implemented the model by aligning all glides greater than 2 m to begin their landing phase at $t = 0$ s, with $t > 0$ s corresponding to further into the landing phase (Figure 4.7a). Glides less than 2 m (n = 2) matched the average tree spacing in the field site and, due to their proximity, may not require a landing trigger. The critical RREV value was calculated as the minima in the coefficient of variation (c.v.) of RREV values between -0.5 s and 0.1 s across all glides (Figure 4.7a).

4.2.8 Steering model

We used an obstacle-avoidance steering model to understand how lizards adjusted their in-flight trajectory (heading direction, ∅, Figure 4.2b) to reach the landing tree. This steering model [17] characterized the goal (landing tree) as an attractor and obstacle(s) as repellers of heading acceleration, modulated by the distance to the goal and obstacle(s). A linear combination of the attractor and all the repellers produced a final heading acceleration function for the track. We modelled the glide tracks based on the simplest obstacle-avoidance case with one obstacle for each glide track (obstacle-aware model, Equation 5).

$$\ddot{\emptyset}_{obstacle} = -b\dot{\emptyset} - k_g(\emptyset - \varphi_g)\left(e^{-c_1 d_g} + c_2\right) + k_o(\emptyset - \varphi_o)(e^{-c_3|\emptyset - \varphi_o|})(e^{-c_4 d_o}) \quad \text{.....(5)}$$

where at any instant of time in the horizontal plane: ∅ is the lizard's heading direction, φ_g and φ_o are the angle subtended by the landing tree (goal) and the obstacle on the lizard's position, d_g and d_o are the lizard's distance from the goal and the obstacle, (b, k_g, k_o and c_{1-4}) are tuning parameters.

By removing the obstacle term, we obtained the no-obstacle model, equation (6)

$$\ddot{\emptyset}_{no-obstacle} = -b\dot{\emptyset} - k_g(\emptyset - \varphi_g)\left(e^{-c_1 d_g} + c_2\right) \quad \text{.....(6)}$$

To test the performance of each of these models, the observed heading direction data were fit to equation (5) and (6) using the *fitnlm* MATLAB function; the relative goodness of fit of the models were compared using the Akaike information criterion corrected for small sample size (AICc).

4.2.9 Statistical analysis

Linear relationships between glide and kinematic variables were tested using a least square regression model (LSR) performed with the *fitlm* function in MATLAB.

4.3 Results

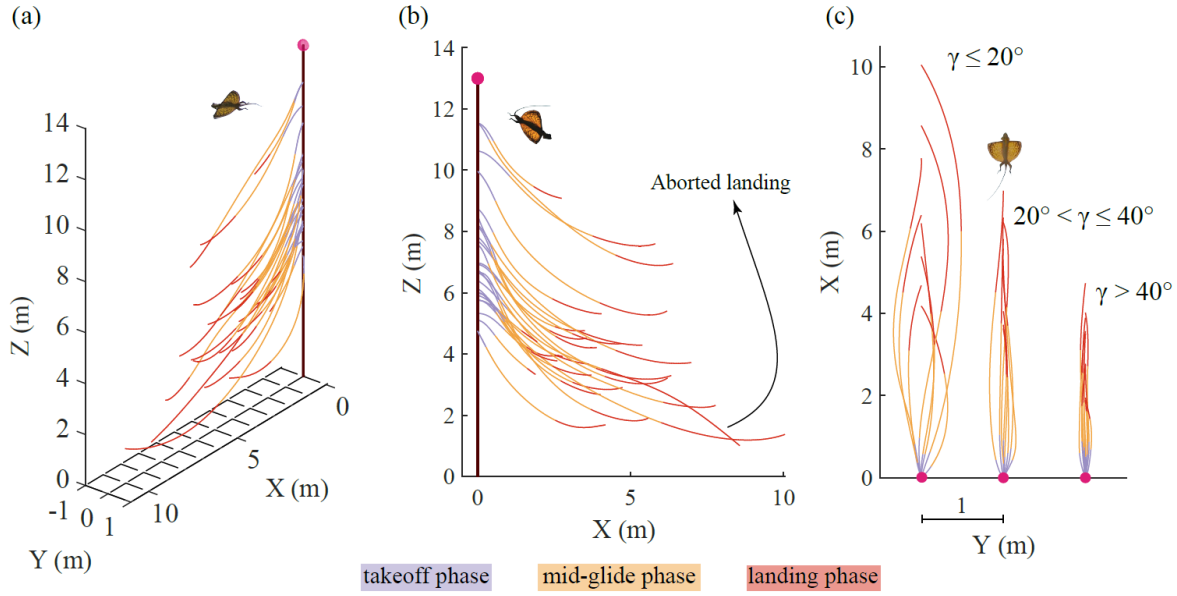

Figure 4.3 2D and 3D views of all 26 glides divided into takeoff, mid-glide and landing phases. (a) 3D plot showing the variation in takeoff height, glide distance and path curvature. (b) Side profile (X-Z plane), with the aborted landing glide not following the stereotypical shallowing glide path. (c) Overhead view (X-Y plane) of glides grouped by the obstacle angles, highlighting the influence of obstacles on the glide path. Note the obstacle avoidance maneuvers, shown by the increasing path curvature with decreasing obstacle angle, also resulting in longer glide distances.

A total of 33 glides were digitized (26 male and 7 female glides), out of which only 25 male glides were used for analysis; one was not considered because the lizard flew past the apparent target tree to land on a nearby tree (Figure 4.3). These 25 male glides excluded any

known repeat glides from the same individual. Nevertheless, the local population density of ~4.7 lizards per 1000 m^2 (i.e., ~33 lizards at the recording site) makes it possible but not certain that some repeated sampling occurred; population exchange between the recording site and surrounding jungle preserve may have prevented even limited resampling. The 7 female glides were excluded because females might be at different stages of their reproductive cycle during the mating season, influencing their gliding behavior. Overall, male recorded glides varied in distance from ~2 m to ~10 m, with maximum glide speeds between ~3.6 - 7.9 ms^{-1} and glide durations of ~0.8 - 2.1 s.

4.3.1 Takeoff phase

Lizards jumped from a height of 7.40 ± 1.91 m (mean ± s.d., n = 25) above ground level, independent of the glide distance (LSR, p = 0.20, Figure 4.4a). In most cases, they did not take off directly towards the target tree, i.e., the takeoff direction (β) was not equal to 0°; β had an absolute value of 10.07 ± 9.46° and a maximum of 40.88°. Lizards directed their jumps farther away from obstacles more in line with the target tree (LSR, $R^2 = 0.22$, p = 0.01, Figure 4.4a) and had higher lateral accelerations (a_{yO}) of 1.74 ± 1.63 ms^{-2} (LSR, $R^2 = 0.39$, $p < 0.001$) while passing the obstacle to reorient their glide towards the landing tree (Figure 4.4b). The maximum a_{yO} observed was 6.34 ms^{-2} for a β of 40.88° and a γ of 5.69°. Average takeoff angles ($\bar{\theta}_{takeoff}$) ranged from -63.90° to -30.78°; steeper $\bar{\theta}_{takeoff}$ was associated with longer glide distances (LSR, $R^2 = 0.16$, p = 0.03, Figure 4.4b) and higher maximum glide speeds (LSR, $R^2 = 0.58$, $p < 0.001$). On average, the takeoff phase lasted for 0.38 ± 0.06 s, independent of the glide distance (LSR, p = 0.64). Overall, lizards tuned their takeoff angle and direction with respect to the obstacle and landing tree position but maintained similar takeoff durations across glide distances.

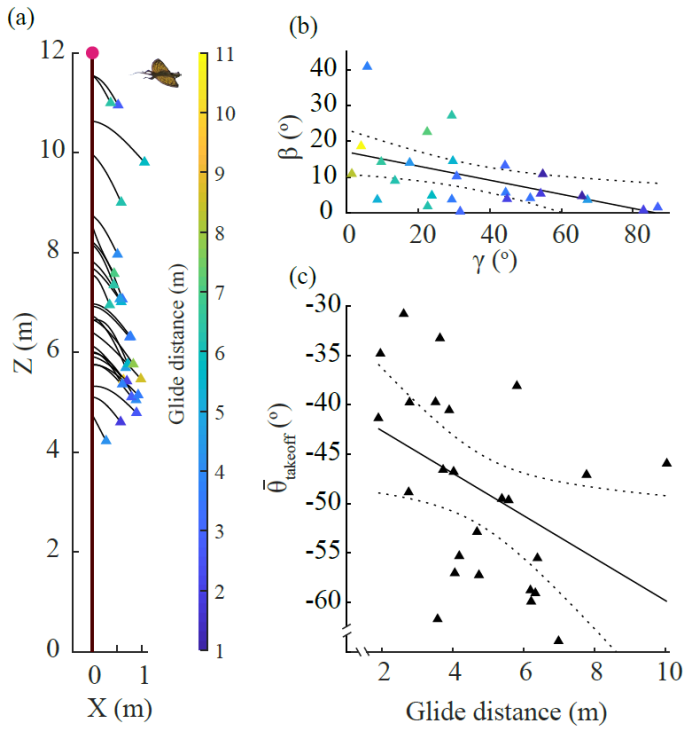

Figure 4.4 Takeoff phase. (a) Side view (X-Z plane) of takeoff phase for all 26 glides, showing variation in takeoff height and average takeoff angle ($\bar{\theta}_{takeoff}$). The end of each takeoff phase is marked by a color-coded triangle denoting the corresponding glide distance. (b) Inverse correlation between the takeoff direction (β) and the obstacle angle (γ), showing that lizards direct their jump farther away from obstacles closer to a straight path between the takeoff and landing tree. (c) Correlation between the average takeoff angle and glide distance indicating steeper dives for longer glide distances.

4.3.2 Mid-glide phase

Longer glides had marginally shallower mid-glide angles ($\bar{\theta}_{mid-glide}$) (LSR, $R^2 = 0.15$, $p = 0.03$); however, the average shallowing rate through mid-glide was $54.15 \pm 14.29°s^{-1}$ and did not vary with glide distance (LSR, $p = 0.11$, Figure 4.5c). Thus, shallower and longer glides were achieved by extending the mid-glide duration, a quantity strongly associated with the final glide distance (LSR, $R^2 = 0.87$, $p < 0.001$). Interestingly, the average glide angle from the initiation of landing (from the RREV cue, see Results section on Visual landing control) to the end of the mid-glide phase was correlated with the total glide distance (LSR, $R^2 = 0.71$, $p < 0.001$). Obstacle position (angle γ) had no significant effect on the average mid-glide angle (LSR, p =

0.12) but corresponded to a marginally lower average shallowing rate (LSR, $R^2 = 0.13$, $p = 0.04$). The roll angle model further emphasized the weak obstacle effects on the mid-glide phase kinematics. Across all glides, we calculated a maximum roll angle of 21.08° from a recording with a γ of 1.38°, corresponding to a loss of 6.69% in the modelled lift force (Figure 4.5b).

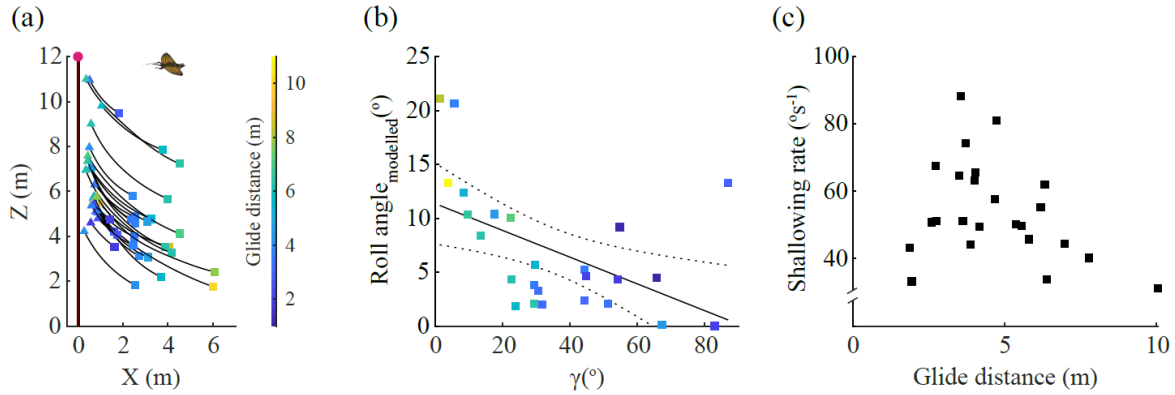

Figure 4.5 Mid-glide phase. (a) Side view (X-Z plane) of mid-glide phase for all 26 glides, color coded with respect to their glide distance. Longer glides have extended mid-glide phases. (b) Model results simulating the roll angles for a fixed wing glider to generate observed a_{yO} while passing the obstacle tree. The model shows a maximum roll angle of ~21° for an obstacle almost in line with the landing tree. (c) A scatter plot showing the mid-glide shallowing rate to be invariant across all glides.

4.3.3 Landing phase

With increasing glide distance, lizards entered the landing phase at higher horizontal speeds (LSR, $R^2 = 0.73$, $p < 0.001$) and had longer landing durations (LSR, $R^2 = 0.41$, $p < 0.001$). Furthermore, longer glides were associated with shallower landing angles ($\bar{\theta}_{landing}$) (LSR, $R^2 = 0.52$, $p < 0.001$) and higher maximum deceleration in the horizontal plane (LSR, $R^2 = 0.26$, $p < 0.01$) (Figure 4.6b). The braking maneuver culminated in touchdown speeds of 0.83 to 5.74 ms^{-1}, ~1 to ~9 m (median height of 3.77 m) above the ground. The touchdown speed was slightly higher for longer glides (LSR, $R^2 = 0.20$, $p = 0.01$) but independent of the average landing angle (LSR, $p = 0.20$) and the maximum horizontal deceleration achieved (LSR, $p = 0.98$). Overall,

with an increase in glide distance, lizards had extended landing durations and shallower landing angles with variable touchdown speeds.

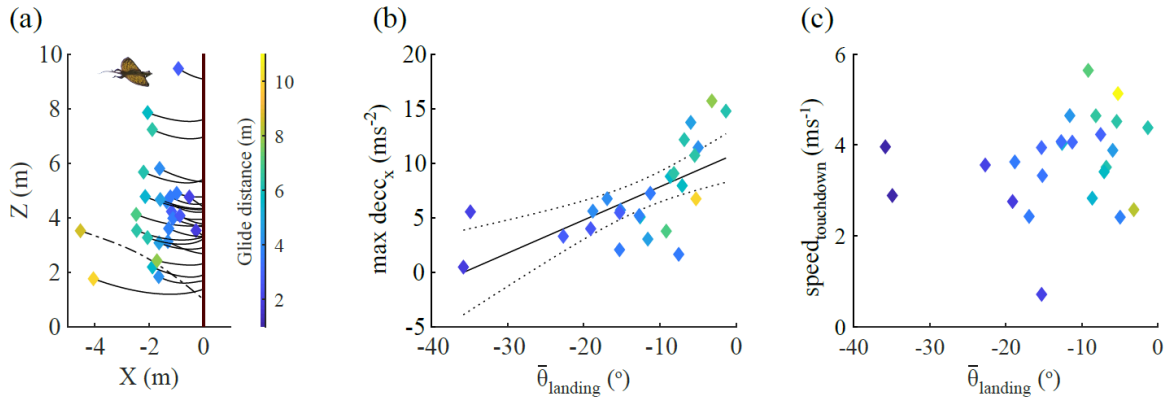

Figure 4.6 Landing phase. (a) Side view (X-Z plane) of landing phase for all 26 glides, color coded with respect to their glide distance. The dashed line shows an aborted landing, not following the stereotypical shallowing curve of other landing trajectories. (b) As expected, shallower average landing angles ($\bar{\theta}_{landing}$) correspond to higher maximum deceleration in the forward direction. (c) The touchdown speed is independent of $\bar{\theta}_{landing}$, showing a range of impact speeds employed by lizards.

4.3.4 Effect of obstacles

Longer glides are expected to have smaller obstacle angles (γ) due to the distribution of trees at the field site (see Methods, γ with glide distance simulation) (Figure 4.7c). However, the observed γ were significantly larger than that predicted by the simulation (Wilcoxon signed-rank test, $p < 0.001$) (Figure 4.7c). Additionally, smaller γ's corresponded to lizards performing high a_{yO} maneuvers (LSR, $R^2 = 0.47$, $p < 0.001$) when passing the obstacle while maintaining a minimum lateral distance (d_{yO}) of 0.5 m from it.

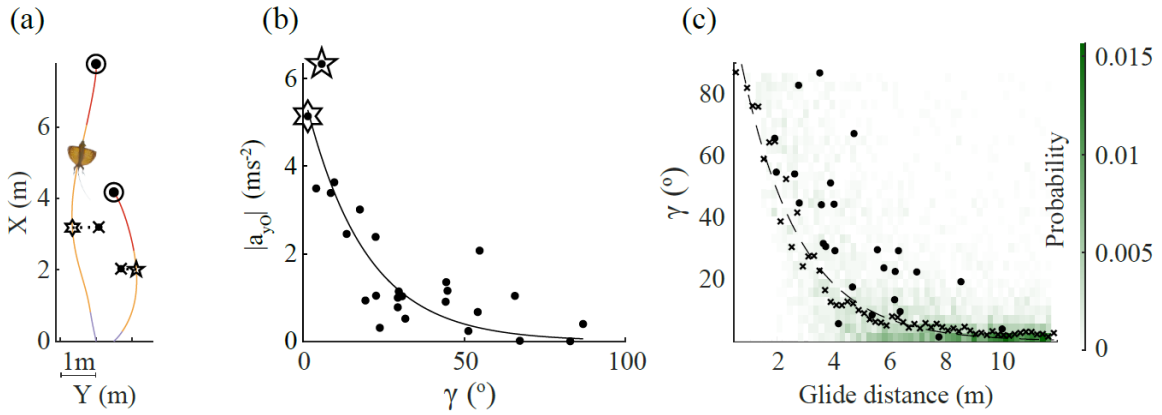

Figure 4.7 Obstacle avoidance and path choice. (a) Overhead view of two representative glides portraying obstacle-avoidance, color coded to show the glide phases. Both glides show the lizard taking off in a direction away from the obstacle. The location of lateral acceleration (a_{yO}) calculation is marked by ✩ and ✩ for each glide. (b) Magnitude of lateral acceleration ($|a_{yO}|$) calculated while passing the obstacle decreases exponentially with an increase in obstacle angle (γ). (c) Probability density map of simulation of obstacle angles varying with glide distances in the topography of our field site. The dashed line shows that the median of simulated obstacle angles, marked by '**x**', decreases exponentially as a function of glide distance. The observed γ's for our recorded glides, marked by '●', were higher for 22 out of 25 glides compared to the simulated γ of similar glide distance.

4.3.5 Visual navigation

The obstacle-aware (Equation 4) and no-obstacle (Equation 5) steering models were fitted to the observed heading data (see Methods, also Figure 4.8). The best fit for both models was obtained with a response lag of 67 ms, with the obstacle-aware model (non-linear LSR, $R^2 = 0.60$, $F_{7,1889} = 402$, $p < 0.001$) performing better than the no-obstacle model (non-linear LSR, $R^2 = 0.57$, $\Delta AICc = 101.12$, $F_{4,1892} = 641$, $p < 0.001$).

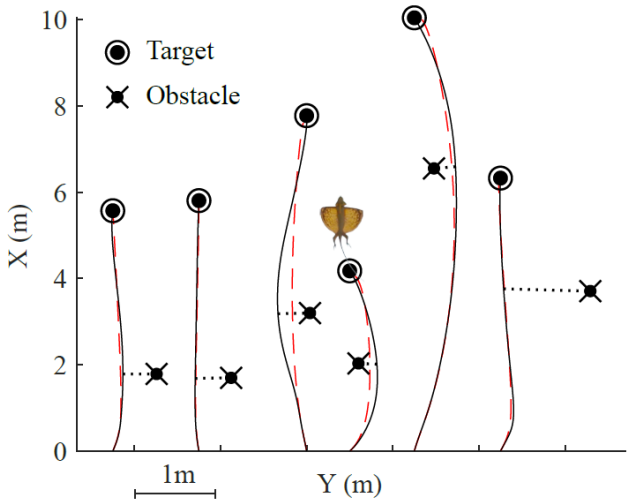

Figure 4.8 Vision-based obstacle-avoidance model. Overhead view (X-Y plane) of 6 out of 25 glides of varying glide distances and obstacle positions showing the observed glide path (solid black line) along with the glide paths predicted by the obstacle-avoidance model (dashed red line). The model agreed with most glides, excluding a few with $\gamma < 20°$.

4.3.6 Visual landing control

Lizards initiated their landing response at a mean RREV of ~1.39 s^{-1} (n = 23) observed at 280 ms before the start of the landing phase, as shown in Figure 4.9a. During the landing phase, we found that τ (inverse of RREV value) varied uniformly with time (Fig 7b), i.e., $\dot{\tau}$ was held constant with a value of -0.84 ± 0.08 (n = 23; LSR, mean R^2 ~1.00, $p < 0.001$; Pearson Correlation Coefficient, mean r ~ -1.00, $p < 0.001$) indicating a 'controlled collision' approach undertaken by lizards to land [18,26].

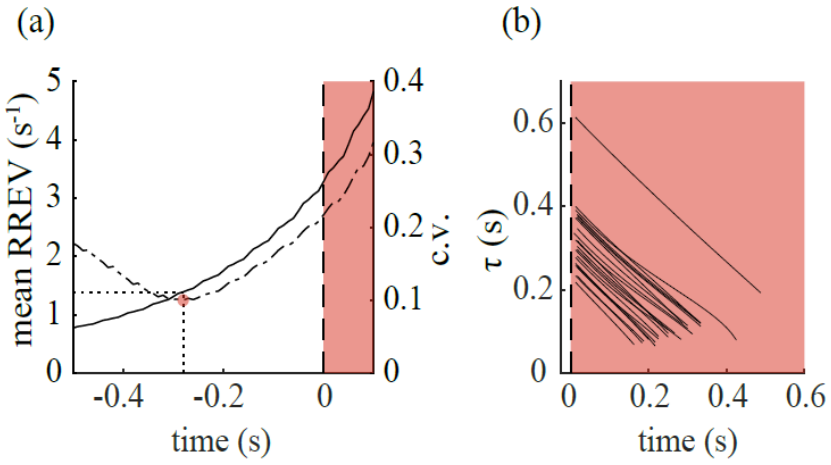

Figure 4.9 RREV model and the τ function. All glides were aligned to begin their landing phase at t = 0 s, with t > 0 s to be further into the landing phase. (a) The coefficient of variation (c.v.) reached a minimum at 280 ms before the start of the landing phase corresponding to a mean RREV value of 1.39 s^{-1}. (b) The τ value for each glide calculated as α/Ω reduced at a constant rate of 0.84 ± 0.08, suggesting a controlled-collision landing approach.

4.4 Discussion

Our study examined behaviorally motivated, complete glides of male flying lizards over varying degrees of spatial complexities and glide distances. In this context, we found that flying lizards employ a visually guided path-planning strategy to traverse their aerially cluttered natural environment. Specifically, lizards performed non-equilibrium glides along paths with relatively less surrounding clutter and adjusted their takeoff to accommodate for topography and the desired glide distance. Furthermore, their glide trajectories were consistent with vision-based control models for navigation, obstacle-avoidance and landing.

4.4.1 Equilibrium v/s non-equilibrium gliding

To perform an equilibrium glide, the animal must hold a static gliding pose for an extended duration along a straight path to balance the gravitational and aerodynamic forces, yielding a constant glide velocity [4,27]. Equilibrium gliding as a common mode of glide execution has been described in colugos [10] and gliding lizards [12] but appears to be absent in flying snakes [14] and squirrels [13], questioning the prevalence and feasible conditions of

equilibrium gliding in nature. In *Draco*, McGuire et al. found that 48% of recorded glides (with complete speed profile) reached equilibrium [12]. However, the individuals were coaxed to glide between a fixed takeoff and landing pole, placed 9.3 m apart, with no other destination options (few landings were on the ground), and no obstacles.

We hypothesized that most natural habitats provide little opportunity for animals to glide the distances required to achieve equilibrium gliding without adjusting their glide path or speed to negotiate obstacles. This implies that non-equilibrium gliding is the predominant mode of glide execution for *Draco* in their natural habitat. Our results support this hypothesis, as none of our quantified glides reached equilibrium. Furthermore, the highest probability for lizards to achieve equilibrium gliding is in the mid-glide phase where they are not accelerating or braking as observed in takeoff and landing. However, we found that flying lizards in mid-glide shallowed their trajectory at a rate of $54.15 \pm 14.29°s^{-1}$, much greater than rates observed in flying snakes [14,28] and sugar gliders [7]. Moreover, the average shallowing rate was independent of the glide distance (Figure 4.5c) but was marginally lower for glides with obstacles more in line with the target tree (smaller γ's), suggesting that lizards exhibit steeper glide paths while performing in-flight lateral maneuvers. To maneuver, the aerodynamic force vector is rotated about the roll axis of the body to cause lateral deviations, thus, reducing the upwardly directed lift force and resulting in a steeper glide path or lower shallowing rate. In our model for a fixed-wing glider generating identical lateral accelerations (a_{yO}) while passing the obstacle, the roll angles varied between ~0 to 21° (Figure 4.5b) with a maximum loss in lift production of ~7%, further emphasizing the relationship between shallowing rate and the obstacle tree location. These results suggest that flying lizards actively manipulate body orientation and/or wing area to alter and direct aerodynamic forces while gliding, similar to mammalian gliders [7,8]. However, the

absence of equilibrium gliding in our study does not show *Draco* to be incapable of attaining constant velocity glides in natural settings, just that lizards might choose not to use equilibrium gliding, or that opportunities to attain steady state dynamics were rare or non-existent at our site. Our simulation of γ, the obstacle angle, as a function of glide distance in our field site yielded high probability of obstacle encounter for glide distances of 10 m or more (Fig 4.7c), roughly the fixed glide distance tested by McGuire et al. In comparison, the majority of our recorded glides were much shorter (median = 4.18 m). Nonetheless, it is also worth noting that McGuire et al. recorded glides in a 2D (X-Z) plane using a single video camera, which would slightly limit the ability to detect lateral variations along the glide path, thus increasing the chances of incorrectly identifying equilibrium glides.

4.4.2 Path planning versus reactive in-flight maneuvers

Reaching the target tree in an aerially cluttered environment can be achieved by implementing a pre-defined collision-free path (path planning) and/or reactively altering the path as and when an obstacle is encountered (reactive maneuvering). To maneuver, a glider must redirect the existing aerodynamic forces to generate centripetal acceleration, resulting in a decrease in upwardly directed force and an increase in gliding costs (energy). Thus, following the assertion of Caple et al. [29], we hypothesized that flying lizards would preferentially use a path planning strategy to minimize energetic costs of negotiating obstacles, or alternatively, perform shorter obstacle-free glides to altogether avoid encountering these issues.

We quantified lizards performing glides of ~2 to 10 m, with obstacle angles (γ) ranging between ~1.4° to 87°. For a given glide distance, lizards jumped in a direction with less surrounding clutter than alternatives, suggesting that they opt for glide paths, which will lead to relatively less loss of altitude due to in-flight maneuvering (see Results – Environmental effects,

Figure 4.7c). Furthermore, they modulated their takeoff to account for the expected glide distance and obstacles, using marginally steeper takeoff angles for longer glides and jumping farther away from obstacles directly in line with the target tree (Figure 4.4b). Though the takeoff angle and direction varied, the takeoff duration was independent of glide distance and obstacle presence. Takeoff duration may instead be related to a morphological constraint of time taken for complete wing and lappet deployment to generate lift. Nonetheless, the unique wing apparatus of *Draco* leads to a relatively streamlined pose immediately after jumping, allowing them to rapidly gain speed with their wings and appendages tucked close to their body. In a cluttered environment, the rapid gain in speed might facilitate maneuvering earlier in the glide compared to mammalian gliders that take an abducted body pose [6] to extend their wing surface, leading to increased overall drag.

Together, these results show that flying lizards pre-select their target tree based on the topography and accordingly adjust their takeoff phase to successfully execute a glide. However, as glide distance increases, planning a collision-free path through a cluttered environment becomes increasingly less feasible, likely increasing the importance of reactive in-flight maneuvers. This was indeed the case, with 2 glides with $\gamma < 10^{o}$ and obstacles greater than 3 m from the takeoff tree exhibiting reactive in-flight maneuvers (Figure 4.7a, glide on the left), indicating that both strategies contribute towards lizards navigating their environment. Overall, we provide evidence for a path planning strategy used by flying lizards in a cluttered environment, with the increased possibility of reactive in-flight maneuvers for smaller γ and longer glide distances.

4.4.3 Visual navigation

Vision is believed to be the primary sensory modality used by most gliders for flight control [4]. Canopy ants *Cephalotes atratus* use brightness cues to orient themselves during a fall and to land on the tree [30], highlighting the role of vision in glide navigation and control. The gliding lizard *Draco sumatranus* adjust their position on the tree relative to the sun to make their dewlap easily visible to conspecifics during social interactions [31], supporting that vision is likely the primary sensory input used by *Draco* to gather information from their surroundings. However, testing the contribution of vision to navigation and/or path control can be extremely challenging, requiring manipulating the visual field of the animal in real time during flight [4]. Instead, here we provide indirect support by fitting pre-existing visual control models to heading direction (navigation) and landing kinematics (control).

We hypothesized that flying lizards navigate towards the landing tree by using an obstacle-avoidance steering model [17]. Even in cases where no obstacles were present, the lizards took off at an angle offset from a straight line between takeoff and landing trees ($\beta > 0°$), thus requiring some in-flight lateral maneuvers. We saw good agreement between the heading direction of lizards and that predicted by the model after incorporating a time shift of 67 ms, implying a visuomotor delay. The time delay was comparable to the minimum retinal integration time of ~67 ms reported in *Anolis* lizards (flicker fusion frequency in the 15-30 Hz range) [32] but short compared to visuomotor delays in other flying species [3], suggesting that our observations include feed-forward and feedback components. Next, we removed the obstacle component from the model and saw reduced predictive power (ΔAICc = 101.12, see Results 4.3.5), suggesting that flying lizards indeed consider obstacles while gliding. Overall, the model suggests that flying lizards adjust their heading direction to align in the direction of their target

while maximizing the bearing angle to the obstacle. Nonetheless, we did observe reactive in-flight maneuvers which were poorly replicated by the model. These maneuvers corresponded to obstacles farther away from the takeoff tree (> 3m), potentially making them less conspicuous at the time of takeoff (Figure 4.8).

4.4.4 Visual landing control

To land, we hypothesized that flying lizards use a RREV model, also known as the tau (τ) strategy. The τ strategy has been used to describe the onset of landing in flies [19,20] and pigeons [18]. In the wild, plummeting gannets were shown to use a τ strategy to trigger streamlining just before entering the water surface to forage [33]. Hence, in vision-based animals, the τ strategy could provide a simple way of integrating surrounding information to control the timing of certain locomotory behaviors. For *Draco,* the locomotory behavior is the initiation of the body pitch-up landing maneuver to decelerate. Our data fit exceptionally well with the RREV model and show 280 ms prior to the start of the landing phase as the decision point to initiate a body pitch-up braking maneuver. Interestingly, for glides less than 3 m, the 280 ms response time corresponds to the start of the mid-glide phase, i.e., in shorter glides (< 3m), lizards prepare to land immediately after the takeoff phase, essentially using the mid-glide to initiate braking.

By pitching up to land, flying lizards present more frontal area in the direction of motion, dissipating part of the accumulated kinetic energy as drag. However, the magnitude of deceleration is limited by the wing area; in other words, long glides with higher speeds require extended landing durations to reach a safe touchdown speed and thus, lizards should enter the landing phase farther away from the target tree. As expected, with an increase in glide distance and speed, lizards had longer landing durations corresponding to shallower landing angles and

higher maximum deceleration. Interestingly, the speed at touchdown was variable (0.83 - 5.74 ms^{-1}, Figure 4.6c) and lizards maintained a constant $\dot{\tau}$ of 0.85±0.08 during landing, suggesting that they approach the target tree using a 'controlled-collision procedure' [18]. Here, flying lizards gradually increase their braking as the target gets closer, culminating in a non-zero touchdown velocity. For unpowered flight, such a strategy might allow maintaining lift during deceleration to alleviate the risk of stalling, or, facilitate evasive maneuvers if the landing site is unfavorable upon closer inspection (e.g., predator and/or a territorial male). We did record an aborted landing in one of our glides where the lizard turned away from the initial target tree to land instead on a nearby tree (Figure 4.6a and 4.3b).

Finally, pitching up also increases the upward force, potentially allowing lizards to regain some lost altitude by performing a terminal upswing, as noted previously in flying lizards [12] and squirrels [13]. From the lowest point in the glide trajectory, we saw marginally increasing gain in altitude of up to ~4.5% of the total height lost, with a maximum gain of 0.19 m for a glide distance of 6.21 m. This small gain increased with glide distance, suggesting that the terminal upswing is likely a feature of longer glides but still represents only a small fraction of the total height lost.

4.5 Conclusion

By integrating aspects of the environment, behavior, and the biomechanical capabilities of the glider, we show flying lizards using a visually guided path-planning strategy to perform collision-free flight in a naturally cluttered habitat. Furthermore, our study provides insight into how gliders use and process visual information from the environment, beginning from pre-selecting the target tree, adjusting their heading direction, to initiating and controlling their braking to land. Together, these unique set of results reveal previously unknown capabilities in

gliding animals and demonstrate the importance of field studies in gaining a more comprehensive understanding of ecologically relevant locomotory behaviors.

4.6 Acknowledgements

We wish to thank two anonymous referees for their comments as well as Jonathan Rader and other members of the Hedrick lab for their feedback on this project. We would also like to thank Dr. Sanjay P. Sane, Deepak CK, Dhiraj Bhaisare, Ajay Giri and the local staff at ARRS for hosting and assisting with field data collection.

REFERENCES

1. Parker SE, McBrayer LD. 2016 The effects of multiple obstacles on the locomotor behavior and performance of a terrestrial lizard. *J. Exp. Biol.* **219**, 1004–1013. (doi:10.1242/jeb.120451)

2. Jayaram K, Mongeau JM, Mohapatra A, Birkmeyer P, Fearing RS, Full RJ. 2018 Transition by head-on collision: mechanically mediated manoeuvres in cockroaches and small robots. *J. R. Soc. Interface* **15**. (doi:10.1098/rsif.2017.0664)

3. Lin HT, Ros IG, Biewener AA. 2014 Through the eyes of a bird: Modelling visually guided obstacle flight. *J. R. Soc. Interface* **11**. (doi:10.1098/rsif.2014.0239)

4. Socha JJ, Jafari F, Munk Y, Byrnes G. 2015 How animals glide: From trajectory to morphology. *Can. J. Zool.* **93**, 901–924. (doi:10.1139/cjz-2014-0013)

5. Essner RL. 2002 Three-dimensional launch kinematics in leaping, parachuting and gliding squirrels. *J. Exp. Biol.* **205**, 2469–2477.

6. Paskins KE, Bowyer A, Megill WM, Scheibe JS. 2007 Take-off and landing forces and the evolution of controlled gliding in northern flying squirrels *Glaucomys sabrinus*. *J. Exp. Biol.* **210**, 1413–1423. (doi:10.1242/jeb.02747)

7. Bishop KL. 2007 Aerodynamic force generation, performance and control of body orientation during gliding in sugar gliders (Petaurus breviceps). *J. Exp. Biol.* **210**, 2593–2606. (doi:10.1242/jeb.002071)

8. Bishop KL. 2006 The relationship between 3-D kinematics and gliding performance in the southern flying squirrel, *Glaucomys volans*. *J. Exp. Biol.* **209**, 689–701. (doi:10.1242/jeb.02062)

9. Bishop KL, Brim-Deforest W. 2008 Kinematics of turning maneuvers in the southern flying squirrel, *Glaucomys volans*. *J. Exp. Zool. Part A Ecol. Genet. Physiol.* **309**, 225–242. (doi:10.1002/jez.447)

10. Byrnes G, Lim NTL, Spence AJ. 2008 Take-off and landing kinetics of a free-ranging gliding mammal, the Malayan colugo (*Galeopterus variegatus*). *Proc. R. Soc. B Biol. Sci.* **275**, 1007–1013. (doi:10.1098/rspb.2007.1684)

11. Byrnes G, Libby T, Lim NTL, Spence AJ. 2011 Gliding saves time but not energy in Malayan colugos. *J. Exp. Biol.* **214**, 2690–2696. (doi:10.1242/jeb.052993)

12. McGuire JA, Dudley R. 2005 The cost of living large: Comparative gliding performance in flying lizards (Agamidae: *Draco*). *Am. Nat.* **166**, 93–106. (doi:10.1086/430725)

13. Bahlman JW, Swartz SM, Riskin DK, Breuer KS. 2013 Glide performance and

aerodynamics of non-equilibrium glides in northern flying squirrels (*Glaucomys sabrinus*). *J. R. Soc. Interface* **10**. (doi:10.1098/rsif.2012.0794)

14. Socha JJ, Miklasz K, Jafari F, Vlachos PP. 2010 Non-equilibrium trajectory dynamics and the kinematics of gliding in a flying snake. *Bioinspiration and Biomimetics* **5**. (doi:10.1088/1748-3182/5/4/045002)

15. Suzuki K, Asari Y, Yanagawa H. 2012 Gliding locomotion of Siberian flying squirrels in low-canopy forests: The role of energy-inefficient short-distance glides. *Acta Theriol. (Warsz).* **57**, 131–135. (doi:10.1007/s13364-011-0060-y)

16. Suzuki KK, Yanagawa H. 2019 Gliding patterns of Siberian flying squirrels in relation to forest structure. *iForest* **12**, 114–117. (doi:10.3832/ifor2954-011)

17. Fajen BR, Warren WH. 2003 Behavioral Dynamics of Steering, Obstacle Avoidance, and Route Selection. *J. Exp. Psychol. Hum. Percept. Perform.* **29**, 343–362. (doi:10.1037/0096-1523.29.2.343)

18. Lee DN, Davies MNO, Green PR, (Ruud). Van Der Weel FR. 1993 Visual control of velocity of approach by pigeons when landing. *J. Exp. Biol.* **180**, 85–104.

19. Wagner H. 1982 Flow-field variables trigger landing in flies. *Nature* **297**, 147–148. (doi:10.1038/297147a0)

20. Van Breugel F, Dickinson MH. 2012 The visual control of landing and obstacle avoidance in the fruit fly *Drosophila melanogaster*. *J. Exp. Biol.* **215**, 1783–1798. (doi:10.1242/jeb.066498)

21. Khandelwal P., Shankar C., Hedrick T. 2018 Take-off biomechanics in gliding lizards. *Soc. Integr. Comp. Biol.* , 38–1. See http://www.sicb.org/meetings/2018/schedule/abstractdetails.php?id=985.

22. Sreekar R, Purushotham CB, Saini K, Rao SN, Pelletier S, Chaplod S. 2013 Photographic capture-recapture sampling for assessing populations of the Indian gliding lizard *Draco dussumieri*. *PLoS One* **8**. (doi:10.1371/journal.pone.0055935)

23. Srinivasulu, C, Srinivasulu, B, Vijayakumar, S.P, Ramesh, M, Ganesan, S.R, Madala, M & Sreekar R. 2013 *Draco dussumieri*. *IUCN Red List Threat. Species 2013*. See http://dx.doi.org/10.2305/IUCN.UK.2013-1.RLTS.T172625A1354495.en.

24. McGuire JA, Dudley R. 2011 The biology of gliding in flying lizards (genus Draco) and their fossil and extant analogs. *Integr. Comp. Biol.* **51**, 983–990. (doi:10.1093/icb/icr090)

25. Colbert EH. 1967 Adaptations for gliding in the lizard Draco. *Am. Mus. Novit.* **2283**, 1–20.

26. Lee DN, Reddish PE, Rand DT. 1991 Aerial docking by hummingbirds. *Naturwissenschaften* **78**, 526–527. (doi:10.1007/BF01131406)

27. Norberg UM. 1985 Evolution of vertebrate flight: an aerodynamic model for the transition from gliding to active flight. *Am. Nat.* **126**, 303–327. (doi:10.1086/284419)

28. Socha JJ, O'Dempsey T, LaBarbera M. 2005 A 3-D kinematic analysis of gliding in a flying snake, *Chrysopelea paradisi*. *J. Exp. Biol.* **208**, 1817–1833. (doi:10.1242/jeb.01579)

29. Caple G, Balda RP, Willis WR. 1983 The physics of leaping animals and the evolution of preflight. *Am. Nat.* **121**, 455–476. (doi:10.1086/284076)

30. Yanoviak SP, Dudley R. 2006 The role of visual cues in directed aerial descent of *Cephalotes atratus* workers (Hymenoptera: Formicidae). *J. Exp. Biol.* **209**, 1777–1783. (doi:10.1242/jeb.02170)

31. Klomp DA, Stuart-Fox D, Das I, Ord TJ. 2017 Gliding lizards use the position of the sun to enhance social display. *Biol. Lett.* **13**. (doi:10.1098/rsbl.2016.0979)

32. Pallus AC, Fleishman LJ, Castonguay PM. 2010 Modeling and measuring the visual detection of ecologically relevant motion by an Anolis lizard. *J. Comp. Physiol. A Neuroethol. Sensory, Neural, Behav. Physiol.* **196**, 1–13. (doi:10.1007/s00359-009-0487-7)

33. Lee DN, Reddish PE. 1981 Plummeting gannets: A paradigm of ecological optics. *Nature* **293**, 293–294. (doi:10.1038/293293a0)

CHAPTER 5: CONCLUSIONS

In my dissertation, I ask the question, how do animals glide in their natural habitat? Although many studies on gliding mechanics and ecology have been conducted before, none have attempted to take a holistic approach to understand gliding performance in the animal's natural habitat where the interplay between different behaviors, body sizes and the habitat can be seen, and their combined effect on the gliding performance can be recorded. Therefore, it remains unclear how and to what extent do each of these factors influence the animal's gliding ability, ultimately affecting its performance and survival.

I attempted to answer these questions using the lesser studied flying lizard *Draco dussumieri* in the wilderness of the Western Ghats in India. I used a novel non-invasive motion capture technique to film them glide and also took qualitative observations of their behavior. Together, this approach allowed me to reveal the underlying kinematics and aerodynamics of gliding and link it to the morphology and behavior of *Draco*, all in its environmental context. My investigations revealed, for the first time, real-world strategies used by the *Draco* to both stay aloft and traverse its cluttered environment and evidence that evolutionary pressures influence performance among and within sexes.

5.1 Aerodynamics

In Chapter 2, I investigated the underlying physical mechanism of gliding, which in the case of gliding animals deals with the aerodynamics to stay aloft. My study is the first to reconstruct an aerodynamic polar plot from actual glide data and provides the most detailed look

at *Draco* gliding aerodynamics currently available. In general, the results are consistent with prior work on mammalian gliders and, to some extent, flying snakes. By describing the aerodynamics, I also made some key advancements in our understanding of gliding flight mechanics.

5.1.1 Angle of attack and camber

I showed that *Draco* airfoil operate largely like a traditional airfoil but with the advantages of a compliant wing. The angle of attack (AoA) was positively correlated with the coefficient of lift and coefficient of drag yet was held surprisingly steady at approximately 26° during the mid-glide phase. The drag polar plot showed that the AoA of 26° corresponded to the maximum value of the lift-to-drag ratio observed in our field recordings. This translates to *Draco* operating at forces which minimize the loss in altitude per unit increase in horizontal distance covered. Though maximizing lift-to-drag ratio had been previously proposed as a favorable strategy to glide, my study is the first to show experimental support for it, with *Draco* impressively maintaining maximum lift-to-drag ratio by continuously changing body orientation in the air. Second, I showed that a compliant airfoil allowed for changes in percentage camber under aerodynamic load. The changes in percentage camber along with AoA were used by *Draco* to modulate the coefficient of lift and coefficient of drag. This was especially advantageous since it allowed *Draco* to achieve higher coefficients of forces at relatively low AoA, providing greater flexibility in terms of its gliding ability.

These advantages were carried over to the landing phase where the *Draco* reached AoA upwards of 40°. Such high AoA are often seen in gliding taxa but represent an extraordinary aerodynamic feat. Where traditional airfoils experience stall (drastic loss of lift after a critical AoA) at an AoA of approximately 15°, gliding animals can achieve AoA almost thrice that

value. Previous simulation on a rectangular wing with the same aspect ratio of 1.4 as the primary *Draco* wing showed that increasing percentage camber to approximately 10 delayed the onset of stall to around 40°. My results were strikingly similar to the simulation and provide the first experimental evidence of how gliding animals might achieve higher AoA than traditionally possible using rigid wings.

5.1.2 Composite airfoil

Gliding taxa with a dedicated well-defined wing such as mammalian gliders and flying lizards are considered to rely largely on their primary wing to glide. Although this is partially true, my study showed that *Draco* body parts including the head, body, and the hindlimb along with the mostly flat body are significant contributors towards increasing the surface area by up to 50% to generate aerodynamic forces. This fundamentally changes the perspective from considering only the primary wing for modelling for various aerodynamic analysis to considering a composite airfoil composed of the primary wing and the body parts. Furthermore, using a composite airfoil also changes the scaling relationships between body size (mass) and aerodynamic performance (surface area). Previously, it was believed that due to isometric scaling of wing area with body size, larger *Draco* would be less capable gliders. By considering the composite airfoil, I showed that larger gliders actually must accommodate negative allometric scaling of surface area with body size, further emphasizing the compensatory behavioral changes in larger *Draco* to reduce the detrimental aerodynamics effects of scaling that was reported in Chapter 3 and is mentioned in the next section.

5.2 Body size and sex

Chapter 3 built on the glide performance description in Chapter 2 by investigating the variation in performance in the context of body size and sex of the individual. Both are equally

important when describing glide performance. Variation in body size sets boundaries on the physical capabilities of the glider, whereas sex relates to different behaviors which ultimately influence the performance level of individuals. For example, behaviors like territoriality and foraging have distinct motivations which can lead to performance differences but must operate within the physical limits defined by the body size of the individual. Such influences though expected have mostly remained unstudied in gliding animals. In my study system there was a stark distinction between behaviors of males and females and a body size variation ranging between 3 gm to 11 gm, allowing me to investigate the effects of body size and sex on glide performance.

Overall, I saw that the effect of body size and sex on glide performance was not mutually independent because of female-biased size dimorphism in *Draco*. However, I was able to observe some key differences between and within males and females.

5.2.1 Body size

I saw the expected negative effects of body size on glide performance with larger *Draco* performing steeper overall glides. However, my analysis revealed compensatory behavior in larger individuals to reduce the detrimental effects of body size. I found that larger *Draco* achieve slightly higher maximum speeds and AoA to operate at higher coefficients of lift and coefficients of drag but lower lift-to-drag ratio. Such adjustments allowed larger individuals to slow their descent potentially to land safely since the speed at touchdown was independent of body size even though larger *Draco* started the landing phase at higher speeds. Therefore, instead of relying on significantly higher flight speeds to achieve similar glide performance as smaller individuals, larger *Draco* behaviorally compensated using higher AoA to slow their descent and potentially prioritized landing safety over glide performance.

5.2.2 Sex

A major goal of Chapter 3 was to investigate if and how different evolutionary pressures manifest in the gliding performance of the individual. To this end, I found support for variation in performance among sexes, highlighting for the first time, how behavior might influence gliding performance. However, it should be noted that my data set was limited to a small sample size of 23 glides with 7 males and 6 females, where females represented the higher end of the body mass spectrum. After accounting for body size, males performed shallower and thus more efficient glides than females, reaching consistently higher landing spots with little variation in landing height. Conversely, females, along with their steeper glides showed large variation in landing height and landed lower than males. Such variation among sexes might represent how evolution has shaped overall glide performance. For example, glide performance in males might be tuned for frequent glides and reducing the transit time between them allowing them to effectively defend territories and seek mates. Conversely, females do not participate in territoriality or mate seeking and thus could afford greater variability in glide performance. Overall, this showed support for the evolution of reversed sexual dimorphism in *Draco*.

An interesting outcome of performance comparison among sexes was the compensatory behavior observed for variation in body size. In the mid-glide phase, I saw opposite effects of body size on performance among sexes. Larger males overcompensated for their body size and performed shallower mid-glides compared to smaller males whereas larger females followed the expected outcome of having steeper glides than smaller females. This level of detail on differences of performance among and within sexes was unexpected but welcomed. It further suggested that glide performance is not only driven by selection pressures but also influenced by ontogenetic variation.

5.2.3 Male territoriality and female home range

Fundamental differences in behavior between males and females, especially in the mating season should translate to differences in spatial distribution among sexes. This was the motivation for recording *Draco* sightings during the mating season and catered to two goals in my dissertation. First, it showed that males formed distinct territories maintaining spatial distancing of approximately 6 m from each other and mostly avoiding territorial overlap. Furthermore, 8 out of 12 male territories overlapped with at least one female home range suggesting that maintaining a territory might be important for gaining access to females. Conversely, females did not form territories and large overlap between their spatial distribution was observed, showing an obvious distinction between male and female behaviors. After quantifying the spatial distribution, I attempted to seek the second, more ambitious goal of my spatial distribution study – relating the territory size of males to their glide performance and morphology to understand what male characteristics influence territory size and access to females. Though this analysis did not lead to any significant relationships, it showed a possible approach to test such hypothesis in the future.

Overall, the spatial distribution analysis in my dissertation is the first quantitative representation of territoriality in gliding animals and cements the expectation that different evolutionary pressures indeed influence glide performance. On a more practical note, it also shows the value that a convenient field site can have on a study, which turned out to be particularly advantageous in the case of *Draco* inhabiting an abandoned areca nut plantation.

5.3 Gliding in the natural habitat

In Chapter 4, the focus was to broaden the scope of the dissertation to understand gliding behavior in the context of the environment. In doing so, I presented the first study elucidating

how gliding animals use and process information from the environment to modulate their glide trajectory and reach their desired target. This is by far the biggest leap in our understanding of how gliding animals traverse their spatially cluttered environment.

It should be noted that Chapter 4 presents a diverse data set of male *Draco* gliding over distances ranging from 2 m to 10 m with varying degrees of spatial complexities. Furthermore, this data set had minimal influence of the data collection setup compared to Chapters 2 and 3 where the recordings were conducted in a flight arena constructed within the same field site.

5.3.1 Path planning strategy

Gliding animals must manage a fixed energy budget to reach their desired target and to power maneuvers to negotiate obstacles in their glide path. Therefore, it would make sense to execute a path planning strategy to minimize expensive energetic losses involved in performing reactive in-flight maneuvers to avoid obstacles in their path and safely reach their target. A path planning strategy requires that the final outcome (glide distance) is pre-determined at the very beginning of the glide (takeoff phase). My results strongly supported this reasoning where numerous takeoff characteristics were associated with the glide outcome. Male *Draco* used a steeper average takeoff angle to cover greater horizontal distance, independent of takeoff height. The direction of takeoff in the horizontal plane was dependent on the relative location of the obstacle with respect to the landing tree; with *Draco* jumping further away from obstacles directly in-line with their target tree. Even before jumping to glide, for a given glide distance, *Draco* chose a glide direction which exposed them to relatively less clutter and reduced the in-flight maneuvering demands.

However, this is not to say that *Draco* did not perform reactive in-flight maneuvers or experience energetic losses associated with path planning. For glides where the obstacle was

more in-line with the target tree, the *Draco* had to execute a higher degree curved glide path by directing part of the resultant aerodynamic force vector sideways resulting in reduction of upward force that was used to counteract the body weight, leading to a marginally lower shallowing rate of the glide. Furthermore, for longer glides, with obstacles further away from the takeoff tree, path planning became less feasible potentially due to difficulty in discerning obstacles and landing tree in a visually rich environment. Therefore, a few glides of more than 6 m showed reactive in-flight maneuvers indicating that both strategies contribute towards lizards navigating their environment.

5.3.2 Visual navigation and landing control

After showing that the glide outcome influenced the takeoff characteristics of the glider, it was important to understand how animals actively controlled their glide trajectory once airborne. Note that active control has two types of interaction described in this dissertation. The first type, discussed in Chapters 2 and 3, deals with the animal and the surrounding fluid medium, air. It describes how the animal stays aloft and exhibits varying degrees of glide performance. The second, and the one discussed here, relates to how the environment influences the glide trajectory which ultimately also feeds into the first interaction.

Once airborne, the changes in *Draco's* heading direction agreed well with a vision-based obstacle avoidance steering model which has been previously described in humans. The model showed that the *Draco* heading direction was modulated by the combined effect of its angular orientation in the horizontal plane with respect to the obstacle and the landing tree. At every instant of time, *Draco* maximized its angular orientation with respect to the obstacle while minimizing its orientation with respect to the target tree, until eventually the *Draco* passed the obstacle tree and perfectly aligned its heading direction towards the landing tree.

Finally, landing initiation was described using a Relative Retinal Expansion Velocity (RREV) model which has been previously described in animals as diverse as plummeting gannets to fruit flies. It suggested that *Draco* initiated the breaking maneuver based on the ratio of its distance from the desired target and the speed at which it was approaching it. The distance from the target was derived from the retinal size of the target and the approach speed was derived from the rate at which the retinal size was changing. The RREV model suggested that *Draco* initiated its landing response 280 ms before the start of the landing phase. The delay of 280 ms potentially corresponded to the time taken to increase drag and induce deceleration by increasing its body pitch.

Overall, Chapter 4 showed how *Draco* were able to execute collision-free gliding on a daily basis to perform various behaviors. It revealed a vision-based path planning strategy employed by *Draco* to navigate their cluttered environment. This study also highlighted the maneuvering capabilities of *Draco* which were previously unknown and showed that collision-free gliding required continuous changes in the gliding kinematics such that the lizards never attained theoretically ideal steady state glide dynamics.

5.4 Gliding in a nutshell

In a nutshell, my dissertation shows that gliding is a complex task and involves various factors at play, both intrinsic and extrinsic to the animal. In doing so, it provides a convincing example of how habitat, behavior, and morphology influence locomotory performance in animals. I found that the *Draco* was aware of its environment and physical capabilities while performing well-choreographed glides in its natural habitat. The glide itself, was executed using a strategy that allowed it to efficiently cover horizontal distance while avoiding obstacles in its path. On a performance level, *Draco* airfoil properties were a surprisingly good match to the

expected properties of low-aspect ratio flexible airfoils, and the lizards made the most of their capabilities by continuously adjusting their posture throughout the glide. Overall, my investigations barely begin to reveal the interplay between locomotor capabilities and natural behavior, and I hope that further investigation in this species and others will continue to bridge the gap between theory, laboratory experiment, and field studies.